January 2013

Continuous Electrowetting in Passivating and Non-passivating Systems

Mehdi Khodayari
University of South Florida, mkhodaya@mail.usf.edu

Continuous Electrowetting in Passivating and Non-passivating Systems

by

Mehdi Khodayari

A dissertation submitted in partial fulfillment
of the requirements for the degree of
Doctor of Philosophy
Department of Mechanical Engineering
College of Engineering
University of South Florida

Co-Major Professor: Nathan B. Crane, Ph.D.
Co-Major Professor: Alex A. Volinsky, Ph.D.
Delcie Durham, Ph.D.
Matthias Batzill, Ph.D.
Alberto A. Sagüés, Ph.D.

Date of Approval:
July 3, 2013

Keywords: Reliable Electrowetting, Symmetric Electrowetting, Electrochemical Diodes, Electrostatic Force, Titanium, Aluminum

ACKNOWLEDGMENTS

I would like to express my gratitude to Professor Nathan B. Crane and Professor Alex A. Volinsky for all of their scientific and financial support during my Ph.D. study at the University of South Florida. Professor Crane was my immediate advisor and from him I learned how a dedicated advisor would be. Professor Volinsky was my great mentor and advisor too. Their approaches to scientific problems have always aided me to do research and publish papers. I appreciate all of their kindness.

TABLE OF CONTENTS

LIST OF TABLES

LIST OF FIGURES

ABSTRACT

Electrowetting is an electromechanical response that can be used to change the equilibrium shape of droplets on a surface through the application of an electric potential. By applying this potential asymmetrically to a droplet, the droplet can be moved. Typical electrowetting devices use an electrode covered by a dielectric to reduce electrochemical interactions. Successful electrowetting requires electrodes and dielectric layers that can resist damage through many cycles of voltage.

Continuous Electrowetting (CEW) is performed on high resistivity silicon wafers. In this process, when an electric potential difference is applied between the substrate ends, the droplet on the substrate moves towards the side with positive voltage. The diode behavior of consecutive metallic spots, placed in the oxide layer, is the root of the droplet movement. This thesis investigates electrode, dielectric, and electrolyte material combinations that can achieve long stable performance with a particular emphasis on continuous electrowetting.

Incorporation of diodes can also improve standard EW conditions to achieve lower voltage operation. In passivating systems, a reverse biased electrode becomes electrochemically passive. This way we have performed low voltage and reliable Electrowetting on Dielectric (EWOD) for 5000 test cycles. This is while, in non-passivating systems, EWOD degrades significantly from the first cycles. In CEW devices, SiO_2 can also serve as a steady dielectric. It is observed that, with larger electrolytes, contact angle change would remain consistent for 10000 cycles with less than 19% degradation, while would be as high as 47% with small electrolytes.

In CEW device, consistent and ideal behavior of electrochemical diodes is expected. Even though diode pairs reduces current flow and the extend of electrochemical reactions, the diode behavior can degrade over test cycles due to electrochemical reactions. To evaluate the diode behavior of different electrodes, a coefficient (referred to as actuation coefficient) is introduced which varies between zero (the least favorable diode behavior) and one (the best diode behavior) It is shown that, with the use of titanium as the electrode, the diodes behave more ideally and they behave consistently over 2000 test cycles. The best diode performance was observed with Na_2SO_4 electrolyte solution, where actuation coefficient remains at around 0.8 for 10000 test cycles. Aluminum can perform well in the beginning of the test cycles, but its performance degrades significantly over the first cycles.

CHAPTER 1: INTRODUCTION

1.1. Technology Life-Cycle Path

Centuries ago, the discovery of a new process could remain as pure science without industrial applications. Yet, these days, with the aid of advanced technologies almost any scientific concept will turn into a new technology. Decades ago, a car working with batteries was just an idea and now it is a reality. Market demands have pushed the industries to manufacture new products. However, a novel concept or method, first, has to pass a research and development phase and then it pays off in vital life phase (as shown in Figure 1-1) and finally the financial return of a technology declines [1]. During vital life phase a technology profits because it is superior to its counterparts. For some technologies such as steel, glass, and cement the vital life span is long, while for some others like pharmaceutical products it is short. The vital life span could be extended through patents and new discoveries in the field.

1.2. Motivation for Electrowetting on Dielectric Process Research

A century ago, electrowetting was also a scientific observation [2]. In this process, a droplet is placed on top of a hydrophobic dielectric substrate. Then, the droplet wets the hydrophobic surface when a potential difference is applied between the droplet and an electrode below the dielectric layer. This process is known as Electrowetting on Dielectric (EWOD). Typically, a thin layer of a hydrophobic layer is coated on a dielectric layer even though the hydrophobic layer alone can also act as a dielectric layer.

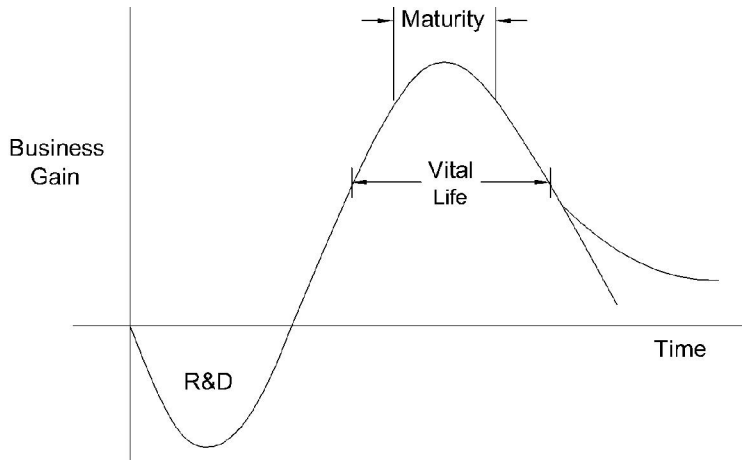

Figure 1-1. Technology life-cycle path.

Likewise, these days EWOD has found applications in different devices and has offered advantages over its conventional alternatives. In cell phone cameras, a droplet can act as a lens and its focal length can be changed via electrowetting process without the need of mechanical motors [2-4]. Reflective displays have been manufactured by using droplets with significantly lower response time than ordinary electronic papers [5-6]. In Lab on Chip devices, electrowetting has been used to move, split, and mix droplets [7-13]. EWOD has even been also used for vibration energy harvesting with a power density as high as 10^3 Wm^{-2} [14].

These accomplishments suggest that electrowetting may soon inter its vital life span and any future researches and inventions in the field can expand the vital life span. So far, amongst the extensive researches on EWOD, only a few have focused on the device reliability. The goal of this study is to investigate the materials, which improve both the device reliability and droplet actuation force.

1.3. Continuous Electrowetting

Before talking about Continuous Electrowetting (CEW), I briefly explain how Electrowetting on Dielectric (EWOD) works. Conventional EWOD is performed by placing a droplet on top of a hydrophobic substrate and applying a potential difference between the droplet

and the substrate. Even though EWOD has found multiple applications such as electrowetting lenses, microprocessors cooler, reflective displays, and etc., this work will focus on a particular actuation scheme called Continuous Electrowetting (CEW), but many of the results have direct application to other actuation schemes. We have already used EWOD to perform CEW (Figure 1-2) [15]. In CEW as shown in Figure 1-2, the diode like behavior of the metallic spots causes an asymmetric potential distribution analogous to bidirectional electrowetting, so that the substrate potential at the reverse biased spot is higher than that at the forward biased spot. The difference in the substrate potential leads to an asymmetric contact angle modulation, so that contact angle at the spot with higher potential would be lower than that at the other spot. Hence, the droplet is actuated towards the spot with higher potential. With a sequence of metallic spots a droplet moves continuously.

The droplet in CEW can be used to move parts placed on top of the droplet. The parts could be used for an assembly process. This is the specific application in our study, yet CEW can be used for any other purposes such as drug delivery.

The prototype CEW device consists of a 270 μm high resistivity silicon substrate (300-500 Ω-cm) with a 500 nm thermally grown SiO_2 layer with small holes (200 μm in diameter), which are filled by a metal via e-beam evaporation. Finally a thin layer of Cytop (50 nm) is spin coated on top of the substrate to render the surface hydrophobic. In CEW devices, the metallic spots act as diodes and the surrounding SiO_2 as dielectric [15].

A droplet can move when an electric potential difference exists between the substrates ends. In this process, the diode-like behavior of the metallic spots causes a potential difference in the high resistivity substrate between adjacent metallic spots (The diode behavior of the metallic spots is caused by the variation of the electrochemical reactions rate with potential polarity. A

metallic spot gets forward and reverse biased respectively when it is polarized to negative and positive voltages). The potential difference results in an asymmetric contact angle due to electrowetting. This asymmetry propels the droplet towards the end with higher potential (lower contact angle) [15]. Figure 1-3 shows the top view of CEW on a high resistivity n-type silicon wafer. In this process, the left side of the shown device is grounded and a voltage of +350 V is applied to the right side. In this figure, the snapshots of the droplet movement are shown. The device width is 28 mm and the droplet volume is 50 µl. It takes about 0.8 second for the droplet to move from the left side of the strip to the right side. In this device, aluminum spots are used as the electrochemical diodes.

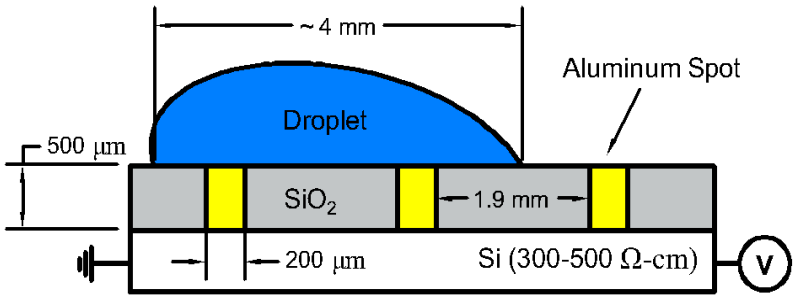

Figure 1-2. Continuous electrowetting schematic.

1.4. Dissertation Goal

Practically, it is possible to move any fluids on the substrates, yet the droplet lateral force and device reliability highly depends on the droplet electrolytes and the metal used in the spots. Reliability is assumed to be limited by electrochemical degradation of the metal spots that form the diode-like droplet/substrate connections and the silicon dioxide dielectric. Thus, this thesis will focus on improving device reliability by improving the consistency of the electrical response of the CEW device components under repeated voltage cycles. There are two components of the device that are required to perform reliably, which are metallic spots and SiO_2 dielectric.

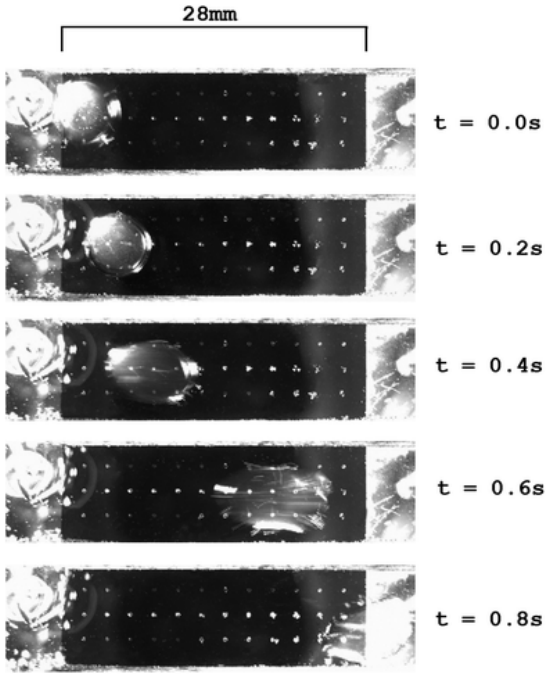

Figure 1-3. Top view of Continuous Electrowetting on a high resistivity n-type silicon wafer [15].

The reliability of both metallic spots and SiO_2 dielectric layer is important. Metallic spots play a significant role in CEW process by providing an electric potential difference in the high resistivity silicon substrate at the two ends of the droplet - without the metallic spots CEW ceases. However, they can be etched away through oxidation after repeated actuation. The metallic spots etching can be minimized by using specific combination of the metal/droplet electrolytes (in this process non-oxidizing metals such as gold cannot be used because they do not show diode like behavior). In addition, the SiO_2 has to behave reliably too. Typically, electrowetting on SiO_2 degrades over many electrowetting cycles, the degree of which depends highly on the droplet electrolytes. However, with the use of some specific electrolytes, the angle modulation degradation decreases significantly. Therefore, the chosen metal/electrolytes combinations have to guarantee both metallic spots and SiO_2 reliability. As will be shown in the next chapters, reliable material systems do not necessarily result in high potential difference

between the spots. Hence, the material systems have to be narrowed down to those which ensure significant potential difference between the metallic spots, too.

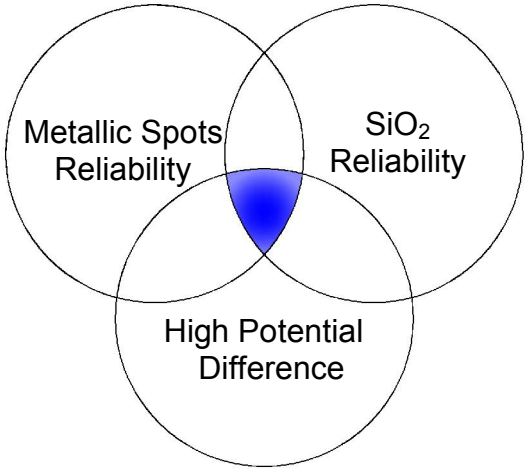

Figure 1-4. The relation between metallic spots reliability, SiO2 reliability, and high potential difference.

The three objectives of this study are metallic spots reliability, SiO_2 dielectric reliability, and high potential difference between the two points of the high resistivity silicon wafer at metallic spots underneath the moving droplet. Since the prototype CEW devices work initially but with decreasing performance after 5-10 cycles, it is believed that there are changes in the electrical performance of the device components from repeated cycling. This thesis will study conditions for consistent response of each independent area. The diagram in Figure 1-4 shows the logical relation between the objectives, which are further explained as follows:

1- Objective 1: metallic spots have to have consistent electrical response and the top left circle is related to the metallic spots reliability. Here, electrical response is related to the diode behavior of the metallic spots, which is diminished if they etch away. The first objective of this study is to find metal/electrolyte combinations, in which the metallic spots withstand the oxidation and etching, and so provide reliable electrical response. In the previous study [15], CEW could be performed for a few cycles (here, each cycle is the droplet movement from one side to other side), which is attributed to the etching of metallic spots. Here, we try to find metal/electrolyte

combinations, with which CEW can be performed for over 1000 cycles. Given the state of the technology, 1000 cycles of consistent CEW means a significant improvement in the reliability of CEW devices and we try to achieve this reliability with the aid of appropriate metal/electrolyte combinations.

2- Objective 2: the SiO_2 dielectric has to be reliable too. Here, reliability is referred to the consistency of contact angle change of the droplet on the SiO_2 dielectric, which depends on the electrical consistency of the SiO_2 dielectric. The top right circle corresponds to the reliability of SiO_2 dielectric. SiO_2, in the CEW devices, acts as a dielectric and when a potential difference is applied between a droplet on SiO_2 electrode and an electrode below, the droplet/substrate contact angle changes. The magnitude of the contact angle change varies with the dielectric properties of the dielectric layer. In CEW, we want the SiO_2 dielectric to show consistent dielectric properties, so that the contact angle change would be consistent over many cycles. We have seen that the SiO_2 reliability highly depends on the electrolytes in the droplet, so the second objective of this study is to find the best SiO_2/electrolyte combinations in terms of the droplet contact angle reliability. To determine the contact angle reliability on SiO_2 dielectric, conventional electrowetting is performed on wafers with SiO_2 as dielectric with different electrolytes. It will be shown that the SiO_2 dielectric acts reliably when large electrolytes are used in the droplet.

Other authors have also conducted researches on the EWOD reliability. Heikenfeld et. al. have performed extensive researches on substrates reliability in EWOD. They have shown that large electrolytes such as SO_4^- hardly penetrates through Al_2O_3 dielectric, and hence the reliability of the EWOD devices can be improved [16]—to show this they have obtained I-V curves with different fluids with various sizes of electrolytes. This way they have observed that with large electrolytes current remains at around zero ampere and also attributed the EWOD

reliability to the zero current passage—zero current guarantees the absence of the electrochemical reactions which damage the substrates.

Alternatively, they have shown that, with the use of nonaqueous fluids, the electrowetting reliability can be improved [17]—in their study, indium tin oxide substrates coated with 1 μm Parylene C were used. Fourteen nonaqueous fluids were used, namely acetonyl acetone, acetophenone, diacetone alcohol, diethyl carbonate, dimethyl malonate, dimethyl sulfoxide, ethyl aceto-acetate, ethyl-L lactate, γ-butyrolactone, N,N-dimethylacetamide, N-methyl formamide, propylene carbonate, propylene glycol, and 2-pyrrolidone. It was shown when the substrate is negatively polarized and small ions such as Na^+ are involved in EWOD, dielectric failure occurs, which is detected by a current raise in I-V curves [17]. However, the contribution of large ions such as ammonium (NH_4^+) and tetrabutyl ammonium (TBA^+) when the substrate is positively polarized results in a significant improvement of the substrates reliability in EWOD.

Additionally, the reliability of Parylene HT as a dielectric in EWOD substrates has been shown [18].In this study, a 300 nm Parylene HT performed reliably without current passage in I-V curves in both polarities of the substrates. The droplet liquid was 0.013 wt% SDS. With Parylene HT, EWOD can be performed for over 6.5 hours with insignificant degradation in contact angle change [18].

Even though zero current is the key criteria to obtain reliable EWOD, the endurance of the EWOD systems with zero current has to be evaluated over repeated cycles. In our study, in addition to the current passage prevention, we also show how reliable contact angle change would be maintained over many cycles (for up to 10000 cycles). In fact, with EWOD systems that perform reliably for many cycles, we can make fabricate long-life devices.

3- Objective 3: last but not least, the bottom circle is associated with the electric potential difference in the high resistivity silicon wafer at the ends of the droplet. Here, the metallic spots etching is not the concern and only the diode behavior of the metallic spots is investigated. It is noteworthy that in some cases metallic spots do not etch away, but their diode behavior is poor. Therefore, beside the resistance against etching, the metallic spots have to posses appropriate diode behavior, which is taken care of in this part of the study objective. When the metallic spots behave as ideal diodes, the lateral electrostatic force moving a droplet sidewise in CEW would be the highest possible. Based on the diode behavior of the metallic spots, we introduce a criterion—referred to as actuation coefficient ($\eta_{actuation}$)—to compare the lateral electrostatic force in different metal/electrolyte combinations. When $\eta_{actuation}$ is zero, it means the metallic spots behave as resistors, and hence the lateral electrostatic force is zero. However, the lateral electrostatic force reaches a maximum when $\eta_{actuation}$ is equal with one, as the metallic spots act as ideal diodes. The third objective of this study is to find the metal/electrolyte combinations with highest electrostatic forces, which is when $\eta_{actuation}$ is close to one . It will be shown that the highest $\eta_{actuation}$ values can be obtained with titanium electrode in contact with all the tested electrolyte solutions (0.1 M citric acid, 0.1 M Na_2SO_4, and NaOH).

In this study, each component of the above diagram is investigated separately and then these results will be used to assess the prospects for reliable CEW. It will be shown that, when aluminum is used as the metallic spots, all the objectives cannot be met. We either see high resistance of aluminum spots against etching or relatively high potential difference between two spots. To improve the resistance of aluminum spots, passivating systems were used, in which aluminum passivates upon anodic polarization—passivating systems consist of appropriate combinations of electrode (aluminum) and electrolytes (e.g. citric acid and tartaric acid). The

problem of passivating systems is that the barrier-like oxide layer on aluminum prevents electrolytes diffusion (through the oxide layer) at both positive and negative potential polarities. Hence, the diode behavior of electrodes diminishes in the passivating systems and the potential difference between two spots drops significantly. However, with the use of titanium instead of aluminum, metallic spots reliability and high potential difference can be met. It is also speculated that with SO_4^{2+} cations, droplet actuation on SiO_2 dielectric is reliable. Therefore, it is recommended that, in CEW devices, titanium be used as the metallic spots and also Na_2SO_4 electrolyte solution be used for the droplet.

1.5. References

[1] R.P.P. Senthilkumar, Project Management, New Delhi, 2010.

[2] F. Mugele, J.-C. Baret, Electrowetting: from basics to applications, Journal of Physics: Condensed Matter, 17 (2005) R705-R774.

[3] B. Berge, J. Peseux, Variable focal lens controlled by an external voltage: An application of electrowetting, Eur. Phys. J. E, 3 (2000) 159-163.

[4] B.H.W. Hendriks, S. Kuiper, M.A.J. As, C.A. Renders, T.W. Tukker, Electrowetting-Based Variable-Focus Lens for Miniature Systems, Optical Review, 12 (2005) 255-259 LA - English.

[5] R.A. Hayes, B.J. Feenstra, Video-speed electronic paper based on electrowetting, Nature, 425 (2003) 383-385.

[6] R. Shamai, D. Andelman, B. Berge, R. Hayes, Water, electricity, and between... On electrowetting and its applications, Soft Matter, 4 (2008) 38-45.

[7] M. Abdelgawad, A.R. Wheeler, Rapid Prototyping in Copper Substrates for Digital Microfluidics, Advanced Materials, 19 (2007) 133-137.

[8] C. Cooney, C.-Y. Chen, M. Emerling, A. Nadim, J. Sterling, Electrowetting droplet microfluidics on a single planar surface, Microfluidics and Nanofluidics, 2 (2006) 435-446.

[9] M.W.L. Watson, M. Abdelgawad, G. Ye, N. Yonson, J. Trottier, A.R. Wheeler, Microcontact Printing-Based Fabrication of Digital Microfluidic Devices, Analytical Chemistry, 78 (2006) 7877-7885.

[10] K.P. Nichols, J.G.E. Gardeniers, A Digital Microfluidic System for the Investigation of Pre-Steady-State Enzyme Kinetics Using Rapid Quenching with MALDI-TOF Mass Spectrometry, Analytical Chemistry, 79 (2007) 8699-8704.

[11] E.M. Miller, A.R. Wheeler, A Digital Microfluidic Approach to Homogeneous Enzyme Assays, Analytical Chemistry, 80 (2008) 1614-1619.

[12] P. Paik, V.K. Pamula, R.B. Fair, Rapid droplet mixers for digital microfluidic systems, Lab on a chip, 3 (2003) 253-259.

[13] E. Miller, A. Wheeler, Digital bioanalysis, Anal Bioanal Chem, 393 (2009) 419-426.

[14] T. Krupenkin, J.A. Taylor, Reverse electrowetting as a new approach to high-power energy harvesting, Nature communications, 2 (2011) 448-448.

[15] C.W. Nelson, C.M. Lynch, N.B. Crane, Continuous electrowetting via electrochemical diodes, Lab on a chip, 11 (2011) 2149-2152.

CHAPTER 2: BACKGROUND MATERIALS

The purpose of this study is to find material systems, which guarantee reliable Continuous Electrowetting (CEW) with high droplet actuation force. In first part of this chapter, electrowetting theories are first explained and then the CEW mechanism is explained. The second part is spent on the background materials of metallic spots etching and prevention. To perform CEW reliably over thousands of cycles, metallic spots must be reliable. The metallic spots could etch away possibly due to oxidation which has to be prevented with an appropriate electrode/electrolyte pair selection. In this chapter, it is explained how passivating systems can be incorporated in CEW to improve the device reliability.

2.1. Wetting Basics

In contact with other phases (gas, liquid, solid), liquids take a shape that minimizes the free energy[1-2]. The gravitational energy acting on the liquid and surface tensions of the other phases are the energies that determine droplet shapes. The ratio of the typical weight ($\rho.g.r^3$) over the force caused by the droplet surface tension ($r.\sigma_{lg}$), which is referred to as the Bond number (Bo), defines the droplet shape, as follows [3]:

$$Bo = {\rho.g.r^2}/{\sigma_{lg}} \tag{2.1}$$

here, ρ, g, r, and σ_{lg} are respectively droplet density, gravitational acceleration, the largest droplet radius (the distance between the droplet surface to a line vertical to the substrate and tangent to the droplet), and the surface tension between the droplet and the second phase (air or oil). For the droplets with bond numbers higher than one, weight is dominant, and hence the droplet tends to

get flat (like a pancake). For aqueous liquids (without surfactants) in air, an 82 µl droplet possesses a Bond number of 1 [4] (in this calculation σ_{lg}=72 mN/m and ρ=1 kg/L). For the droplets with a Bond number lower than one, droplets are like a spherical cap [5]. Typically, in this study we have used droplets smaller than 20 µL, so the contribution of the gravitational energy is negligible and it is presumed that only the surface would be effective (the bond number of a 20 µL droplet in air is around 0.24). Additionally, the droplets are spherical cap due to their bond number.

In the next sections, it is explained how a droplet takes shape on a solid surface. Then it is explained how the droplet shape can be manipulated in Electrowetting on Dielectric (EWOD) process.

2.1.1. Surface Energy

Material surfaces, typically, host physical reactions (e.g. dust absorption) and chemical reactions (e.g. rust formation). In fact, due to missing intermolecular bonds, material surfaces possess higher energy than in the bulk, which leads to reactions to reduce their energy. For liquids, surface energy variation of the liquid and/or adjacent phases brings about droplet shape manipulation with or without reactions on the surfaces.

2.1.2. Contact Angle (Young's Equation)

For a droplet on a solid surface, the droplet shape can be defined by the contact angle of the droplet at Three Phase Contact Line (TCL), the contact line where the three phases meet.

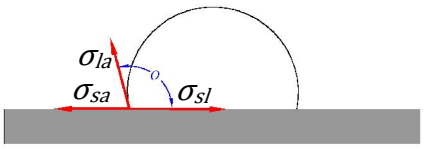

Figure 2-1. The effect of surface tensions interaction on droplet contact angle.

The contact angle can be calculated by balancing horizontal vectors of the forces at TCL. In equilibrium, the net force per unit length acting on TCL must be zero. Typically, three forces are

acting on TCL, droplet/air (σ_{la}), substrate/droplet (σ_{sl}), and substrate/air (σ_{sa}) surface tensions. Balancing the surface tensions, the droplet contact angle can be obtained through Young's equation as follows:

$$\cos\theta = \frac{\sigma_{sa} - \sigma_{sl}}{\sigma_{la}} \tag{2.2}$$

This equation is the basis of the Lippman equation that predicts EWOD behavior.

2.2. Electrowetting

Electrowetting is a process, in which a droplet shape is modulated on a hydrophobic substrate by applying an electric potential difference between the droplet and the substrate. Typically, the contact angle between the droplet and substrate is associated with the droplet modulation.

First, Lippman derived the electrowetting equation based on the substrate/droplet surface tension reduction with voltage [6]. At the time, the electrowetting tests were performed on bare mercury exposed to an acidic electrolyte solution. Hence, the surface tension reduction was attributed to charge accumulation in the double layer formed on the mercury droplets. The surface tension reduction with voltage can be explained by the following equation:

$$\mathrm{d}\sigma_{sl}^{eff} = -\rho_{sl}\mathrm{d}U \tag{2.3}$$

here, U is the surface electrochemical potential and σ_{sl}^{eff} is the effective surface tension. The effective surface tension is associated to the surface tension that is caused by the deliberate variation of the metal potential, not by the initial charge accumulation. When a metal is immersed in an electrolyte solution, electrolytes accumulate on the metal surface due to the metal surface free energy. The electrolytes accumulation reduces the effective surface tension of the metal. ρ_{sl} is the electrolyte's concentration on the metal, which varies with the metal potential and is obtained as follows:

$$\rho_{sl} = C_H U \tag{2.4}$$

C_H is the double layer capacitance formed on the metal surface exposed to an electrolyte solution. Combining equations (2.3) and (2.4) and integrating both sides, one reaches an equation that relates surface tensions before and after electric potential application as follows [7-8]:

$$\sigma_{sl}^{eff} = \sigma_{sl} - \int_{U_{pzc}}^{U} C_H U \, \mathrm{d}U = \sigma_{sl} - \frac{\varepsilon_0 \varepsilon_1}{2d_H}(U - U_{pzc})^2 \tag{2.5}$$

here ε_0 and ε are respectively the vacuum permittivity (8.854×10^{-12} farads per meter) and double layer dielectric constant (~81). d_H is the double layer thickness (around 2 *nm*) and U_{pzc} is the potential of zero charge, the metal potential without spontaneous electrolytes accumulation. Combining equations 2.2 and 2.5, the Lippman equation is obtained as follows:

$$cos\theta = cos\theta_0 + \frac{\varepsilon_0 \varepsilon_1}{2d_H \sigma_{la}}(U - U_{pzc})^2 \tag{2.6}$$

here Θ and Θ_0 are the droplet/substrate contact angles respectively before and after voltage application.

Equation 2.6 was derived in a metal/electrolyte system where the spontaneous charge accumulation on the metal surface has to be taken into account via the U_{pzc} consideration. However, after coating a dielectric material on the metal surface, the charge accumulation effect can be neglected [8] and the Lippman basic electrowetting equation would be as follows:

$$cos\theta = cos\theta_0 + \frac{\varepsilon}{2\delta\sigma_{la}}V^2 \tag{2.7}$$

here, θ_0 and θ are the initial and actuated angles, V is the electric potential difference between the droplet and wafer, σ_{la} is the surface tension between the droplet and the second phase, δ is the dielectric thickness, and ε the dielectric permittivity. Figure 2-2 schematically shows the apparent contact angle change in the generic EWOD.

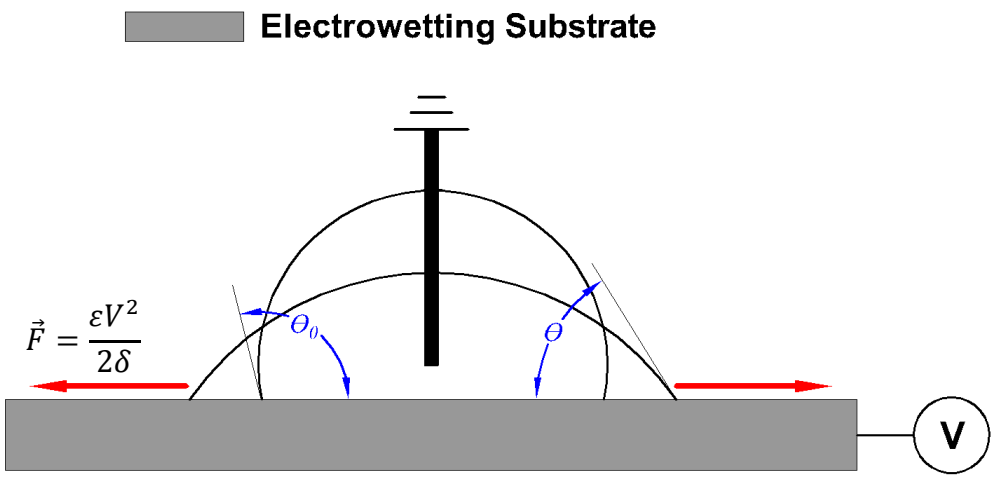

Figure 2-2. Contact angle variation in conventional electrowetting process.

Electrochemical interpretation of electrowetting, as discussed above, could predict contact angle through the Lippman equation. Researchers have already validated the Lippman model capability to predict the electrowetting process [4, 9-11]. However, the electrochemical derivation of equation 2.7 overlooks the mechanical aspects of the droplet modulation. In addition, the stability of contact angle at Three Phase Contact Line (TCL) raises doubt as to whether the substrate surface tension actually changes. In this regard, the electromechanical interpretation of electrowetting addresses the issue of the contact angle stability and also provides an image of the mechanical aspects of electrowetting.

The basis of electromechanical interpretation of electrowetting is the Korteweg-Helmholtz body force density which shows the electrical force on liquids as follows [12]:

$$\overrightarrow{f_k} = \rho_f \vec{E} - \frac{1}{2} E^2 \nabla \varepsilon + \nabla \left[\frac{1}{2} E^2 \frac{\partial \varepsilon}{\partial \rho} \rho \right] \tag{2.8}$$

here, ρ_f is the volume density of free charges, ε is the liquid permittivity, and ρ is the mass density of the liquid. The third term on the right hand of equation 2.8 is the contribution of electrostriction in the electric force, which can be ignored in homogeneous and incompressible

liquid media [13] like electrowetting droplets. Hence, the Korteweg-Helmholtz body force density can be written as follows:

$$\overrightarrow{f_k} = \rho_f \vec{E} - \frac{1}{2} E^2 \nabla \tag{2.9}$$

Within the droplet volume, the free charge density is zero, while it is nonzero on the droplet surface [14]. Hence, the electrical force is only applied on the droplet surface [13-14]. In addition, the free charge density is high on the three phase contact line (TCL) and decreases exponentially by distance from TCL [15]. Therefore, in the vicinity of TCL, the electrostatic force on the droplet surface would be significant. The electrostatic force is perpendicular to the droplet surface and the lateral component causes the translational modulation of droplets. Through mathematical examination, it is shown that the lateral electrostatic force inserted on the droplet close to TCL is equal with the electrowetting number as follows [15]:

$$\vec{F} = \frac{\varepsilon V^2}{2\delta} \tag{2.10}$$

here, ε and d are respectively the dielectric permittivity and thickness. Kang [15] has also shown that the balance of the lateral forces close to TCL would be as follows:

$$\sigma_{la} cos\theta = \sigma_{sa} - \sigma_{sl} + \frac{\varepsilon}{2\delta} V^2 \tag{2.11}$$

Equation 2.11 is, in fact, the Lippman equation which originally was obtained via the electrochemical interpretation. However, in equation 2.11, the electrical force causes the droplet modulation. In EWOD, contact angle remains constant at TCL. The electrostatic force, in fact, applies a drag right above the contact line, which vanishes asymptotically towards TCL. Therefore, *local contact angle* remains constant at TCL while the *apparent contact angle* changes [16-17].

2.2.1. Applications

EWOD has found multiple applications such as microprocessor cooling, micromechanical systems, electrowetting lenses, reflective displays, energy harvesting, and lab on chip, which are briefly explained here.

2.2.1.1. Microprocessors Cooling

Microprocessors and integrated chips are getting smaller rapidly and their thermal management is getting more challenging. The conventional method for the microprocessor heat management is air cooling with the cooling limit of around 200W per microprocessor (this number shows the device cooling capacity), which is not enough for the contemporary microprocessors [18]. One way to decrease microchip temperature is to incorporate channels with a fluid flow in the microchips. This way, heat can be efficiently transferred from a heat source to a heat sink through fluids flowing in microchannels with the aid of microscale pumping technologies [19]. However, due to the high heat generation in microprocessors chips, the fluid has to be pumped with high rates through the microchannels, which consumes significant power.

Instead, electrowetting on Dielectric (EWOD) consumes low power and has provided a promising method for microchips cooling [20]. In this method, a droplet moves over the hot spots via electrowetting, which results in a significant temperature drop in the hot plates.

2.2.1.2. Micromechanical Systems

In this application, a vertical force is applied on a flat surface by an electrowetting based microactuator. The microactuator device consists of two flat plates connected by a liquid bridge. The liquid bridge is actuated via electrowetting on one the plates and then pressure is applied on the plates [21]. Figure 2-3 shows the schematic of the electrowetting based microactuator.

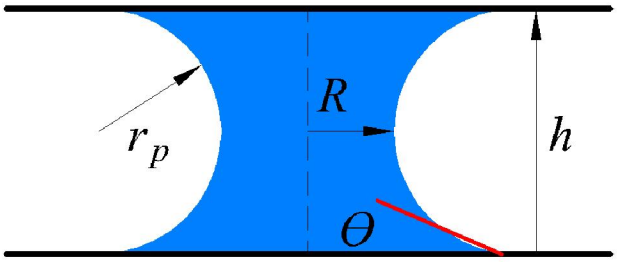

Figure 2-3. Schematic of the electrowetting based microactuator. The blue area shows the liquid bridge that is actuated by electrowetting [21].

here, h, R, r_p, and Θ are respectively the bridge height, the bridge waist radius, the bridge profile radius of curvature, and the apparent contact angle. In the electrowetting based microactuator, the actuation force is obtained as follows:

$$f = -\sigma_{la}\pi R(1 + \frac{2R}{h}cos\theta) \tag{2.12}$$

In this kind of microactuator, due to the capillary pressure variation via electric field application, the actuation force is higher than conventional electrostatic actuation. In addition, the actuator displacement is significantly higher. The limitation of this device is the saturation of the contact angle, which limits the actuator force [21].

One goal of this project is to move objects on top of droplets via continuous electrowetting. The schematic of the device is shown in Figure 2-4.

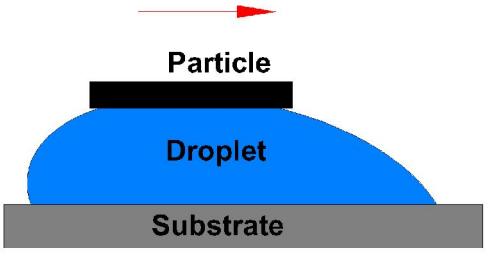

Figure 2-4. The schematic of continuous electrowetting application to move particles.

2.2.1.3. Electrowetting Lenses

To use a droplet as a lens, a droplet is placed on a transparent substrate and then its focal length is changed via electrowetting process without the need of mechanical motors [22-24]. In

this application, indium tin oxide (ITO) on a glass substrate can be used as the substrate for its transparency [25-26]. However, the commercial electrowetting lenses are based on electrowetting on the walls of cylindrical cells with a transparent bottom that does not contribute in the electrowetting process. Varioptic [27] manufactures electrowetting based lenses.

2.2.1.4. Reflective Displays

Reflective displays provide the same quality as the regular ink on paper. In conventional backlit displays, the light is emitted from the display backside, but the reflective displays work similar to ink on paper, which is based on light reflection. Reflective display technology have been already commercialized based on capsules with particles inside [28], which could change their color via electrophoresis.

In electrophoresis based displays, there are black and white dispersed pigments in thousands of capsule units. When a potential difference is applied through a capsule unit, the dispersed black and white particles inside the capsules are separated via the electrophoretic effect. This way, the apparent color of the capsule unit can be manipulated via the variation of the electric field polarity. Hence, an image can be created by controlling the color of all the capsules.

The time response of the electrophoretic process made the conventional reflective displays noticeably slow in speed. However, it has been shown that, instead of the electrophoretic capsules, EWOD cells can be employed in the reflective displays with much faster response time [29-30]. Another advantage of the electrowetting reflective displays is that they can be much brighter than the conventional ones by using a reflective substrate (white substrate) [29]. On and off response times of respectively 12 and 13 ms have been found in the electrowetting display pixels, which are fast enough to show video films [29]. Electrowetting, in addition, is a low power process, so the electrowetting based display is a low power and green generation of

displays. Gamma Dynamics and Liquavista are the main manufacturers of electrowetting displays.

2.2.1.5. Energy Harvesting

EWOD has even been also proposed for vibration energy harvesting with a predicted power density as high as 10^3 Wm^{-2} [31]. This method uses a variable capacitor based harvesting device, in which the contact area between the droplets and the substrate act as the variable capacitor. Upon vibration, the contact area surface area is changed, and then the vibration mechanical energy is transformed into electricity [31].

2.2.1.6. Lab on Chip

In the realm of micro total analysis systems (μTAS) also known as "lab on a chip", small sizes of liquid samples can reduce the time and cost of analysis [32]. In Lab on Chip devices, electrowetting has been used to move, split, and mix droplets [27, 33-38]. Electrowetting can be used for droplets mixing in a timely manner, which helps to investigate enzyme kinetics [36].

Electrowetting has been also employed for field Trinitrotoluene (TNT) detection with the colorimetric method [39]. In this device, a TNT solution droplet is moved and mixed with a nucleophile (e.g. hydroxides and alkoxides), which produce a colored Jackson-Meisenheimer droplet. Then the colored droplet is analyzed via a LED and photodiode.

In another application, it has been shown that a magnetic bed can be extracted from a droplet with the aid of magnet coils, and then the droplet can be moved away from the magnetic bed [40]. The magnetic particles are DNA carriers, so they can be used to extract DNA from a droplet carrying the DNA [41]. The challenging step for the DNA extraction is moving the droplet away from the magnetic bed. The magnetic bed movement should be avoided, as it minimized the DNA extraction efficiency [40]. In DNA extraction process, EWOD aids the droplet lateral movement.

Droplets manipulation can be performed on a substrate with patterned conductive plates adjacent to each other. One example of droplet manipulation has been shown in Figure 2-5 [42].

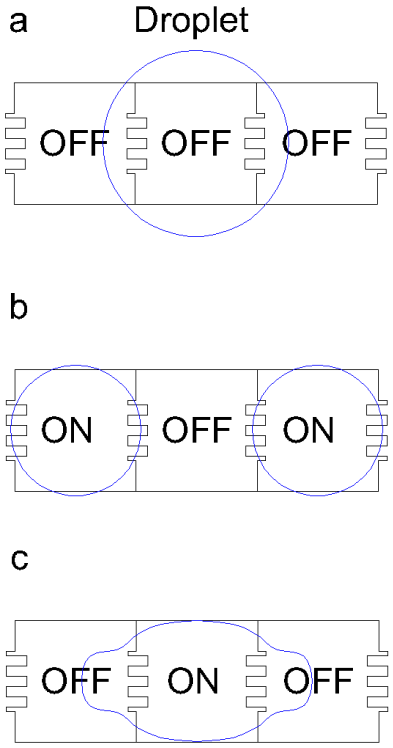

Figure 2-5. Droplet manipulation on substrates with adjacent conductive plates [adapted from 42].

In this process, a droplet is sandwiched between a substrate and a conductive plate [42]. The substrate consist of adjacent conductive plates coated with a hydrophobic layer. A plate is on when a potential difference is applied between the plate and the grounded top conductive plate. A droplet on a plate is split when two plates, adjacent to the off plate, are on as shown in Figure 2-5b. Then, the droplets can be remerged by turning on the middle plate and turning off the adjacent plates, as shown in Figure 2-5c.

2.2.2. Actuation Methods

Three main actuation methods have been used in electrowetting, including conventional electrowetting, bidirectional electrowetting, and continuous electrowetting, which are explained

in the following sections. Before discussing different methods of electrowetting, two methods of grounding are briefly explained.

To actuate a droplet via electrowetting, a potential difference is held between the droplet and the conductive layer. Either droplet or conductive layer can be grounded. For this section we assume the droplet is grounded. The droplet grounding can be done either from above or from below. Figure 2-5 shows one example of grounding droplet from above. To ground from above, the droplet is grounded via either a conductive layer or a piece of wire that is connected to the droplet from above.

2.2.2.1. Grounding from below

Grounding from below method has been shown schematically in Figure 2-6. In this method of droplet grounding, the ground electrode is laid on the substrate below the hydrophobic surface. Hence, all the required electrical connections are in the substrate, enabling agile droplet movements [4].

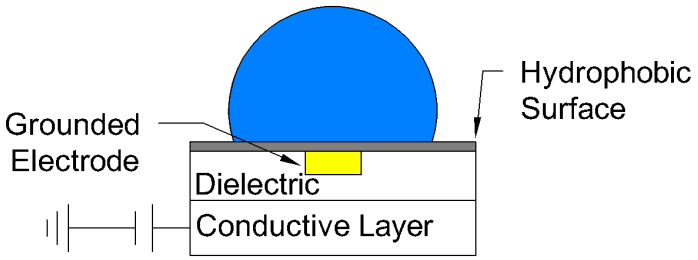

Figure 2-6. Schematic of grounding electrode from below [adapted from 4].

2.2.2.2. Conventional Electrowetting

Conventional electrowetting is performed by placing a droplet on top of a hydrophobic substrate and applying a potential difference between the droplet and the substrate as shown in section 2.2. . Conventional electrowetting process has been used in electrowetting lenses where a transparent substrate and a droplet on top—with the capability of changing its focal length via electrowetting—constitute the lens component [22]. The conventional electrowetting setup is

also appropriate to investigate electrowetting reliability in the passivating and non-passivating systems, which is used in this study.

The conventional electrowetting is also the basis of digital manipulation of droplets as shown in Figure 2-5. In the next section we introduce another scheme of electrowetting, which is used for bidirectional electrowetting; in this method, instead of switching the adjacent plates on and off, diode like behavior of conductive layers is employed to move the droplets laterally.

2.2.2.3. Optoelectrowetting

When an ac voltage is applied on a photoconductive layer in the absence of light, its impedance changes with the ac voltage frequency. At a certain frequency its impedance would be significantly high and it is said the photoconductive layer is in the dark state. However, in the present of a light beam, the photoconductive—otherwise in the dark state—impedance drops and it acts like a conductor.

In the optoelectrowetting method, the substrate is connected to the power source through a photoconductor layer below the conductive layer. Then, between the droplet and the substrate, an ac voltage is applied. The frequency of the ac voltage has to be in a range that keeps the photoconductor layer in the dark state. This way, the significant part of the voltage drop would be through the photoconductor layer, and hence electrowetting does not occur. However, when a light beam is applied on the photoconductor layer, it acts like a conductor, and then the potential drop would be between the droplet and the dielectric layer, so electrowetting occurs [43].

In the optoelectrowetting process, all the conductive and dielectric layers have to be transparent, so the photoconductor impedance can be adjusted by a light beam from above. The advantage of this method is that a droplet can be moved to different parts of the substrate by only a light beam without the maze of electrical connections [23].

2.2.2.4. Bidirectional Electrowetting

In the conventional electrowetting, because of the voltage uniformity over the droplet perimeter, the contact angle variation would be identical all over the perimeter, so the droplet remains steady without any lateral movement. As a result, upon voltage application, contact angle changes without droplet lateral movements [15]. However, if we apply a nonuniform voltage on the droplet, the net force on TCL would be greater than zero, causing a planar movement of the droplet. Traditionally this is accomplished using a series of different electrodes. However, in bidirectional electrowetting the diode properties of some electrode/electrolyte systems are used to create a nonuniform voltage drop that is voltage polarity dependent. as shown in Figure 2-7.

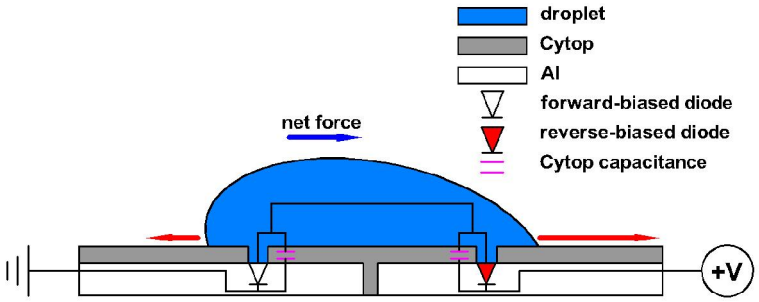

Figure 2-7. Bidirectional electrowetting on patterned Al wafer.

In bidirectional electrowetting, a droplet is placed on two aluminum electrodes, which are electrically isolated. Upon applying a voltage between the electrodes, the diode like behavior of aluminum causes potential difference between the aluminum sides. Here the aluminum electrode with higher electrical potential is the reverse biased diode with a large voltage change because of its high resistance to charge transfer. On the grounded side, the aluminum diode gets forward biased, and hence the voltage change from electrode to droplet is insignificant. The potential difference between the aluminum sides results in droplet actuation. Droplet actuation is changed by changing the polarity of the electrode voltages.

In bidirectional electrowetting, aluminum has to be in contact with the electrolyte solution to act like a diode. By applying a scratch in Cytop or applying very thin Cytop (~50 nm), aluminum diodes are created. Thin spin-coated Cytop is inherently porous, so electrochemical diodes would take action at the pores without scratch application [44].

2.2.2.5. Continuous Electrowetting (CEW)

In bidirectional electrowetting, the lateral movement of the droplet occurs on two separate plates below the droplet. CEW integrates this effect on a resister to create a continuous voltage gradient along the substrate with just one electrode pair [45]. In CEW the diode like behavior of the metallic spots causes an asymmetric potential distribution analogous to bidirectional electrowetting, so that the potential at the reverse biased spot is higher than the forward biased spot. Therefore, the contact angle modulation at the spot with higher potential would be more than that at the other spot and the droplet moves towards the spot with higher potential. With a sequence of metallic spots a droplet can be moved continuously on the substrate as shown schematically in Figure 2-8. This simplifies motion control by eliminating the need for numerous electrodes. This is particularly advantageous for 2D motion. In our work, CEW will be used to move objects which can be used for a microassembly/microactuation.

2.2.1. Materials Issues

As discussed before, in electrowetting, an electric potential difference is applied between a droplet and a substrate to modulate the droplet contact angle. The main components of the electrowetting experiments are the substrate (a stack of conductive layer, dielectric layer, and hydrophobic layer), the droplet electrolyte solution, and an auxiliary electrode.

The auxiliary electrode can be in the form of a piece of rod or a plate in the conventional electrowetting, a narrow line in the *grounding from below* setup, and a metallic spot in the continuous electrowetting (CEW).

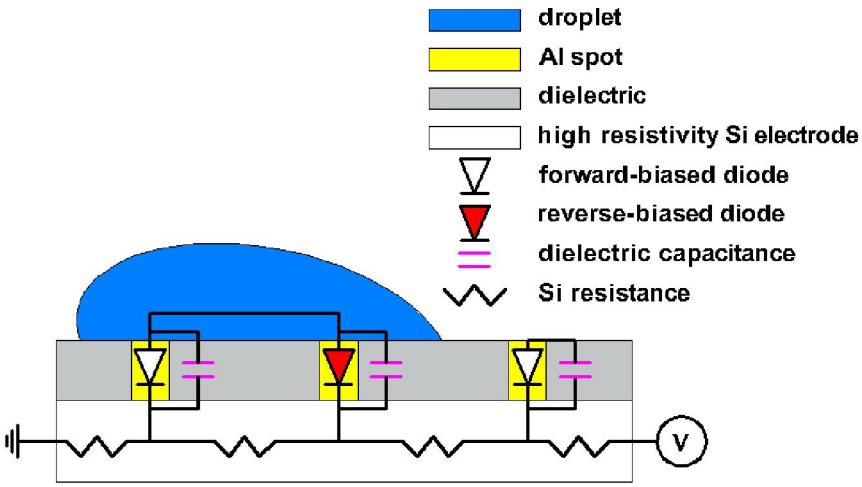

Figure 2-8. Schematic of continuous electrowetting on processed high resistivity silicon wafers.

In our experiments, we have used a piece of platinum wire as the auxiliary electrode in the conventional test method. Platinum is a noble metal and also shows low resistance against electrochemical reactions [46-47], so the voltage drop on the auxiliary electrode is minimized, which is desired. In CEW, a droplet has to touch two metallic spots and none of the spots should be considered as the auxiliary electrode. The reason is that depending on the applied voltage polarity, significant contact modulation can occur on either metallic spot.

The droplet consists of a solvent (e.g. water) and electrolytes. Upon electric field application, the electrolytes diffuse through the dielectric layer [44], which results in electrochemical reactions on the conductive layer [48-49]. The dielectric failure is highly dependent on the electrolyte size. It has been shown for bigger electrolytes the dielectric failure occurs at higher voltages [44].

The dielectric failure is determined by the onset of current impulses, which are the sign of electrochemical reactions [44]. If cathodic reactions occur on the conductive layer, extensive electrochemical reactions occur, which appear as bubbles [48]. However, upon anodic reactions, aluminum etches away. Figure 2-9 shows a case of aluminum etching in conventional and bidirectional electrowetting.

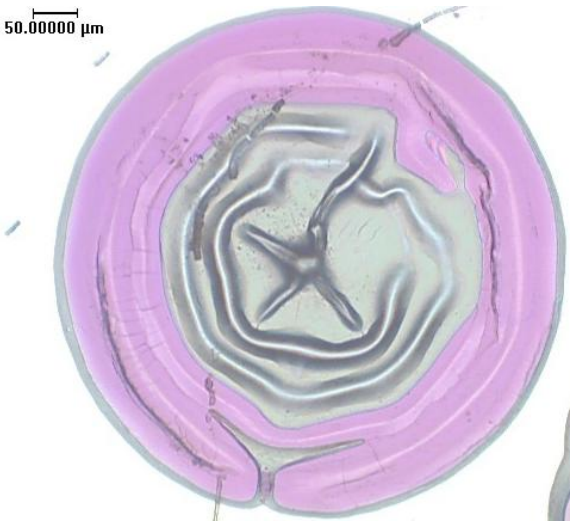

Figure 2-9. Aluminum etching upon anodic polarization of an electrowetting wafer. The conductive layer is aluminum and the electrolyte solution 0.1 M NaCl. The purple side shows SiO_2 after aluminum etching. The wrinkled appearance is due to delamination of the Cytop coating, probably due to gas generation during aluminum etching.

Our concern is the metallic spots reliability in CEW, so the incorporated metal/electrolyte system has to show both reliability and diode-like behavior. EWOD with either non-oxidizing metals (like gold) or barium strontium titanate and SiO_2 dielectrics [50] show resistance against oxidation, yet they do not act like diodes. On non-oxidizing metals, fast cathodic and anodic electrochemical reactions occur and hence the substrate acts more like a conductive element in EWOD circuit with poor diode like behavior. On the other hand, barium strontium titanate and SiO_2 dielectrics prevents electrochemical reactions in both cathodic and anodic polarizations of the substrate [50], which also minimizes diode like behavior due to the high electrochemical reactions resistance in both potential polarities, and so they are inappropriate for CEW [45]. We will introduce a system that can act like diodes and also perform a reliable EWOD process.

2.3. Electrochemistry

The knowledge of the electrochemical reactions in EWOD is important because it helps us steer the electrochemical reactions towards favorable conditions. Electrowetting requires the use of electrolytes in the presence of an electrode and an electric potential, all the conditions required

for electrochemical reactions. Traditionally, the focus has been on eliminating or at least minimizing these reactions by using such strong oxide layers as silicon dioxide or barium strontium titanate [50]. Silicon dioxide and barium strontium titanate have been employed by researchers in different electrowetting applications such as lab on chip [50], microgripper [51], electrowetting displays [52], and lab on chip [42]. However, this project looks at the electrochemical reactions that can improve CEW performance by providing high potential difference between electrodes with opposite polarizations. This is possible when the conductive metal (in contact with electrolytes) is acting like a diode. Here, metals that act like diodes in contact with electrolytes are referred to as electrochemical diodes [45].

The underpinning mechanism of the diode like behavior is the variation of the metal resistance against electrochemical reactions at different polarities [53]. In CEW, the diode like behavior of the metallic spots provides the electric potential difference between the spots, required for the asymmetric contact angel modulation of the droplet and the subsequent continuous droplet movement. Electrochemical diodes show high and low resistance against electrochemical reactions respectively at anodic and cathodic polarity. Hence, in CEW, the droplet moves towards the side with higher voltage [45].

2.3.1. Basic Reactions

Before explaining the aluminum oxidation processes, anodic and cathodic reactions are briefly explained. The most common example of electrochemical reactions is what occur during metals corrosion. In this process, when a metal surface is exposed to a medium with electrolytes, different parts of the metal take different electrochemical potentials due the heterogeneity of the surface. The variation of the electrochemical potentials causes electrochemical reactions, which consist of cathodic and anodic reactions. On the cathode, cationic electrolytes (e.g. protons, H_3O^+) are reduced by taking electrons on cathode through charge transfer. On the anode,

however, the metal cations are removed from the metal structure, which leaves behind electrons [54]. If we consider two parts of the metal surface as two separate metal sheets with different electrochemical potentials, then the corrosion process can be simplified as a galvanic cell as shown in Figure 2-10.

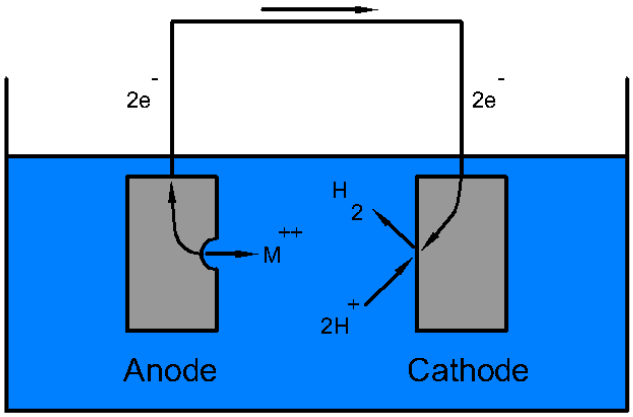

Figure 2-10. Basic electrochemical reactions in a galvanic cell [adapted from 54].

The galvanic cell shown in Figure 2-10 illustrates the basic components required for electrochemical reactions. In corrosion process, the intrinsic electrochemical potential difference over a metal surface is the moving force, yet an external power source can also induce electrochemical reactions between two conductive electrodes. In electrowetting, electrochemical reactions could also happen via the external potential difference which is applied to modulate the droplet. When a potential difference is applied between a droplet and an electrowetting substrate, electrolytes first diffuse through the dielectric layer until they reach the conductive layer [44]. Then, electrochemical reactions occur on the conductive layer. Anodic and cathodic reactions occur respectively at positive and negative polarities of the substrate [48].

The anodic reactions can be prevented in passivating systems, while cathodic reactions cannot. In the next section, the basic anodic reactions on aluminum (which is mostly used in this study) are explained.

2.3.2. Basic Aluminum Electrochemistry

In most experiments, we have used aluminum electrodes. In continuous electrowetting, the metallic spots were originally aluminum and the reliable electrowetting system is based on aluminum oxidation in certain electrolyte solutions. Hence, general electrochemical reactions on aluminum are explained in this section. In contact with pure water, aluminum oxidizes via the following reaction:

$$2Al^{3+} + 9H_2O = Al_2O_3 + 6H_3O^+ \quad (2.13)$$

with a free energy of -864.6 Kj/mol this reaction occurs spontaneously. Aluminum oxide (alumina) is formed concurrently with protons formation. Hence, once either alumina covers all the sites for proton formation or the oxide layer porosity becomes tight, the oxidation process ceases. As a result, two interfaces of Al/Al_2O_3 and Al_2O_3/electrolyte solution are created. If aluminum is polarized anodically, oxidation and hydrogen evolution continue at the interfaces via the following reactions [55]:

$$2Al \rightarrow Al^+ + Al^{3+} + 4e^- \quad (2.14)$$

$$Al^+ + 2H_3O^+ \rightarrow Al^{3+} + H_2 + 2H_2O \quad (2.15)$$

$$Al^+ + 2H_2O \rightarrow Al^{3+} + H_2 + 2OH^- \quad (2.16)$$

$$2Al^{3+} + 9H_2O \rightarrow Al_2O_3 + 6H_3O^+ \quad (2.17)$$

In EWOD, Cytop gets damaged upon electric field application, and then water reaches the aluminum layer. If the substrate is anodically polarized, alumina is formed and after repeated electrowetting processes the aluminum layer could etch away, which results in the electrowetting failure [48-49]. If the substrate is cathodically polarized, then fast cathodic reactions occur on the aluminum surface, which also results in EWOD failure [48].

If electrochemical reactions are prevented, reliable EWOD is feasible [48]. In section 2.3.2. , we explain how it is possible to prevent electrochemical reactions in some specific

electrode/electrolyte systems called *passivating systems* [48]. First, porous and barrier like alumina layers are introduced.

2.3.3. Incorporation of Anions in Aluminum Oxidation

Aluminum oxidation results in either a porous or barrier alumina layer formation, depending on the available electrolytes. The porous alumina is formed due to the anion incorporation (up to 17 wt%) in the alumina layer adjacent to the electrolytes [56]. Aluminum oxidation with such electrolytes as sulfuric acid, oxalic acid, phosphoric acid, chromic acid, and etc. results in porous alumina formation [57]. However, in the barrier like alumina layers the anions incorporation is insignificant (around 1 wt%) [58].

2.3.4. Porous Alumina

Porous alumina consists of a barrier layer at the aluminum/alumina interface and a porous layer on top. The porous layer thickness depends on the electrolytes contribution in the oxidation process. However, the barrier layer thickness varies by the electric field strength (the ratio of voltage drop through the barrier layer over its thickness) and the ions diffusivity. In fact, the electric field aids the ions diffusion, which decreases upon the oxide thickening. In practice, the oxide (at a voltage) gets stable once it reaches a certain thickness. The barrier layer thickness is commonly represented by the *anodizing ratio*, which is a ratio of thickness over the applied voltage. Anodizing ratio varies with electrolytes [55, 57]. Table 2-1 shows the alumina thicknesses formed with some common electrolytes.

2.3.1. Barrier like Alumina

In contact with some specific electrolytes such as tartaric acid and citric acid, aluminum forms barrier like alumina without the porous layer [59]. It has been shown that the electrolytes constitute insignificant part of the barrier like alumina layers (around 1 wt%) [57]. Current conduction and ion transport occurs with high resistance through the barrier like alumina. For

barrier like alumina, anodizing ratios between 13 and 13.7 AV^{-1} has been reported in [55]. It is noteworthy that alumina properties can be influenced by the aluminum surface roughness before oxidation [60-62].

Table 2-1. Anodizing ratio of barrier layer of alumina with some common electrolytes [55].

Electrolyte Concentration	Anodizing Ratio ($ÅV^{-1}$)
15% Sulfuric Acid	10.0
2% Oxalic Acid	11.8
4% Phosphoric Acid	11.9
3% Chromic Acid	12.5

2.3.2. Passivating Systems in EWOD

Dielectric failure due to the electrolytes diffusion and the subsequent conductive layer oxidation and etching make reliable EWOD a challenge. As mentioned before, one way to avoid the dielectric failure is to use a dielectric layer that can withstand intense electrical fields. It has been shown that such strong dielectric layer as barium strontium titanate and SiO_2 dielectrics can provide reliable electrowetting at both potential polarities of the substrate [50]. These dielectric layers can be used for manufacturing reliable electrowetting devices. However, in our study the diode behavior of the substrate is required, which is eliminated by barium strontium titanate and SiO_2 dielectrics. Another way to improve EWOD reliability is to use thick dielectric layers [63] at the expense of low voltage EWOD. However, high actuation voltages are not desirable for portable devices; in addition, thick dielectrics prevent the electrolytes diffusion which is required for the electrode diode behavior, and hence they also eliminate the electrodes diode behavior. In

another study [64], it has been also shown that parylene dielectric layers in combination with surfactant electrolytes can be used for low voltage EWOD.

Alternatively, we have used aluminum combined with tartaric acid and citric acid at anodic polarities of the wafers to perform low voltage reliable EWOD. This way, the barrier like nature of the alumina prevents the aluminum etching, and hence EWOD continues without any damages to the wafers. The electrode (with barrier like oxide)/electrolyte combinations are referred to as *passivating systems*. It is noteworthy that systems with porous alumina layers could also yield reliable EWOD, as they also show resistance against etching. However, as in reliable EWOD only the barrier layer is used, so in our experiments we have used only barrier like alumina layers. It should be mentioned that barrier property is not peculiar to alumina, as some other metal oxides such as tantalum, titanium, and bismuth can also form barrier oxide layers [65].

The passivating systems show diode behavior. An I-V curve of aluminum wafers in passivating systems is shown in Figure 2-11 which illustrates the diode behavior of an aluminum wafer. Similar to non-passivating systems, the EWOD substrates here also become reverse and forward biased respectively upon anodic and cathodic polarization. Hence, their performance in the CEW devices is evaluated and compared with those of the non-passivating systems.

In the next chapters, the experimental results of droplet actuation over many cycles in passivating and non-passivating systems are presented. It will be shown that, in passivating systems, EWOD is reliable, while in non-passivating systems EWOD fails after a few cycles. Passivating systems can be also used to perform low voltage electrowetting on thin Cytop layers. However, for CEW devices passivating systems are not recommended, as droplet actuation is less than what is observed in non-passivating systems—the degradation in the droplet actuation in the passivating systems is attributed to the barrier like oxide layer, which impedes the cathodic

reactions as well as the anodic reactions. The passivating systems performance in CEW is also evaluated and the results are presented in chapter 6.

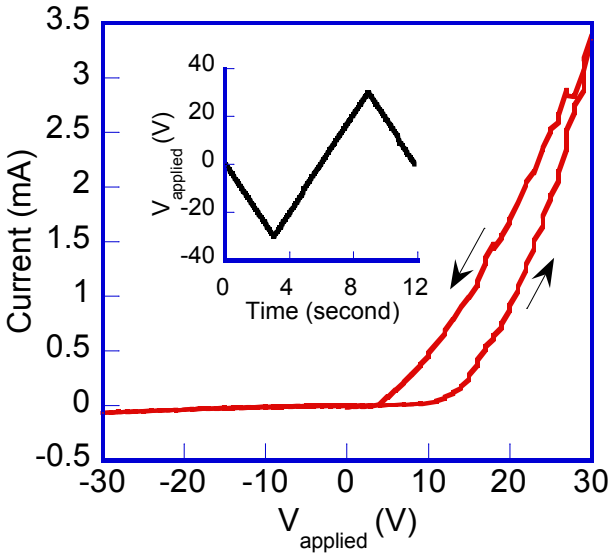

Figure 2-11. I-V curve obtained in a passivating system of aluminum and 0.1 M citric acid. In this test a 16 µl droplet was placed on an aluminum wafer with 60 nm Cytop. Then the wafer was grounded and a triangle voltage was applied over 12 seconds as shown in the inset.

2.4. References

[1] K. G. Hans-Jürgen Butt, Michael Kappl, *Physics and Chemistry of Interfaces*: John Wiley & Sons, 2003.

[2] J. B. Hudson, *Surface Science: An Introduction*: John Wiley & Sons, 1998.

[3] S. W. Rienstra, "The shape of a sessile drop for small and large surface tension," *Journal of Engineering Mathematics,* vol. 24, pp. 193-202, 1990/08/01 1990.

[4] C. Cooney, *et al.*, "Electrowetting droplet microfluidics on a single planar surface," *Microfluidics and Nanofluidics,* vol. 2, pp. 435-446 LA - English, 2006.

[5] V. A. Lubarda and K. A. Talke, "Analysis of the Equilibrium Droplet Shape Based on an Ellipsoidal Droplet Model," *Langmuir,* vol. 27, pp. 10705-10713, 2011/09/06 2011.

[6] A. W. Adamson, *Physical Chemistry of Surfaces*, 5th ed.: New York: Wiley, 1990.

[7] J. A. M. Sondag-Huethorst and L. G. J. Fokkink, "Potential-Dependent Wetting of Electroactive Ferrocene-Terminated Alkanethiolate Monolayers on Gold," *Langmuir,* vol. 10, pp. 4380-4387, 1994/11/01 1994.

[8] W. J. J. Welters and L. G. J. Fokkink, "Fast Electrically Switchable Capillary Effects," *Langmuir,* vol. 14, pp. 1535-1538, 1998/03/01 1998.

[9] R. Olivier, *et al.*, "On the influence of surfactants in electrowetting systems," *Journal of Micromechanics and Microengineering,* vol. 17, p. 2217, 2007.

[10] A. Quinn, *et al.*, "Contact Angle Saturation in Electrowetting," *The Journal of Physical Chemistry B,* vol. 109, pp. 6268-6275, 2005/04/01 2005.

[11] A. G. Papathanasiou, *et al.*, "Illuminating the connection between contact angle saturation and dielectric breakdown in electrowetting through leakage current measurements," *Journal of Applied Physics,* vol. 103, pp. 034901-4, 2008.

[12] H. H. Woodson and J. R. Melcher, *Electromechanical dynamics, part I: Discrete systems*: Wiley: New York, 1968.

[13] C. E. Rosenkilde, "A Dielectric Fluid Drop an Electric Field," *Proceedings of the Royal Society of London. A. Mathematical and Physical Sciences,* vol. 312, pp. 473-494, 1969.

[14] T. B. Jones, *et al.*, "Frequency-Based Relationship of Electrowetting and Dielectrophoretic Liquid Microactuation," *Langmuir,* vol. 19, pp. 7646-7651, 2003/09/01 2003.

[15] K. H. Kang, "How electrostatic fields change contact angle in electrowetting," *Langmuir,* vol. 18, pp. 10318-10318, 2002.

[16] J. Buehrle, *et al.*, "Interface profiles near three-phase contact lines in electric fields," *Phys. Rev. Lett.,* vol. 91, pp. 86101-86101, 2003.

[17] F. Mugele and J. Buehrle, "Equilibrium drop surface profiles in electric fields," *Journal of Physics: Condensed Matter,* vol. 19, pp. 375112-375112, 2007.

[18] K. Joonho, *et al.*, "Recent thermal management techniques for microprocessors," *ACM Comput. Surv. %@ 0360-0300,* vol. 44, pp. 1-42, 2012.

[19] V. Singhal, *et al.*, "Microscale pumping technologies for microchannel cooling systems," *Applied Mechanics Reviews,* vol. 57, pp. 191-221, 2004.

[20] J. T. Cheng and C. L. Chen, "Adaptive Chip Cooling Using Electrowetting on Coplanar Control Electrodes," *Nanoscale and Microscale Thermophysical Engineering,* vol. 14, pp. 63-74, 2010/04/30 2010.

[21] C. Knospe and S. Nezamoddini, "Capillary force actuation," *Journal of Micro-Nano Mechatronics,* vol. 5, pp. 57-68, 2009/12/01 2009.

[22] B. Berge and J. Peseux, "Variable focal lens controlled by an external voltage: An application of electrowetting," *The European Physical Journal E,* vol. 3, pp. 159-163, 2000/10/01 2000.

[23] F. Mugele and J.-C. Baret, "Electrowetting: from basics to applications," *Journal of Physics: Condensed Matter,* vol. 17, pp. R705-R774, 2005.

[24] B. H. W. Hendriks, *et al.*, "Electrowetting-Based Variable-Focus Lens for Miniature Systems," *Optical Review,* vol. 12, pp. 255-259 LA - English, 2005.

[25] S. Millefiorini, *et al.*, "Electrowetting of Ionic Liquids," *Journal of the American Chemical Society,* vol. 128, pp. 3098-3101, 2006/03/01 2006.

[26] D. R. Link, *et al.*, "Electric Control of Droplets in Microfluidic Devices," *Angewandte Chemie International Edition,* vol. 45, pp. 2556-2560, 2006.

[27] Available: http://www.varioptic.com/

[28] B. Comiskey, *et al.*, "An electrophoretic ink for all-printed reflective electronic displays," *Nature,* vol. 394, pp. 253-255, 1998.

[29] R. A. Hayes and B. J. Feenstra, "Video-speed electronic paper based on electrowetting," *Nature,* vol. 425, pp. 383-385, 2003.

[30] R. Shamai, *et al.*, "Water, electricity, and between... On electrowetting and its applications," *Soft Matter,* vol. 4, pp. 38-45, 2008.

[31] T. Krupenkin and J. A. Taylor, "Reverse electrowetting as a new approach to high-power energy harvesting," *Nature communications,* vol. 2, pp. 448-448, 2011.

[32] T. Vilkner, *et al.*, "Micro Total Analysis Systems. Recent Developments," *Analytical Chemistry,* vol. 76, pp. 3373-3386, 2004/06/01 2004.

[33] M. Abdelgawad and A. R. Wheeler, "Rapid Prototyping in Copper Substrates for Digital Microfluidics," *Advanced Materials,* vol. 19, pp. 133-137, 2007.

[34] C. Cooney, *et al.*, "Electrowetting droplet microfluidics on a single planar surface," *Microfluidics and Nanofluidics,* vol. 2, pp. 435-446, 2006/09/01 2006.

[35] M. W. L. Watson, *et al.*, "Microcontact Printing-Based Fabrication of Digital Microfluidic Devices," *Analytical Chemistry,* vol. 78, pp. 7877-7885, 2006/11/01 2006.

[36] K. P. Nichols and J. G. E. Gardeniers, "A Digital Microfluidic System for the Investigation of Pre-Steady-State Enzyme Kinetics Using Rapid Quenching with MALDI-TOF Mass Spectrometry," *Analytical Chemistry,* vol. 79, pp. 8699-8704, 2007/11/01 2007.

[37] E. M. Miller and A. R. Wheeler, "A Digital Microfluidic Approach to Homogeneous Enzyme Assays," *Analytical Chemistry,* vol. 80, pp. 1614-1619, 2008/03/01 2008.

[38] P. Paik, *et al.*, "Rapid droplet mixers for digital microfluidic systems," *Lab on a chip,* vol. 3, pp. 253-259, 2003.

[39] E. Miller and A. Wheeler, "Digital bioanalysis," *Analytical and Bioanalytical Chemistry,* vol. 393, pp. 419-426, 2009/01/01 2009.

[40] V. K. Pamula, *et al.*, "A droplet-based lab-on-a-chip for colorimetric detection of nitroaromatic explosives," in *Micro Electro Mechanical Systems, 2005. MEMS 2005. 18th IEEE International Conference on*, 2005, pp. 722-725.

[41] Y. Fouillet, *et al.*, "Digital microfluidic design and optimization of classic and new fluidic functions for lab on a chip systems," *Microfluidics and Nanofluidics,* vol. 4, pp. 159-165, 2008/03/01 2008.

[42] U. Lehmann, *et al.*, "Droplet-Based DNA Purification in a Magnetic Lab-on-a-Chip," *Angewandte Chemie International Edition,* vol. 45, pp. 3062-3067, 2006.

[43] C. Sung Kwon, *et al.*, "Creating, transporting, cutting, and merging liquid droplets by electrowetting-based actuation for digital microfluidic circuits," *Microelectromechanical Systems, Journal of,* vol. 12, pp. 70-80, 2003.

[44] P. Y. Chiou, *et al.*, "Light actuation of liquid by optoelectrowetting," *Sensors and Actuators A: Physical,* vol. 104, pp. 222-228, 2003.

[45] B. Raj, *et al.*, "Ion and liquid dependent dielectric failure in electrowetting systems," *Langmuir : the ACS journal of surfaces and colloids,* vol. 25, pp. 12387-92, 2009.

[46] C. W. Nelson, *et al.*, "Continuous electrowetting via electrochemical diodes," *Lab on a chip,* vol. 11, pp. 2149-2152, 2011.

[47] F. Kadirgan, *et al.*, "Electrocatalytic oxidation of ethylene-glycol: Part II. Behaviour of platinum-ad-atom electrodes in alkaline medium," *Journal of Electroanalytical Chemistry and Interfacial Electrochemistry,* vol. 143, pp. 135-152, 1983.

[48] H. Möller and P. C. Pistorius, "The electrochemistry of gold–platinum alloys," *Journal of Electroanalytical Chemistry,* vol. 570, pp. 243-255, 2004.

[49] M. Khodayari, *et al.*, "A material system for reliable low voltage anodic electrowetting," *Materials Letters,* vol. 69, pp. 96-99, 2012.

[50] M. Dhindsa, *et al.*, "Electrowetting without Electrolysis on Self-Healing Dielectrics," *Langmuir,* vol. 27, pp. 5665-5670, 2011/05/03 2011.

[51] H. Moon, *et al.*, "Low voltage electrowetting-on-dielectric," *Journal of Applied Physics,* vol. 92, pp. 4080-4087, 2002.

[52] A. Vasudev and J. Zhe, "A low voltage capillary microgripper using electrowetting," in *Solid-State Sensors, Actuators and Microsystems Conference, 2009. TRANSDUCERS 2009. International*, 2009, pp. 825-828.

[53] K.-T. Chen, *et al.*, "METHOD FOR FABRICATING ELECTROWETTING DISPLAYS," 2010.

[54] B. M. Grafov, "On the theory of the electrochemical diode," *Bulletin of the Academy of Sciences of the USSR, Division of chemical science,* vol. 13, pp. 763-769, 1964/05/01 1964.

[55] J. W. Diggle*, et al.*, "Anodic oxide films on aluminum," *Chemical Reviews,* vol. 69, pp. 365-405, 1969/06/01 1969.

[56] R. B. Mason, "Factors Affecting the Formation of Anodic Oxide Coatings in Sulfuric Acid Electrolytes," *Journal of The Electrochemical Society,* vol. 102, pp. 671-675, 1955.

[57] F. Keller*, et al.*, "STRUCTURAL FEATURES OF OXIDE COATINGS ON ALUMINIUM," *Journal of The Electrochemical Society,* vol. 100, pp. 411-419, 1953.

[58] W. J. Bernard and J. J. Randall, "An Investigation of the Reaction between Aluminum and Water," *Journal of The Electrochemical Society,* vol. 107, pp. 483-487, 1960.

[59] G. D. Sulka and A. Eftekhari, Nanostructured Materials in Electrochemistry, 2008.

[60] J. M. Montero-Moreno*, et al.*, "Influence of the aluminum surface on the final results of a two-step anodizing," *Surface and Coatings Technology,* vol. 201, pp. 6352-6357, 2007.

[61] P. Bocchetta*, et al.*, "Influence of initial treatments of aluminium on the morphological features of electrochemically formed alumina membranes," *Materials Science and Engineering: C,* vol. 23, pp. 1021-1026, 2003.

[62] M. T. Wu*, et al.*, "Effect of polishing pretreatment on the fabrication of ordered nanopore arrays on aluminum foils by anodization," *Journal of Vacuum Science & Technology B: Microelectronics and Nanometer Structures,* vol. 20, pp. 776-782, 2002.

[63] H. Liu*, et al.*, "Dielectric materials for electrowetting-on-dielectric actuation," *Microsystem Technologies,* vol. 16, pp. 449-460, 2010/03/01 2010.

[64] M. Dhindsa*, et al.*, "Reliable and low-voltage electrowetting on thin parylene films," *Thin Solid Films,* vol. 519, pp. 3346-3351, 2011.

[65] M. M. Lohrengel, "Thin anodic oxide layers on aluminium and other valve metals: high field regime," *Materials Science and Engineering: R: Reports,* vol. 11, pp. 243-294, 1993.

CHAPTER 3: EXPERIMENTS

There are two goals in this project. First goal is to improve the reliability of the metallic spots and the silicon dioxide to fabricate reliable continuous electrowetting (CEW) devices. Second goal is to improve the droplet actuation force.

Metallic spots act as the electrochemical diodes and are inlaid to SiO_2 layer, which are connected to the silicon layer below SiO_2. A thin Cytop layer is coated on the substrate, which renders the surface hydrophobic. The thin layer of Cytop is porous, permitting the electrolytes diffusion and subsequent electrochemical reactions on the metallic spots. Therefore, the diode like behavior of the metallic spots—which requires variation of electrochemical reactions rates at different electric potential polarities—is observed. The metallic spots have to be stable over many EWOD cycles to ensure the CEW device reliability. In part of this chapter, it is explained how the EWOD reliability is evaluated.

Additionally, the droplet will cover the metallic spots, but (because of the small size of the metallic spots) electrowetting mostly occurs on the SiO_2 regions. Hence, the reliability of the SiO_2 dielectric is an important parameter too. The same tests (as used for metallic spots reliability evaluation) are used to investigate the SiO_2 reliability over many cycles.

The improvement of the droplet actuation force is the second objective of this study. To evaluate the droplet actuation force, the electric potential of the metallic spots are measured and with a proposed model is related to the actuation force. The measurement of the metallic spots voltage is performed using a test setup with two separate metallic electrodes, which is referred to as electrode pair measurement. The schematic of this measurement is shown in Figure 3-1.

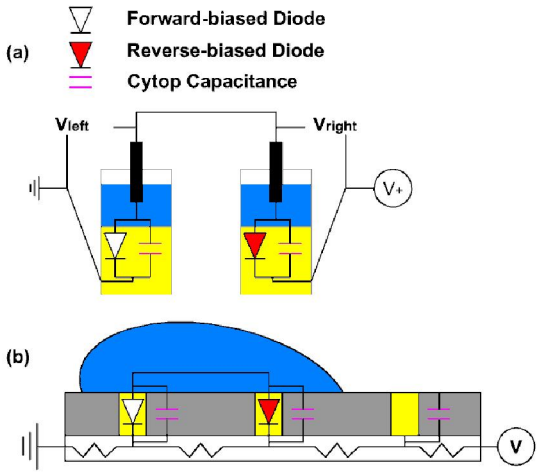

Figure 3-1. A comparison between the test setup circuit and Continuous Electrowetting circuit. (a)Schematic of the diodes and capacitors in the test setup constituting of the hypothetical circuit in CEW (the diodes and capacitors respectively indicate electrochemical diodes and Cytop), (b) schematic of Continuous Electrowetting with the underlying circuit.

With the aid of electrostatic force equation on the droplet perimeter, it is shown that the actuation force is given by:

$$\vec{F} = \frac{\varepsilon.\pi.r}{4d}.V_{\max}(V_{\max} - 2V_{drop}) \tag{3.1}$$

here, F is the total lateral force on the droplet, which has the dimension of Newton. In equation 3.1, the variables are defined as follows:

ε: dielectric permittivity

r: droplet radius

d: dielectric thickness

V_{max}: substrate voltage at the reverse biased spot

V_{drop}: droplet voltage which is equal with V_{left}

The V_{max} is equal with the applied voltage, V_{drop} is the droplet voltage and can be measured directly (Figure 3-1a), and ε, r, and d are known. Hence, theoretical lateral force can be calculated using equation 3.1. In this study, we are looking for electrolyte/electrode combinations where the metallic spots act like ideal theoretical diodes (V > 0 → R = infinity, V

< 0→ R = 0). In this case, V_{drop} would be either zero or V_{max} respectively when V_{max} is positive and negative, so:

$$\vec{F} = \pm \frac{\varepsilon.\pi.r}{4d}.V_{\max}^2 \tag{3.2}$$

A criteria that shows the actuation effectiveness of electrode/electrolyte combinations is obtained by dividing equation 3.1 by equation 3.2 as follows:

$$\eta_{actuation} = \left| \frac{\frac{\varepsilon.\pi.r}{4d}.V_{\max}(V_{\max} - 2V_{drop})}{\frac{\varepsilon.\pi.r}{4d}.V_{\max}^2} \right| = \left| 1 - 2\frac{V_{drop}}{V_{\max}} \right| \tag{3.3}$$

The $\eta_{actuation}$ is the coefficient of actuation and varies between zero and one. The goal of these measurements is to find electrode/electrolyte combinations with $\eta_{actuation}$ close to one. Due to the high resistance of the wafer on the CEW substrates, it is not possible to directly measure the metallic spots electric potential, so an electrode pair test setup is designed to directly measure the metallic spots electric potential. In this chapter, the designed test setup is explained.

3.1. Dielectric Characterization

Dielectric materials resist the movement of charges within the dielectric body. When they are placed in an electric field, the charges are oriented in the material. Positive charges are accumulated towards the negative side of the electric field and vice versa. Dielectric loss in such materials is associated with the permanent charges orientation, which is insignificant in low-loss dielectrics. The dielectric material withstand the electric fields up to a level that defines the dielectric strength. After dielectric breakdown, the dielectric material cannot hold charges and conduction occurs.

In electrochemical media, upon application of excessive voltage, the dielectric breakdown might occur similar to that in dry conditions. Yet, this is not the mechanism associated with the

EWOD dielectric failure. Typically, the EWOD dielectric failure happens below the dielectric breakdown voltage [1], due to electrolytes diffusion through the dielectric layer and subsequent electrochemical reactions on top of the conductive layer. Electrochemical reactions aggravate the dielectric damage, which ultimately result in EWOD failure. In EWOD, the existence of electrolytes in conjunction with high electric fields create electrochemical harsh conditions that need to be addressed to obtain reliable systems.

3.1.1. Resonant Methods

Resonant methods are highly accurate methods for low-loss dielectrics, which works at microwave frequencies [2]. Typically, in this method relaxation time of a dielectric is obtained over a frequency range, and then a model (i.e. Cole-Cole, Davidson-Cole, or Gavril'yak-Negami function [3]) is fitted on the results. The model parameters could reveal such information as dipole alignment and molecular interaction in the dielectric [4]. There are fundamental studies on the resonant methods and they have been used to characterize dielectric materials. Yet understanding the dielectrics behavior in molecular scale is beyond the scope of this study. In this study, the characterization of macroscopic dielectric damages and their effects on EWOD are desired, so resonant methods are not appropriate. Resonant methods have not been used in this study.

3.1.2. Electrochemical Impedance Spectroscopy

Another method for dielectric characterization is the electrochemical impedance spectroscopy (EIS) [5]. In this method, the electrochemical potential of a substrate is oscillated around the substrate equilibrium potential and the current response is collected at various frequencies. The response of the system depends on the electrical characteristics of the system. To analyze the experimental results, a circuit model is assumed and fitted on the experimental results, and then the circuit parameters are used to understand such properties as the dielectric

constant [6]. It can also be used to observe the dielectric damage [7] upon electric field application, as it is in this study. The advantage of this method is that it is a well-known method for electrochemical systems characterization, which is the case of electrowetting systems. However, it is usually limited to small voltage changes while EW is conducted with much larger voltages.

3.1.3. Contact Angle versus Voltage

In EWOD, the direct method to evaluate dielectric condition is to measure contact angle with respect to voltage. The voltage is related to the droplet contact angle via Lippman equation as follows [8]:

$$cos\theta = cos\theta_0 + \frac{\varepsilon}{2\delta\sigma_{la}}V^2 \tag{3.4}$$

here, θ_0 and θ are the initial droplet angle and actuated droplet angle, V is the applied voltage, σ_{la} is the surface tension between the second phase and the droplet, δ is the dielectric thickness, and ε the dielectric permittivity. In this equation, all parameters are know, so θ can be predicted. Dielectric failure affects the contact angle modulation, so deviations from Lippman equation can be related to changes in the dielectric layer.

3.1.4. I-V Measurements

In CEW, the diode like behavior of the metallic spots is critical because it determines the difference in voltage between the droplet and electrode on the leading and trailing edges of the droplet. These in turn determine the droplet actuation force. A common method to characterize semiconductor diodes is I-V measurements. In this test, the voltage of a diode is ramped up with respect to ground and the current is measured concurrently. It is more appropriate to ramp the voltage instead of current, as even small magnitudes of current could result in the breakdown of a reverse biased diode. A diode demonstrates a characteristic I-V curve as shown in Figure 3-2.

A perfect diode prevents the current flow when reverse biased and passes the current when forward biased. However, a reverse biased diode can fail to prevent the current passage at a certain voltage called breakdown voltage as shown in Figure 3-2.

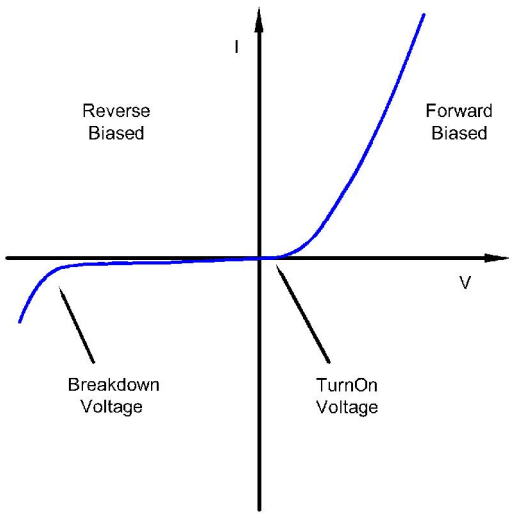

Figure 3-2. I-V characteristics of a perfect diode.

Oxidizing metals show similar I-V characteristics [9]. Here, we also use I-V curves to observe diode like behaviors. In addition, a part of our study is on the EWOD saturation phenomenon investigation. I-V measurement is also used to observe any electrical signs of saturation phenomenon. Hysteresis in the I-V measurements and changes in the patterns indicate degradation of the metallic layers.

3.2. Experiments Setup

3.2.1. Electrochemical Impedance Tests Setup

Here, Cytop dielectric damage upon electric field application is characterized by electrochemical ac-impedance spectroscopy (EIS). A three electrode setup has been used as shown in Figure 3-3 and EIS measurements with an excitation voltage of 5 mV in a frequency range of 100 KHz to 0.04 Hz were performed. Activated titanium electrodes [10] have been used as both reference and auxiliary electrodes. 0.1 M tartaric acid is used as the electrolyte solution.

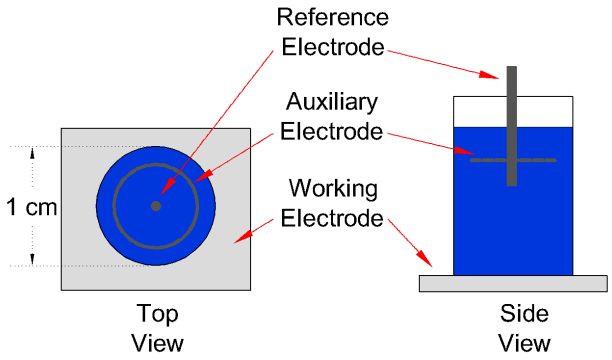

Figure 3-3. A schematic of the electrochemical impedance measurement setup. Working electrode is the electrowetting substrate, consisting of Si/SiO2(500 nm)/Al(300 nm)/Cytop(595±18 nm). The potentiostat working output is connected to the aluminum layer. Auxiliary and reference electrodes are both activated titanium [10].

Considering Cytop as a porous dielectric layer, the equivalent circuit shown in Figure 3-4 is used to model the electrowetting systems.

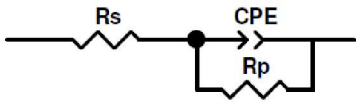

Figure 3-4. Equivalent circuit of electrowetting systems.

In this circuit, R_s, CPE and R_p are respectively solution resistance, constant phase element and charge transfer resistance. CPE is a capacitance substitute due to capacitance distribution [11]. Capacitance distribution could occur due to "*surface roughness and heterogeneities*" [12], "*electrode porosity*" [13], "*variation of coating composition"* [14], "*slow adsorption reactions*" [15], or "*Non-uniform potential and current distribution*" [16]. In our experiments, the CPE existence is attributed to the electrode porosity.

3.2.2. I-V Experimental Setup

For I-V measurements, a platinum auxiliary electrode was placed in the droplet. Then, using a Keithley 2612A SourceMeter, the potential difference between the droplet and the substrate was ramped while the substrate was grounded as shown in Figure 3-5.

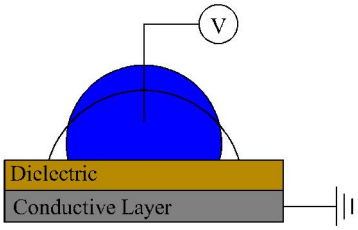

Figure 3-5. Schematic of I-V tests setup.

To do I-V tests, the voltage is ramped down and up to a certain voltage (depending on the Cytop thickness). One example of the voltage ramp is shown in Figure 3-6. In the next sections, the details of each I-V measurement are explained.

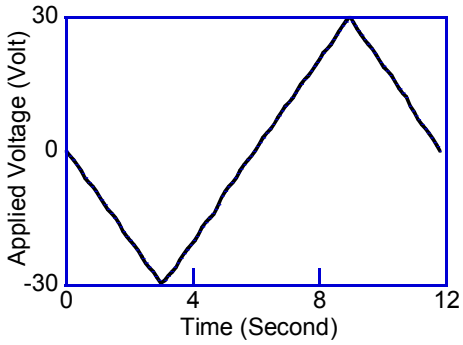

Figure 3-6. One example of voltage ramp in I-V measurements. Ramp rates and peak voltages were varied during testing.

In this measurement, the voltage magnitude influences the I-V curves because, depending on the size of the ions in the electrolyte, the dielectric failure occurs at various voltages (the dielectric failure appears as a current increase in the I-V curves) [1]. Since the contact angle modulation ceases at saturation voltage, in our experiments we have applied a voltage above saturation voltage. This way all the reactions which can affect the droplet modulation are observed and interpreted in the I-V curves.

In addition, the voltage ramp rate can affect the I-V curves due to the capacitive time constant or due to the cumulative effects of increased current through the system. At high frequencies, the measurement time could be less than the system time constant. Therefore, the

dielectric breakdown might not occur. We have used a frequency between 0.1 to 1 Hz, which in our electrowetting systems proved low enough for us to collect the dielectric failure information.

During I-V measurement, the droplet contact angle and droplet/substrate area change. During droplet tests, the dielectric affects are coupled with droplet/substrate area change—introduces undesirable variations in I-V curves. This area change was eliminated by confining the droplet liquid in a tube as shown in Figure 3-7 when contact angles were not required.

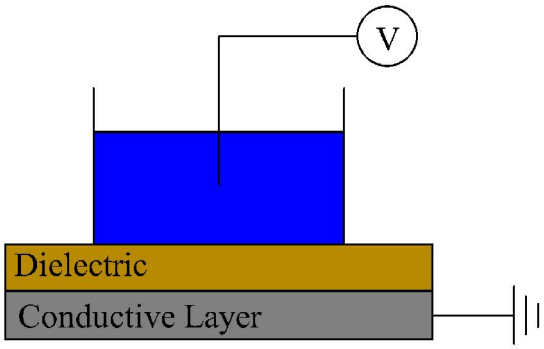

Figure 3-7. Schematic of I-V tests setup with tube.

3.2.3. Contact Angle Measurement Methods

A method of measuring surface energy is the Wilhelmy method [17]. In this method, half of a thin plate is vertically immersed in a liquid and then the force on the plate is measured. The measured force consists of the plate weight plus the force caused by the liquid surface tension minus the upward force due to the buoyant effect of the liquid which is displaced. The contact angle can be obtained as follows:

$$cos\theta = \frac{(w_i - w_a + a.b.h.\rho)g}{2\gamma_{la}(a+b)} \tag{3.5}$$

here, a, b, h, g, and γ_{la} are respectively the plate width, the plate thickness, immersion depth, the gravitational acceleration, and liquid/air (the second phase) surface tension [17]. This

measurement is fast and requires basic laboratory components. The limiting factor in this method is that an EW plate would have to be multilayered. This method would require the same multilayer structure on both sides of the plate making it difficult for electrowetting purposes, yet not impossible.

In electrowetting, direct observation and measurement of contact angle using a camera and a goniometer is the widely used method for droplet contact angle measurement. We also use a camera to capture droplets images and then the contact angles are extracted from the images using Imagej Drop Analysis plug-in [18]. The camera setup is shown in Figure 3-8.

This setup consists of different parts as follows:

1- Camera takes the droplet images. Then the images are saved in a computer.

2- Light intensifies the contrast between the droplet and the second phase (air or oil). The light intensity can be aligned by an aperture built in the light.

3- Stage hosts the EWOD substrates. It can be moved in three dimensions. The stage is aligned to the camera axis and field of view so the measured angles in different conditions will be comparable.

4- Auxiliary electrode is used in the *grounding from above* electrowetting setup, which is used in this study too. The auxiliary electrode aids to apply the potential difference between the wafer and the droplet. To do so, a droplet is placed on the substrate with a pipette, then an auxiliary electrode is dipped in the droplet, and finally an electrical potential difference is applied between the wafer and the auxiliary electrode. The electrical potential difference is provided by a power source. Substrate is connected to the power source via a piece of copper tape, connected to the wafer. To secure the substrate connection to the copper tape during the tests, the copper tape is glued to the substrate using a silver epoxy.

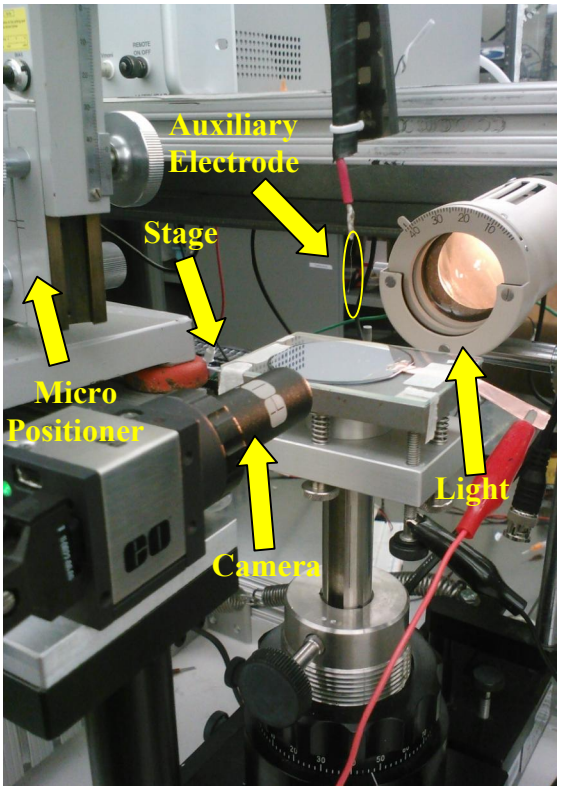

Figure 3-8. Goniometer and camera setup.

5- Micro positioner moves the auxiliary electrode in three dimensions to position it in the center of the droplet to minimize distortion.

3.2.4. Test Setup of the Electrode Pair Measurement

In Continuous Electrowetting (CEW), the $\eta_{actuation}$ is the criteria that is employed to evaluate the effectiveness of the metallic spots, which is calculated with equation 3.3. The $\eta_{actuation}$ values vary between zero and one. At value of one, the metallic spots act as ideal diodes and can cause the highest possible actuation force.

To characterize the $\eta_{actuation}$ values in various electrode/electrolyte systems, the knowledge of potential variation of metallic spots is critical (as equation 3.3 shows). The two spots behave electrically as two diodes in series, one forward biased and one reverse biased. The voltage across the pair of diodes (metal spots) is easily measured, but the electrowetting performance depends on the distribution of the voltage between the two spots. Ideally, the forward biased

diode would have negligible voltage while the reverse-biased diode maintained a high voltage difference. The voltage division is determined by the point at which the current through the two metal spots (diodes) is the same.

While I-V measurements could inform us as to the behavior of the individual spots, the behavior is not as stable as a semiconductor diode and is easily damaged by high currents. Fortunately, when used in pairs, the diode spots reduce the net current through the system, reduce eletrochemical reactions, and minimize electrode damage. To better understand the response in CEW, the behavior of pairs of spots is evaluated using a test that simulates two consecutive metallic spots in CEW, which enable us to measure the potential of metallic spots as illustrated in Figure 3-9.

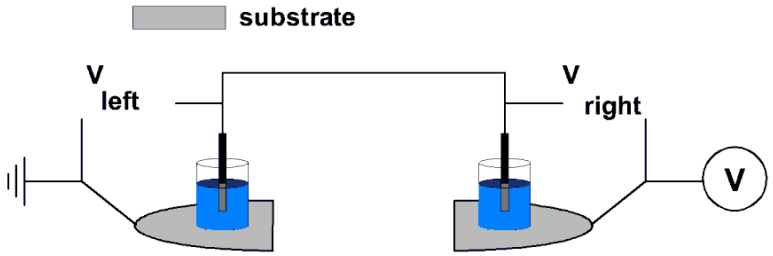

Figure 3-9. Schematic of the test setup for the potential difference measurement.

In this setup, a conductive substrate is spin-coated with a 50 nm Cytop layer and then is divided into two pieces. Then a tube (diameter=4.5 mm) is glued on both pieces and the electrolyte solution is purred in the tubes, which are electrically connected via the auxiliary electrodes placed in the tubes. This combination resembles the droplet condition in CEW with each tube representing one half of the droplet and the electrical connection between them the droplet bulk.

The voltage is applied using one channel of a Keithley 2612A SourceMeter while the other measures V_{left}, and then the potential of the other spot is calculated (V_{right}) as follows:

$$V_{right} = V_{app.} - V_{left} \tag{3.7}$$

The $V_{right.}$, $V_{app.}$, and V_{left} are respectively calculated potential (on the right-hand side of Figure 3-9), applied voltage, and the measured potential (on the left-hand side of Figure 3-9). Here, V_{left} is equal with V_{drop} which is then used to calculate the $\eta_{actuation}$ values via equation 3.3. The impact of the ramp rates of $V_{app.}$, electrolyte solutions, the electrode pre-anodization, and the electrode material are investigated. To do so, first V_{right} and V_{left} are plotted against $V_{app.}$ in two separate graphs. Then, to determine the effects of different electrode/electrolyte combinations in the droplet actuation in CEW, the $\eta_{actuation}$ values are plotted versus $V_{app.}$ and the results in different combinations are compared.

3.3. Microfabrication Methods

There are two main experiments in this study. First, reliability is characterized and, second, the potential difference of the two sides is investigated as explained above. The sample preparation for these tests is explained here. In addition, the microfabrication of CEW device is explained here too. We have already demonstrated continuous electrowetting on patterned samples [19]. The finding of this study will be also examined for CEW as a future study.

3.3.1. Reliability Tests Samples

There are two reliability experiments in this study. First, the reliability experiments on the metallic spots and, second, the reliability experiments on the SiO_2 dielectric layer.

To prepare the samples for the metallic spot reliability experiments, the desired metal is first evaporated on a thermally oxidized 2" silicon wafer. The SiO_2 layer is 500 nm and the metal layer is 300 nm. Then Cytop is spin-coated on top of the metallic layer. The original Cytop solution we used is CTX-807M. Figure 3-10 shows how Cytop codes reflect their properties.

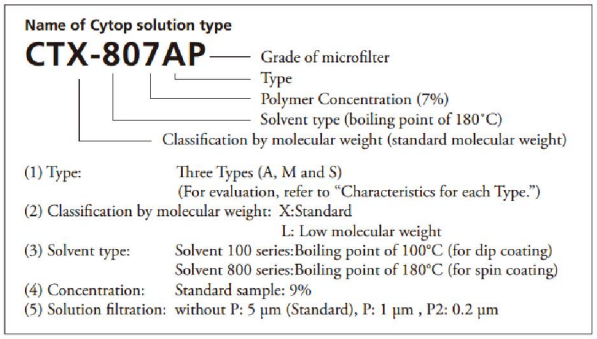

Figure 3-10. Cytop solutions properties based on their codes [20].

The Cytop polymer concentration can be adjusted by adding solvent to the original Cytop solution. Then, Cytop thickness can be changed by tuning the spinning rate as shown in Figure 3-11.

To be able to make the electrical connection to the wafer after Cytop coating, a part of metallic layer is covered by a piece of Kapton tape before spinning and is removed after prebaking Cytop. After spinning, Cytop is first prebaked at 100º C for 100 s on a hot plate and then is baked at 200º C for two hours in an oven.

In these samples, the electrical connection is made to the metallic layer. To make the electrical connection, a piece of copper tape is connected to the uncoated part of the metallic layer using a conductive epoxy and later the connection is secured by gluing the copper tape to the wafer with an epoxy. Two wafers with aluminum and gold metallic layers are shown in Figure 3-12.

For the SiO_2 dielectric reliability experiments, Cytop is directly spin-coated on a thermally oxidized 2" silicon wafer with a SiO_2 oxide thickness of 500 nm. Then, the substrate is divided in half and the electrical connection is made to the silicon layer (to the edge of the broken wafer) below the SiO_2 layer by connecting a piece of copper tape using a conductive pen (Precision Conductive Ink Dispenser, CircuitWriter) as shown in Figure 3-13.

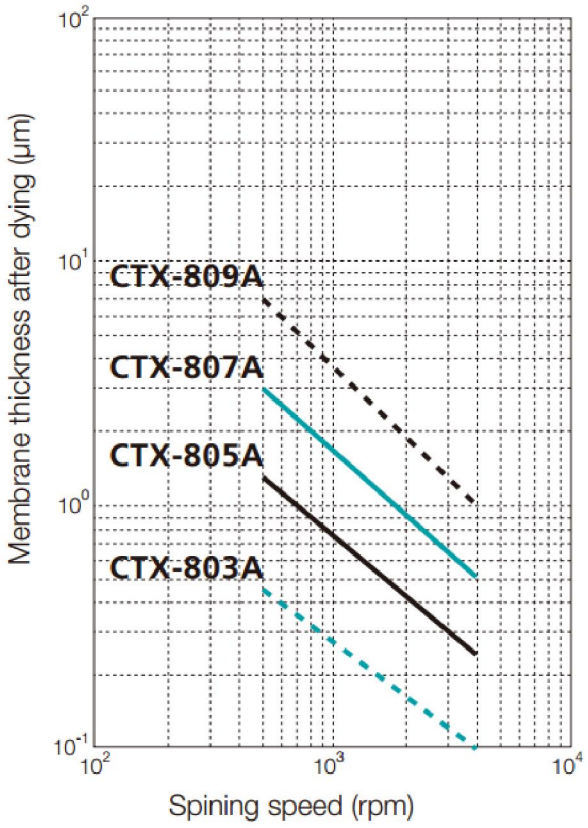

Figure 3-11. Cytop thickness variation by the spinning speed [20]. The spinning duration is 20 s.

Figure 3-12. Electrowetting wafers with aluminum (left wafer) and gold (right wafer) as conductive layers.

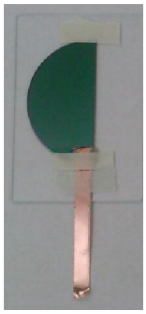

Figure 3-13. An Si/SiO_2/Cytop electrowetting substrate used in this study.

3.3.2. Test Samples of the Electrode Pair Measurements

Two kinds of samples are prepared for the electrode pair measurements. Two kinds of substrates are used in these measurements, which are non-preanodized and preanodized substrates. Non-preanodized substrates are identical to that of the metallic spot reliability experiments. That is, a metal layer is evaporated on SiO_2 and then Cytop is spin-coated on top. In the preanodized substrates preparation, the metallic layer is first oxidized electrochemically and then Cytop is spin coated on the oxidized metallic layer.

The electrochemical oxidation is performed on aluminum in 0.1 M citric acid bath at room temperature. The aluminum layer is oxidized by keeping the aluminum layer potential at +50 V with respect to an activated titanium auxiliary electrode. The oxidation was stopped when the oxidation current density reached a plateau at around 0.046 mA/cm^2.

3.3.3. Continuous Electrowetting Tests Samples

Figure 3-14 shows the schematic of continuous electrowetting substrate micro-fabrication.

The substrates were fabricated in cleanroom area through 22 main steps as follows:

1- A high resistivity four inch silicon wafer is cleaned.

2- The wafer is thermally oxidized with a thickness of 500 nm.

3- Positive photoresist is spin-coated and baked on hot plate.

4- Selective areas of the photoresist are exposed to UV light using a mask aligner.

5- The photoresist is developed and then post-baked.

6- SiO_2 was etched with Buffered Oxide Etch (BOE) solution.

7- Photoresist is stripped.

8- Phosphorous dopant is spin-coated on the substrate, preheated, and then annealed. First, the spinning is performed at 4000 RPM for 30 seconds and then the substrate is preheated at 200º C in an oven for 10 minutes. Finally, the substrate is annealed at 1050º C in 75% N and 25% O_2

ambient for 2.5 hours. The goal of this step is to dope the silicon spots in order to make a proper ohmic contact between silicon and aluminum which is deposited in step 16.

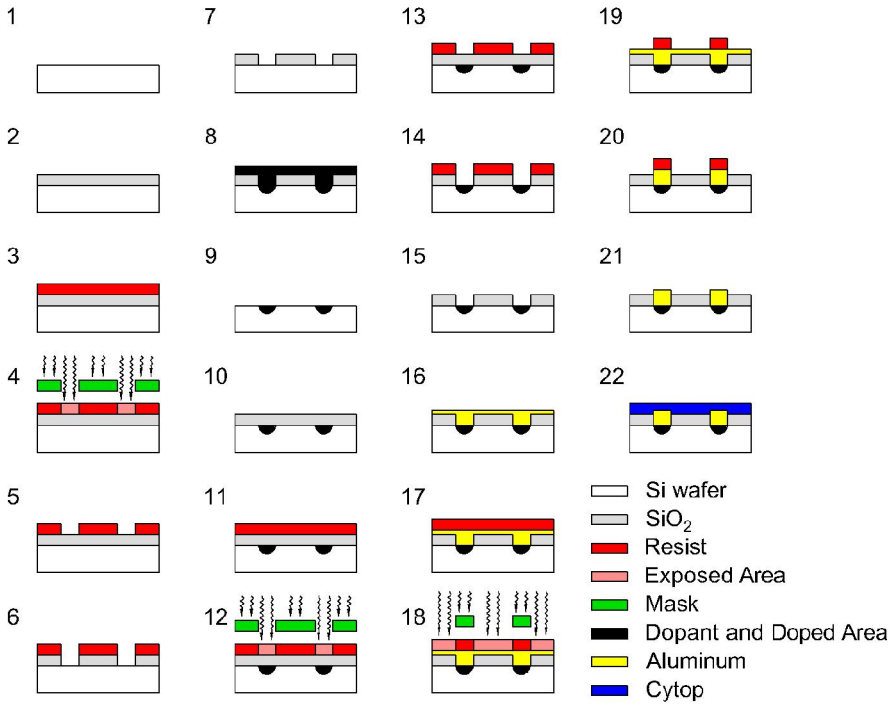

Figure 3-14. Schematic of continuous electrowetting substrate microfabrication. Here, only two spots are shown.

9- The dopant and SiO_2 layers are etched with BOE solution and then the sample is cleaned.

10- The wafer is again thermally oxidized with 500 nm oxide thickness. Here a new SiO_2 layer is grown on the wafer because the dopant can change the dielectric property of the initial SiO_2 layer.

11-15- These steps are identical to steps 3-7.

16- Aluminum is evaporated on the substrate with e-beam.

17- Positive photoresist is spin-coated and baked.

18- The photoresist are exposed to UV light using a mask aligner.

19- The photoresist is developed.

20- Aluminum around the doped silicon spots is etched.

21- Photoresist is stripped and the wafer is cleaned.

22- Cytop is spin-coated and baked.

3.4. Conclusion

Two test methods are used to characterize dielectrics in electrowetting systems. First, electrochemical impedance spectroscopy is used to detect dielectric damage after electric field application. Second, direct contact angle measurement is also performed to investigate the electrowetting systems over many cycles.

In continuous electrowetting, the diode like behavior of electrowetting substrates is used to perform lateral droplet movements. To show the diode like behavior, I-V measurements are performed.

The diode behavior of the metallic spots in continuous electrowetting (CEW) creates a potential difference between two consecutive metallic spots that moves the droplet. The higher potential difference between the metallic spots cause higher droplet actuation force, which is desired. A test setup is designed to monitor the metallic spots electrical potentials, so the spots potential difference can be directly calculated. Variation of the metallic spots voltages with ramp rate, electrolyte solutions, metallic spots pre-anodization, and metallic spot material is to be investigated using this method.

3.5. References

[1] B. Raj*, et al.*, "Ion and liquid dependent dielectric failure in electrowetting systems," *Langmuir : the ACS journal of surfaces and colloids,* vol. 25, pp. 12387-92, 2009.

[2] J. Baker-Jarvis*, et al.*, "Dielectric characterization of low-loss materials a comparison of techniques," *Dielectrics and Electrical Insulation, IEEE Transactions on,* vol. 5, pp. 571-577, 1998.

[3] R. R. Nigmatullin and Y. E. Ryabov, "Cole-Davidson dielectric relaxation as a self-similar relaxation process," *Physics of the Solid State,* vol. 39, pp. 87-90, 1997/01/01 1997.

[4] P. Undre*, et al.*, "Microwave dielectric characterization of binary mixture of formamide with N, N-dimethylaminoethanol," *Pramana,* vol. 68, pp. 851-861, 2007/05/01 2007.

[5] V. F. Lvovich, "Fundamentals of Electrochemical Impedance Spectroscopy," in *Impedance Spectroscopy*, ed: John Wiley & Sons, Inc., 2012, pp. 1-21.

[6] A. Amirudin and D. Thieny, "Application of electrochemical impedance spectroscopy to study the degradation of polymer-coated metals," *Progress in Organic Coatings,* vol. 26, pp. 1-28, 1995.

[7] H.-K. Song*, et al.*, "The effect of pore size distribution on the frequency dispersion of porous electrodes," *Electrochimica Acta,* vol. 45, pp. 2241-2257, 2000.

[8] F. Mugele and J.-C. Baret, "Electrowetting: from basics to applications," *Journal of Physics: Condensed Matter,* vol. 17, pp. R705-R774, 2005.

[9] N. B. Crane*, et al.*, "Bidirectional electrowetting actuation with voltage polarity dependence," *Applied Physics Letters,* vol. 96, pp. 104103-104103, 2010.

[10] P. Castro*, et al.*, "Characterization of activated titanium solid reference electrodes for corrosion testing of steel in concrete," *Corrosion,* vol. 52, pp. 609-617, 1996.

[11] J.-B. Jorcin*, et al.*, "CPE analysis by local electrochemical impedance spectroscopy," *Electrochimica Acta,* vol. 51, pp. 1473-1479, 2006.

[12] Z. Kerner and T. Pajkossy, "Impedance of rough capacitive electrodes: the role of surface disorder," *Journal of Electroanalytical Chemistry,* vol. 448, pp. 139-142, 1998.

[13] C. Hitz and A. Lasia, "Experimental study and modeling of impedance of the her on porous Ni electrodes," *Journal of Electroanalytical Chemistry,* vol. 500, pp. 213-222, 2001.

[14] C. A. Schiller and W. Strunz, "The evaluation of experimental dielectric data of barrier coatings by means of different models," *Electrochimica Acta,* vol. 46, pp. 3619-3625, 2001.

[15] T. Pajkossy*, et al.*, "Impedance aspects of anion adsorption on gold single crystal electrodes," *Journal of Electroanalytical Chemistry,* vol. 414, pp. 209-220, 1996.

[16] M. E. Orazem*, et al.*, "Critical issues associated with interpretation of impedance spectra," *Journal of Electroanalytical Chemistry,* vol. 378, pp. 51-62, 1994.

[17] J. L. Ihrig and D. Y. F. Lai, "Contact angle measurement," *Journal of Chemical Education,* vol. 34, p. 196, 1957/04/01 1957.

[18] A. F. Stalder*, et al.*, "A snake-based approach to accurate determination of both contact points and contact angles," *Colloids and Surfaces A: Physicochemical and Engineering Aspects,* vol. 286, pp. 92-103, 2006.

[19] C. W. Nelson, *et al.*, "Continuous electrowetting via electrochemical diodes," *Lab on a Chip,* vol. 11, pp. 2149-52, 2011.

[20] C. K. Dyer and J. S. L. Leach, "Breakdown and Efficiency of Anodic Oxide Growth on Titanium," *Journal of The Electrochemical Society,* vol. 125, pp. 1032-1038, July 1, 1978 1978.

CHAPTER 4: A MATERIAL SYSTEM FOR RELIABLE LOW VOLTAGE ANODIC ELECTROWETTING

The objective of this chapter is to show how a passive electrode/electrolyte combination can be incorporated to perform reliable Electrowetting on Dielectric (EWOD). The passive combination used in this study is aluminum/citric acid. With the passive combinations, it is possible to actuate a droplet for thousands of cycles without the dielectric breakdown. It is also possible to perform low voltage reliable electrowetting via the use of a thin dielectric layer. With non-passivating combinations, the dielectric failure occurs quickly, which results in the droplet actuation failure. Before showing how the passivating systems work, some evidence of dielectric breakdown upon electric field application are shown via Electrochemical Impedance Spectroscopy (EIS).

4.1. Electrochemical Impedance Spectroscopy

Here, to show the Cytop damage upon electric field application, three electrode electrochemical impedance measurements are performed before and after an electric field application on Cytop coated directly on a conductive layer. Two pieces of activated titanium were used as reference and counter electrodes [1].

Figure 4-1 shows the Nyquist plots before and after an electrical field application, respectively, on a single layer of Cytop as the dielectric.

Here, a resistor-resistor/capacitor equivalent circuit is considered for the EWOD system. The impedance of the assigned equivalent circuit is calculated as follows:

$$Z(\omega) = R_s + \frac{1}{CPE \cdot (j \cdot \omega \cdot C)^n + 1/R_P} \tag{4.1}$$

where R_s and ω are the droplet resistance and angular frequency ($2\pi f$), respectively, *CPE* is the Cytop Constant Phase Angle Element, and R_p is charge transfer resistance on the conductive layer. n is a constant representing the ideality of the Cytop capacitance, which varies between zero and one. *CPE* has been attributed to the capacitance distribution [2].

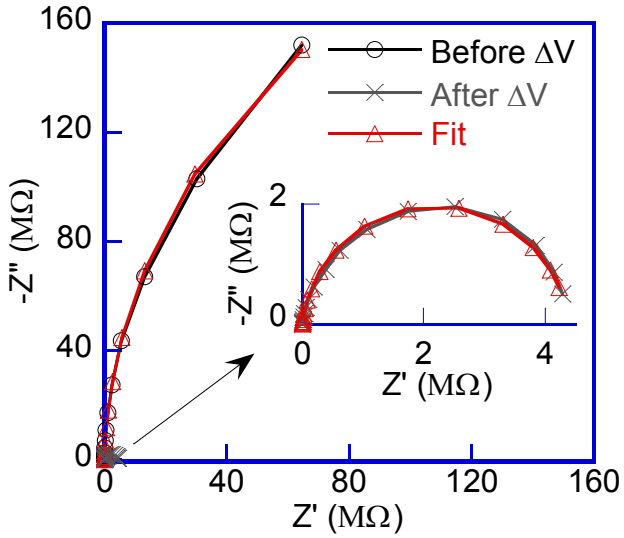

Figure 4-1. EIS results on an aluminum wafer with a 595±3% nm Cytop: Nyquist plots before and after keeping the electrolyte solution voltage at +70 V for two seconds. 0.1 M tartaric acid was the electrolyte solution, which was confined in a tube glued to the Cytop with a surface area of about 1 cm^2. Pieces of activated titanium rod were the auxiliary and reference electrodes. The frequency ranged from 10^5 to 0.04 Hz with an excitation voltage of 5 mV.

Table 4-1 shows the circuit parameter variation after the electric field application.

Table 4-1. Variation of the equivalent circuit parameters after the application of +70 V between the wafer and the droplet.

	n	*CPE (Farad)*	R_P *(Ω)*
Before ΔV	0.984	2.2e-8	4.5e8
After ΔV	0.931	1.2e-7	4.3e6

As Table 4-1 shows, after electrical field application, n changes from 0.984 to 0.931, which is attributed to the capacitance distribution caused by the damage spots in Cytop before and after

the electric field application, respectively [3]. In addition, after electric field application, CPE increases, which is attributed to water absorption [4-5] into the Cytop. Moreover, R_p reduces significantly because of Cytop damage.

EIS results show the Cytop damage during the EWOD process. Cytop damage results in electrochemical reactions at the damage spots, which affect EWOD behavior, depending on the droplet potential polarity with respect to the wafer: cathodic and anodic reactions occur when the droplet potential is either positive or negative, respectively. In the passivating systems, the electrochemical reactions stop at the bottom of Cytop damage spots due to the passivating nature of the conductive layer/electrolyte system [6-7]. However, in non-passivating systems, the electric field damages Cytop and the subsequent electrochemical reactions cause substrate damage and results in quick loss of EWOD response. In the next sections it is shown how passivating systems can aid EWOD to actuate the droplets consistently[1].

4.2. Abstract

Electrowetting on dielectric is demonstrated with a thin spin-coated fluoropolymer over an aluminum electrode. Previous efforts to use thin spin-coated dielectric layers for electrowetting have shown limited success due to defects in the layers. However, when used with a citric acid electrolyte and anodic voltages, repeatable droplet actuation is achieved for 5000 cycles with an actuation of just 10 V. This offers the potential for low voltage electrowetting systems that can be manufactured with a simple low-cost process.

Keywords: electrowetting, fluoropolymer, anodic, passivation, low voltage

[1] The following part of chapter four has been published (M. Khodayari, J. Carballo, N.B. Crane, A material system for reliable low voltage anodic electrowetting, Materials Letters, 69 (2012) 96-99). The published paper is presented here.

4.3. Introduction

Droplet manipulation has found applications in various fields including lab-on-chip [8-9], displays [10], optics [11], chip cooling [12], and energy harvesting [13]. Droplet shape and motion can be controlled by many methods including thermocapillary[14], dielectrophoresis[15] and magnetic forces [16], but electrowetting on dielectric (EWOD) [17-18] is a particularly promising method for low-cost, flexible and swift droplet actuation. In EWOD, droplet shape and equilibrium positions are changed due to an electromechanical effects of an electrical field applied across a fluid interface [19]. Typically, the electric field is created by applying a potential difference between an auxiliary electrode (often an electrode placed inside or on top of the droplet) and an electrode underneath a thin dielectric. Below a limiting saturation voltage, the wetting angle is given as [20]:

$$\cos\theta_1 = \cos\theta_0 + \varepsilon_0\varepsilon_r V^2 / 2\delta\gamma_{LO} \tag{4.2}$$

where θ_0 and θ_1 are the initial and electrowetting droplet angles, V is the applied voltage, γ_{LO} is the surface energy between the droplet and the second phase (here, hexadecane), δ is the dielectric thickness, and $\varepsilon_0\varepsilon_r$ the permittivity.

One challenge in EWOD is to manipulate the droplet with a low voltage, since many EWOD devices require tens to hundreds of volts while most electronics operate at much lower voltages. Those systems that have been demonstrated to operate below 30 V [21-24], typically require slow and/or expensive deposition processes such as atomic layer deposition [23], and chemical vapor deposition [7, 23] to create the dielectric layer. While spin-coated fluoropolymer dielectrics have been demonstrated, dielectric lifetime is often limited or not reported [22, 24-25]. Low voltage operation is typically limited by declining dielectric properties in thin layers which could be the result of high electric field, local defects, and electrode oxidation[22].

However, recently, it has been shown that, in passivating metals, the electrodes can passivate at defects [7, 26-27]. These tests were done on Parylene coated on pre-oxidized aluminum layer (V > 16 volts) and thick Cytop dielectric layers over a passivating metal electrode (V > 60 volts). Electrolyte solutions (citric acid, tartaric acid) were chosen that form a passive oxidation layer with predominately anodic actuation voltages.

This paper reports on a reliable EWOD process with large contact angle modulation at voltages as low as 10 V using only a thin spin-coated polymer dielectric on bare aluminum. This compares favorably with previous thin spin-coated dielectrics requiring 15 V [21]for actuation. Other tests with thin flouropolymer dielectrics have shown very poor reliability at thin levels [22]. The authors are unaware of any previous reports of low voltage EWOD with demonstrated reliability and low voltage modulation.

4.4. Experiments

A 300 nm thick aluminum layer was deposited by e-beam evaporation on a thermally oxidized silicon wafer and then various thickness of Cytop fluoropolymer (20 nm, 50 nm, 1100 nm) were deposited on the aluminum layer via spin-coating. The wafer was placed in hexadecane as the second phase and an 8 µl droplet of the electrolyte was pipetted on the wafer. Tested electrolytes include 0.1 M sodium sulfate (Na_2SO_4), 0.1 M tartaric acid and 0.1 M citric acid. A platinum auxiliary electrode was placed in the droplet. Then, using a Keithley 2612A SourceMeter, potential difference between the droplet and the wafer was applied in steps while the auxiliary electrode was grounded. The applied voltages were +13 V, +22 V and +60 V on wafers with 20, 50 and 1100 nm Cytop thicknesses, respectively. These voltages were chosen to achieve a 75 deg angle change. Horizontal images of the droplets were recorded at each voltage step. The contact angles were extracted from the images using the Drop Analysis plug-in for

ImageJ [28]. Figure 4-2 shows the experimental setup schematics. Reliability was assessed by measuring the change in contact angle with repeated voltage application.

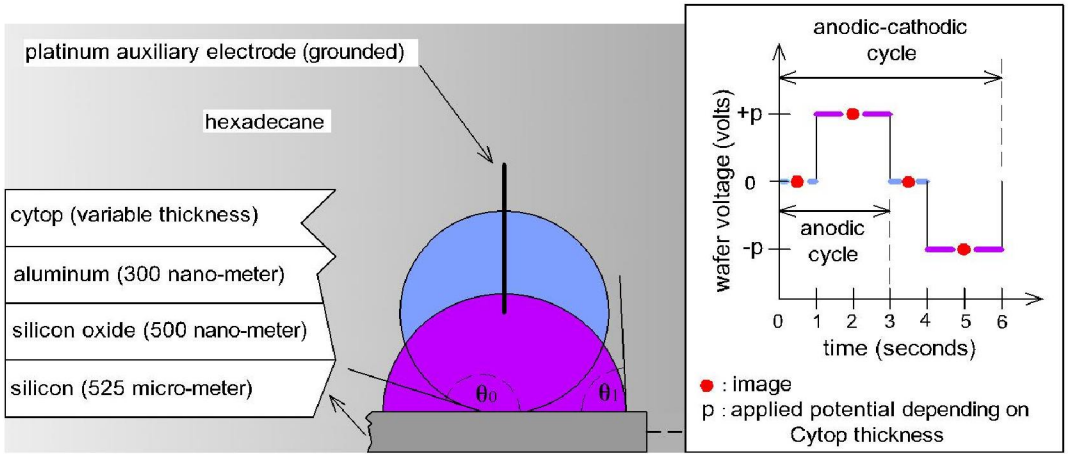

Figure 4-2 Schematic of the experimental setup. Anodic-Cathodic electrowetting used alternating positive and negative voltage pulses as illustrated. In anodic electrowetting only positive pulses were used. These tests were performed on multiple wafers and reproducible results were observed.

4.5. Discussion

Aluminum films show diode-like current-voltage response [26-27] with high resistivity at positive potentials due to the passivation of the aluminum surface. If the proper voltage polarity is maintained, the leakage current is minimized and stable operation is possible. The role of voltage polarity in EWOD life is seen by comparing angle modulations from pure anodic cycles to alternating anodic and cathodic cycles as seen in Figure 4-3. EWOD with alternating voltage polarities (Figure 4-3, dashed lines) degrades rapidly with no angle response after a few cycles, presumably because of the high rate of cathodic reactions causing degradation of the aluminum surface and dielectric. In contrast, positive voltage alone exhibited only modest degradation of the zero voltage angle, and maintained steady operation for 1100 cycles of 2 sec voltage application (FIG. 3b, c).

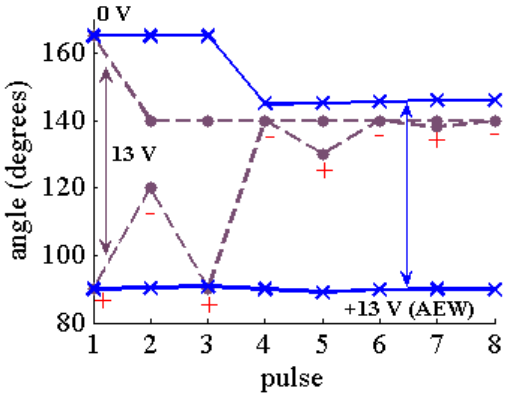

Figure 4-3. Droplet electrowetting modulation with only +13 V pulses (solid line) and both +13 and -13 V pulses (dashed line) with 0.1 M citric acid. The systems with negative applied voltages (dashed lines) show rapid electrowetting degradation due to destructive effects of cathodic reactions.

Typically, the EWOD reliability decreases with decreasing layer thickness. Figure 4-4(a) shows how a sodium sulfate shows much quicker degradation for thinner Cytop layers even when the voltage is adjusted to maintain a nearly constant contact angle. Similar results are seen with sodium chloride solutions.

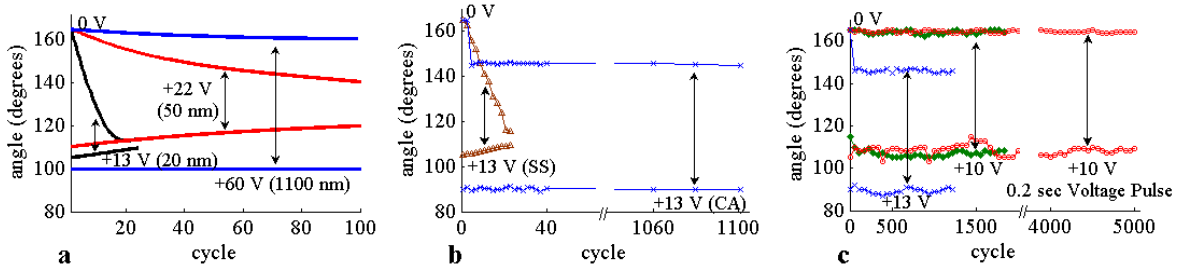

Figure 4-4. (Color Online) Contact angle with and without applied voltages graphed for repeated cycles. In these graphs CA and SS indicate 0.1 M citric acid and 0.1 M sodium sulfate solution. a) Contact angle change for repeated cycles with different Cytop thickness with Na_2SO_4 electrolyte. In this figure fitted curves have been shown for better clarity. The tests were performed on 1100, 50 and 20 nm Cytop thicknesses with electrowetting voltages of +60, +22 and +13 volts, respectively. These voltages were chosen to achieve an electrowetting angle of 90 degrees with the citric acid solution, b) the effects of electrolyte composition on low voltage AEW lifetime on 20 nm Cytop and c) the effects of modulation voltage and voltage pulse length on low voltage AEW on 20 nm Cytop.

When a passivating electrolyte (citric acid) is used, the same dielectric shows larger angle changes for the same applied voltage and more stable operation (Figure 4-4(b)). Citric acid is known to form an effective passivating oxide on aluminum [29-30]. Other solutions such as tartaric acid [29, 31-32] that form passivating oxides also show good performance though tartaric acid electrolytes did not have as long of life as citric acid.

Applied potential magnitude could cause some differences in anodic electrowetting (AEW). Figure 4-3 and Figure 4-4 b shows a drop in the contact angle at zero potential after just a few steps of the 13 V AEW. This could be due to charge entrapment [33]. However, when the voltage is slightly reduced from 13 V to 10 V, negligible angle change is seen over 1800 cycles (Figure 4-4c, Figure 4-5). After 1100th and 1650th cycles in respectively 13 and 10 V AEW, the droplets tended to jump off which is possibly related to a gradual aluminum oxidation and/or charge entrapment that would create differential dielectric properties over the wetting area. However, after the droplet motion, there was no visible damage to the dielectric or the electrode. In addition to potential magnitude, pulse duration can alter AEW life. When the same substrates were tested with shorter voltage pulses the droplet motion occurred at a higher number of cycles. For instance, with a voltage pulse length of 0.2 seconds, one tenth the time used in the other plotted data, droplet motion was not observed until after 5000 cycles (Figure 4-4c). Thus the length of time the voltage is applied affects the ultimate system life.

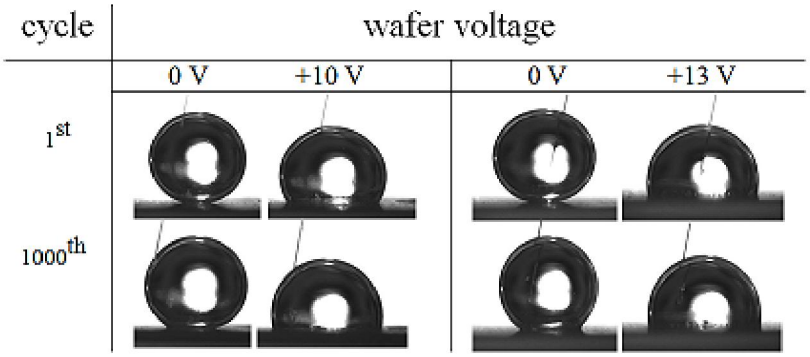

Figure 4-5. Droplet images before and after AEW at the first and 1000th cycles. The droplet solution is 0.1 M citric acid.

4.6. Conclusion

Under anodic actuation voltages, valve-metal electrodes can be used with thin hydrophobic polymers as dielectric to achieve stable operation at low voltages. Typically, these layers have defects that permit significant electrochemical damage to the electrodes. However,

combinations of electrodes and electrolyte known to form a passive oxide perform reliably even for thin spin-coated dielectric layers subject to many defects as long as the electrode is at a more positive potential than the droplet. A passivating oxide is believed to form at the defects to prevent continued electrode damage or droplet/electrode shorting.

This work used aluminum electrodes and compared the system performance for different droplet compositions. The success of this approach requires the proper selection of electrode and droplet composition to create a passivating oxide film. Metals such as Al, Hf, Nb, Ta, Ti, and Zr (sometimes referred to as valve metals) [34] can form such passivating oxide layers. Similar results should be possible with these metals. These electrode/electrolyte material combinations permit reliable electrowetting using simple dielectric deposition methods such as spin-coating and dip-coating processes. This enables experimental study of EW with simplified fabrication and could dramatically reduce the costs of producing commercial devices compared to alternative methods that utilize techniques like chemical vapor deposition or atomic layer deposition to deposit the dielectric.

The results of this study can also help us understand the failure mechanisms in CEW devices, and hence to prevent it with the use of proper materials. Two parts of the CEW devices contribute in the lateral droplet actuation, which are the metallic spots and the dielectric layer. Hence, the reliability of these two parts has to be evaluated.

First, the metallic spots creates a potential difference in the substrate via their diode behavior, which is the cause of the droplet lateral movement. The metallic spots have to resist etching, so that they can create the electric potential difference consistently. To do so, an appropriate selection of electrode/electrolyte combinations is required. In this study we saw that

the passivating combinations can resist etching, and hence they are a candidate in CEW fabrication and will be studied in the chapter 6.

Second, the modulation of the droplet contact angle occurs on the dielectric layer. Therefore, in the fabrication of reliable CEW devices, the dielectric reliability has to be considered. In this study, it was shown that electrochemical reactions and the subsequent dielectric breakdown lead to the EWOD degradation. Hence, in the fabrication of the reliable CEW devices, the electrolytes diffusion through the dielectric layer and the subsequent electrochemical reactions have to be prohibited. Here, SiO_2 is used as dielectric layer and in the next chapter it is shown how it resists electrochemical reactions, which is apparent in I-V curves. However, with small electrolytes, a degradation in contact angle modulation is observed, which is attributed to the electrolytes entrapment in the dielectric layer.

Support for this work was provided through NSF Grant CMMI-092637, the state of Florida through the Florida Energy Systems Consortium (FESC), and by NACE International. The assistance of Dr. Alex Volinsky with manuscript preparation is gratefully acknowledged.

4.7. References

[1] P. Castro, A.A. Sagues, E.I. Moreno, L. Maldonado, J. Genesca, Characterization of activated titanium solid reference electrodes for corrosion testing of steel in concrete, Corrosion, 52 (1996) 609-617.

[2] J.-B. Jorcin, M.E. Orazem, N. Pébère, B. Tribollet, CPE analysis by local electrochemical impedance spectroscopy, Electrochimica Acta, 51 (2006) 1473-1479.

[3] H.-K. Song, H.-Y. Hwang, K.-H. Lee, L.H. Dao, The effect of pore size distribution on the frequency dispersion of porous electrodes, Electrochimica Acta, 45 (2000) 2241-2257.

[4] A.S. Castela, A.M. Simões, An impedance model for the estimation of water absorption in organic coatings. Part I: A linear dielectric mixture equation, Corrosion Science, 45 (2003) 1631-1646.

[5] M. Del Grosso Destreri, J. Vogelsang, L. Fedrizzi, F. Deflorian, Water up-take evaluation of new waterborne and high solid epoxy coatings. Part II: electrochemical impedance spectroscopy, Progress in Organic Coatings, 37 (1999) 69-81.

[6] M. Khodayari, J. Carballo, N.B. Crane, A material system for reliable low voltage anodic electrowetting, Materials Letters, 69 (2012) 96-99.

[7] M. Dhindsa, J. Heikenfeld, W. Weekamp, S. Kuiper, Electrowetting without Electrolysis on Self-Healing Dielectrics, Langmuir, 27 (2011) 5665-5670.

[8] S.-K. Fan, H. Yang, W. Hsu, Droplet-on-a-wristband: Chip-to-chip digital microfluidic interfaces between replaceable and flexible electrowetting modules, Lab on a Chip, 11 (2011) 343-347.

[9] D. Witters, N. Vergauwe, S. Vermeir, F. Ceyssens, S. Liekens, R. Puers, J. Lammertyn, Biofunctionalization of electrowetting-on-dielectric digital microfluidic chips for miniaturized cell-based applications, Lab on a Chip, 11 (2011) 2790-2794.

[10] J. Heikenfeld, N. Smith, M. Dhindsa, K. Zhou, M. Kilaru, L. Hou, J. Zhang, E. Kreit, B. Raj, Recent Progress in Arrayed Electrowetting Optics, Opt. Photon. News, 20 (2009) 20-26.

[11] N.R. Smith, L. Hou, J. Zhang, J. Heikenfeld, Fabrication and Demonstration of Electrowetting Liquid Lens Arrays, J. Display Technol., 5 (2009) 411-413.

[12] J.T. Cheng, C.L. Chen, Active thermal management of on-chip hot spots using EWOD-driven droplet microfluidics, Experiments in Fluids, 49 (2010) 1349-1357.

[13] T. Krupenkin, J.A. Taylor, Reverse electrowetting as a new approach to high-power energy harvesting, Nat Commun, 2 (2011) 448.

[14] V. Pratap, N. Moumen, R.S. Subramanian, Thermocapillary Motion of a Liquid Drop on a Horizontal Solid Surface, Langmuir, 24 (2008) 5185-5193.

[15] W. Tianzhun, Y. Suzuki, N. Kasagi, K. Kashiwagi, Oil droplet manipulation using liquid dielectrophoresis on electret with superlyophobic surfaces, in: Micro Electro Mechanical Systems (MEMS), 2010 IEEE 23rd International Conference on, 2010, pp. 1055-1058.

[16] Z. Long, A.M. Shetty, M.J. Solomon, R.G. Larson, Fundamentals of magnet-actuated droplet manipulation on an open hydrophobic surface, Lab on a Chip, 9 (2009) 1567-1575.

[17] H. Ren, R.B. Fair, M.G. Pollack, Automated on-chip droplet dispensing with volume control by electro-wetting actuation and capacitance metering, Sensors and Actuators B: Chemical, 98 (2004) 319-327.

[18] C. Sung Kwon, M. Hyejin, K. Chang-Jin, Creating, transporting, cutting, and merging liquid droplets by electrowetting-based actuation for digital microfluidic circuits, Microelectromechanical Systems, Journal of, 12 (2003) 70-80.

[19] T.B. Jones, An electromechanical interpretation of electrowetting, Journal of Micromechanics and Microengineering, 15 (2005) 1184.

[20] F. Mugele, J.C. Baret, Electrowetting: from basics to applications, Journal of Physics: Condensed Matter, 17 (2005) 705-774.

[21] M. Dhindsa, S. Kuiper, J. Heikenfeld, Reliable and low-voltage electrowetting on thin parylene films, Thin Solid Films, 519 (2011) 3346-3351.

[22] H. Moon, S.K. Cho, R.L. Garrell, C.-J.C. Kim, Low voltage electrowetting-on-dielectric, Journal of Applied Physics, 92 (2002) 4080-4087.

[23] B. Raj, N.R. Smith, L. Christy, M. Dhindsa, J. Heikenfeld, Composite dielectrics and surfactants for low voltage electrowetting devices, in: 2008 17th Biennial University/Government/Industry Micro/Nano Symposium, 13-16 July 2008, IEEE, Piscataway, NJ, USA, 2008, pp. 187-190.

[24] A. Vasudev, A. Jagtiani, L. Du, J. Zhe, A low-voltage droplet microgripper for micro-object manipulation, Journal of Micromechanics and Microengineering, 19 (2009) 075005.

[25] Y. Li, W. Parkes, L.I. Haworth, A.A. Stokes, K.R. Muir, P. Li, A.J. Collin, N.G. Hutcheon, R. Henderson, B. Rae, A.J. Walton, Anodic Ta2O5 for CMOS compatible low voltage electrowetting-on-dielectric device fabrication, Solid-State Electronics, 52 (2008) 1382-1387.

[26] N.B. Crane, A.A. Volinsky, P. Mishra, A. Rajgadkar, M. Khodayari, Bidirectional electrowetting actuation with voltage polarity dependence, Applied Physics Letters, 96 (2010) 104103.

[27] C.W. Nelson, C.M. Lynch, N.B. Crane, Continuous electrowetting via electrochemical diodes, Lab on a Chip, 11 (2011) 2149-2152.

[28] W.S. Rasband, ImageJ, in, vol. 2009, U.S. National Institutes of Health: Bethesda, MD.

[29] J.W. Diggle, T.C. Downie, C.W. Goulding, Anodic oxide films on aluminum, Chemical Reviews, 69 (1969) 365-405.

[30] A. Mozalev, I. Mozaleva, M. Sakairi, H. Takahashi, Anodic film growth on Al layers and Ta-Al metal bilayers in citric acid electrolytes, Electrochimica Acta, 50 (2005) 5065-5075.

[31] S. Ono, M. Saito, H. Asoh, Self-ordering of anodic porous alumina formed in organic acid electrolytes, Electrochimica Acta, 51 (2005) 827-833.

[32] V.F. Surganov, G.G. Gorokh, Anodic oxide cellular structure formation on aluminum films in tartaric acid electrolyte, Materials Letters, 17 (1993) 121-124.

[33] S. Berry, J. Kedzierski, B. Abedian, Irreversible Electrowetting on Thin Fluoropolymer Films, Langmuir, 23 (2007) 12429-12435.

[34] M.M. Lohrengel, Thin anodic oxide layers on aluminium and other valve metals: high field regime, Materials Science and Engineering: R: Reports, 11 (1993) 243-29.

CHAPTER 5: ELECTROCHEMICAL EXPLANATION FOR ASYMMETRIC ELECTROWETTING RESPONSE

In chapter 4 it was shown that, with the use of a passivating electrode/electrolyte combination, a reliable EWOD can be performed due to the dielectric layer integrity. To have reliable CEW devices, EWOD has to be reliable in CEW devices too. In fact, it is the dielectric layer of the CEW devices that has to be reliable. In this study, a SiO_2(500 nm)/Cytop(50 nm) dielectric stack is used in the CEW devices. Hence, reliability tests are performed in a substrate with the same dielectric stack (the substrate is made of Si/ SiO_2(500 nm)/Cytop(50 nm)) with two different electrolyte solutions over 10000 cycles. The following sections will show the reliability of the tested substrate [1].

5.1. Abstract

In electrowetting, a droplet/substrate contact angle is modulated by applying a potential difference between the droplet and substrate. Typically, the droplet potential is changed via an auxiliary electrode dipped in the droplet. Here, it is shown that electrochemical reactions lead to a potential drop on the auxiliary electrode in electrowetting, which degrades the droplet contact angle modulation. The magnitude of this effect depends on the voltage polarity. This problem can be addressed by using a dielectric layer, such as SiO_2, which can prevent electrochemical reactions with the electrowetting substrate and the auxiliary electrode.

[1] At the time of writing, this chapter has been submitted for publication. The submitted manuscript is presented hereafter.

5.2. Introduction

Electrowetting on dielectric (EWOD) is an electromechanical process, in which a droplet apparent contact angle changes by applying a voltage between the droplet and the substrate underneath [1]. It has found applications in lenses [2], screens [3], energy harvesting [4], and lab-on-a-chip devices [5-8]. Devices consist of a conductive layer, a single or stacked dielectric layer, and typically, a hydrophobic layer (the hydrophobic layer could also act as a dielectric layer). Typically, the droplet voltage is changed via an auxiliary electrode which is placed in the droplet as shown in Figure 5-1.

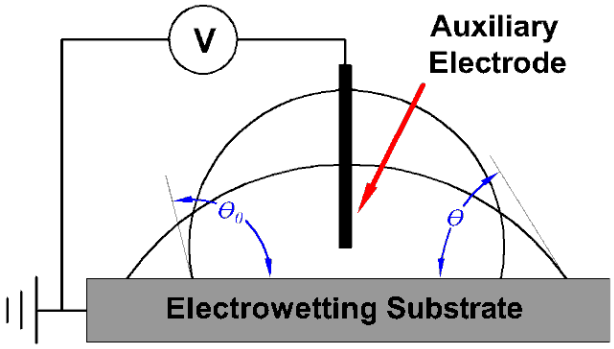

Figure 5-1. Schematic of conventional electrowetting setup. In this process, an electric potential difference is applied between the droplet and substrate, upon which the droplet/substrate contact angle changes. The droplet potential is changed via an auxiliary electrode. In this study, a platinum wire (0.051 mm diameter, 99.95% pure) is used as the auxiliary electrode.

In EWOD, contact angle varies with voltage, following the Lippman equation [9]

$$\cos\theta_1 = \cos\theta_0 + \varepsilon_0 \cdot \varepsilon_r \cdot V_{source}^2 / 2 \cdot \delta \cdot \gamma_{LO} \tag{5.1}$$

Here, θ_0 and θ_1 are the initial and actuated contact angles, V_{source} is the power source voltage, γ_{LO} is the interfacial energy between the droplet and the second phase (here, air), δ and $\varepsilon_0\varepsilon_r$ are the dielectric thickness and permittivity, respectively. Droplet angle decreases with voltage following the Lippman equation. However, the droplet modulation ceases at a certain voltage, which is referred to as saturation voltage, and the corresponding angle is the saturation angle [9]. Saturation angle typically varies between 60° and 70° [10]. Typically, saturation angle is

independent of the droplet voltage polarity. However, it has been shown that saturation angle could vary with voltage polarity [11]. Such voltage polarity-dependent saturation angle appears with the use of thin hydrophobic dielectric layers, which has been attributed to the susceptibility of thin dielectrics to adsorb negative ions [11]. Here, another cause is introduced, which is based on a potential drop on the auxiliary electrode. Electrochemical reactions on the electrowetting substrate are followed by counter reactions on the auxiliary electrode, introducing a potential drop in the auxiliary electrode. It is shown that, for anodic polarizations of the droplet, the auxiliary electrode potential drop intensifies, attributed to fast cathodic reactions on the substrate. When a high resistance substrate, such as thermally grown SiO_2 [12] or electrochemically grown Al_2O_3 [13] is used, saturation angle is independent of the droplet voltage polarity and a symmetrical electrowetting is observed, which is attributed to the prevention of electrochemical reactions. We use a stack dielectric layer of SiO_2/Cytop to prevent the electrochemical reactions and to demonstrate symmetric electrowetting.

In addition to symmetrical electrowetting, the prevention of electrochemical reactions also leads to reliable electrowetting. Here, electrowetting reliability with the SiO_2 substrates is also demonstrated, which is another advantage of the SiO_2 substrates. Two electrolyte solutions, namely 0.1 M NaCl and 0.1 M citric acid are used. Some degradation in droplet modulation is observed over 10,000 trials with 0.1 M NaCl electrolyte solution, while with 0.1 M citric acid, the droplet modulation is quite consistent.

5.3. Discussion

Upon electric field application, electrolytes diffuse through the dielectric, which is accompanied by electrochemical reactions [14]. In this study, hydrophobic Cytop with a nominal dielectric constant of 2.1 is used. During electrowetting, Cytop damage results in electrochemical reactions at the damage spots. This affects EWOD behavior differently, depending on the

droplet potential polarity with respect to the wafer (cathodic and anodic reactions occur when the droplet potential is either positive or negative, respectively).

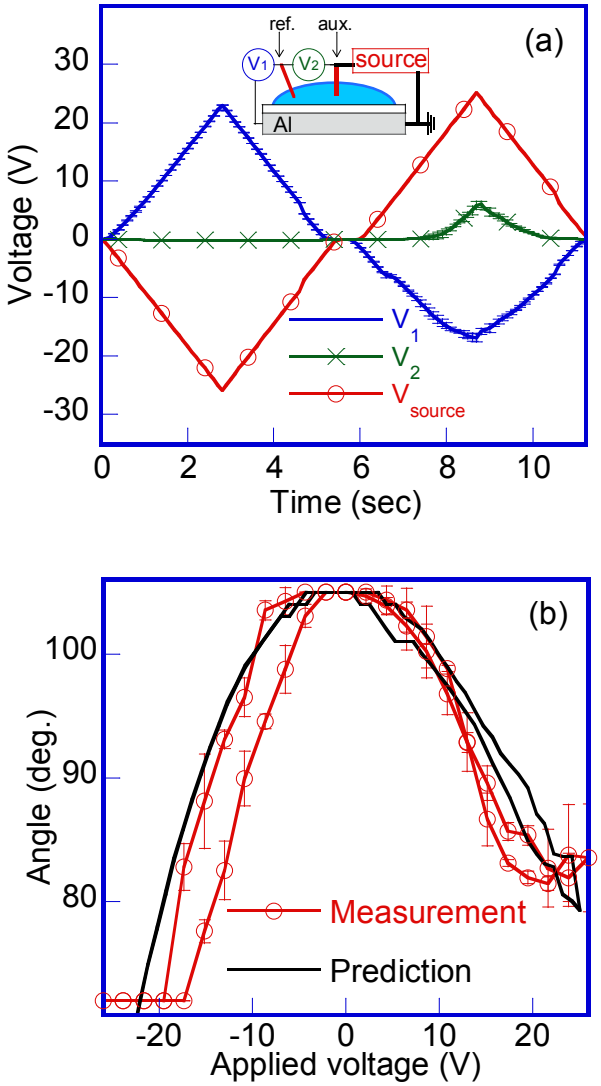

Figure 5-2. Measurement of the wafer and auxiliary electrode potentials. Reference and auxiliary electrodes are platinum. Vsource, V1, and V2 are the power source voltage, potential drop on the wafer, and potential drop on the auxiliary electrode, respectively; (a) Direct measurement of the wafer and auxiliary electrode potentials, and (b) Effect of V1 deviation on the contact angle variation in EWOD. The contact angle values used in Figure 5-2b were collected concurrently with the test in Figure 5-2a. Contact angles are also predicted with the Lippman equation with V1 (the average of V1 curves obtained on the four spots on two wafers as shown in Figure 5-2a) is used for contact angle prediction. Two aluminum wafers with 74±3 nm Cytop were used, and two tests were performed on each wafer.

Cathodic reactions continue at high rates, create bubbles, and cause a potential difference between the droplet/substrate interface and the auxiliary electrode due to a potential drop on the

auxiliary electrode. The wafer, droplet, and auxiliary electrode potentials were directly measured by adding a platinum reference electrode, as shown in Figure 5-2a. In these tests, two electrowetting substrates of Si/SiO_2(500nm)/Al(300 nm)/Cytop(74±3 nm) were used and the electrical connection was made to the aluminum layer. On each substrate two measurements were performed.

As seen in Figure 5-2a, the potential distribution between the wafer and the auxiliary electrode varies with the polarity of the droplet potential. In these tests a passivating system (aluminum/0.1 M citric acid) is used [15]. In passivating systems, the substrate passivates at negative voltage of the droplet, which suppresses electrochemical reactions in the substrate. However, at positive droplet voltages, cathodic and anodic reactions occur in the substrate and the auxiliary electrode, respectively, which results in a potential drop at the auxiliary electrode, as well as the dielectric-coated substrate. Lippman equation can show the impact of the auxiliary electrode potential drop on the actuation angle by replacing V_{source} with V_1:

$$\cos\theta_1 = \cos\theta_0 + \varepsilon_0.\varepsilon.V_1^2/2\delta.\gamma_{LO} \tag{5.2}$$

Here, $V_1 = V_{source} - V_2$, and is equal to the electrical potential difference between the wafer and the reference electrode, as shown in Figure 5-2a. V_{source} is the power source voltage and V_2 is the potential drop at the auxiliary electrode. V_2 increases with the charge transfer resistance on the auxiliary electrode, which creates a difference between V_1 and V_{source}.

When V_{source} tends towards negative values, the electrochemical reactions on the auxiliary electrode and also V_2 magnitude are insignificant because of the reduction of electrochemical reactions due to substrate passivation. In this case, V_1 is equal to V_{source}, and hence Lippman theory predicts EWOD behavior, so either V_{source} or V_1 is used in equation 5.2.

However, when V_{source} becomes positive, V_2 increases. Therefore, V_1 becomes less than V_{source} and EWOD contact angle behavior can be predicted only if V_1 is used in the Lippman equation. Figure 5-2b shows the V_1 deviation effect on the contact angle variation. The Lippman equation predictions with V_1 (V_1 pred.) are also shown (a dielectric thickness of 74 nm, and a droplet surface tension of 72 mN/m have been used in the Lippman equation). The contact angle prediction with V_1 correlates with the contact angle measurements, which substantiates the auxiliary electrode contribution to the contact angle modulation.

The potential drop between the auxiliary electrode and the wafer can be prevented by using a dielectric layer that prevents electrochemical reactions. To achieve this, Cytop was spin-coated over thermally grown SiO_2 on silicon wafers. The electrical connection was made to the silicon layer, below SiO_2. The corresponding wafer and the auxiliary electrode potential variations are shown in Figure 5-3a. Two measurements were performed on two substrates. For the angle prediction with the Lippman equation, a dielectric thickness of 151 nm and a dielectric constant of 3.03 were considered for the SiO_2 (100 nm)/Cytop (51±4 nm) stack. To calculate SiO_2/Cytop dielectric constant, an equation for two capacitors in series was used as follows:

$$\frac{d_t}{\varepsilon_t} = \frac{d_{cytop}}{\varepsilon_{cytop}} + \frac{d_{sio_2}}{\varepsilon_{sio_2}}$$

$$\frac{d_t}{\varepsilon_t} = \frac{d_{cytop}}{\varepsilon_{cytop}} + \frac{d_{SiO2}}{\varepsilon_{SiO2}} \tag{5.3}$$

here, d_t, d_{cytop}, and d_{sio_2} are respectively, the total thickness, the Cytop thickness, and SiO_2 thickness and ε_t, ε_{cytop}, and ε_{sio_2} are the total, Cytop, and SiO_2 dielectric constants. For d_t=151 nm, d_{cytop}=51 nm, d_{sio_2}=100 nm, ε_{cytop}=2.1, and ε_{sio_2}=3.9, ε_t is equal to 3.024.

With thermal SiO_2, contact angle varies symmetrically with voltage, as shown in Figure 5-3b and V_2 varies between -0.09 V and +0.06 V.

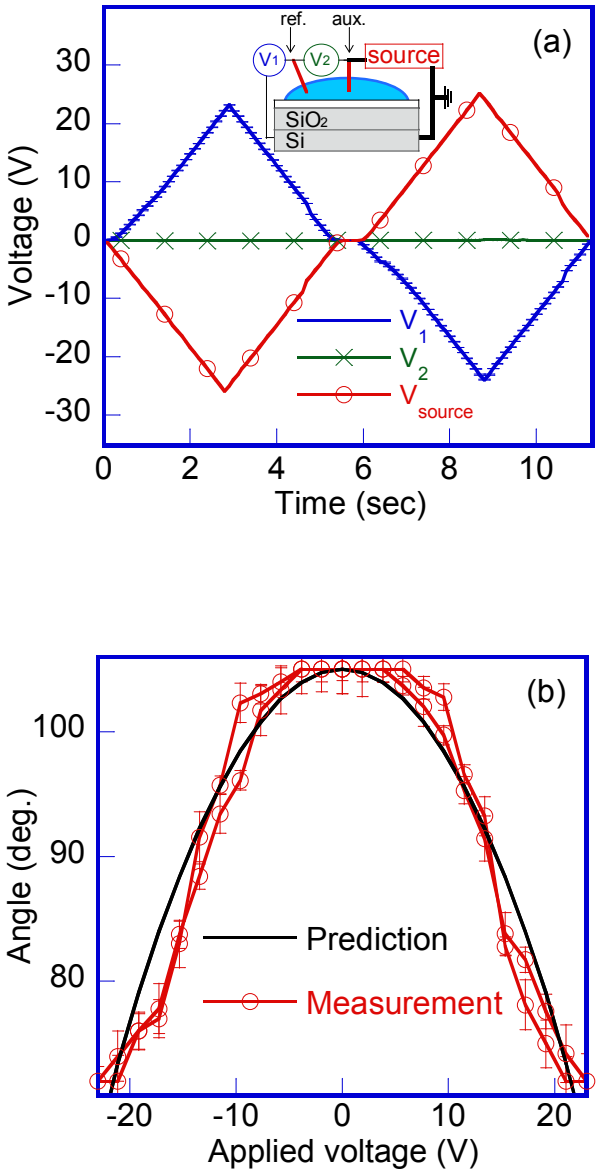

Figure 5-3. Potential distribution with an SiO_2 wafer. A 51±4 nm Cytop layer was coated on 100 nm SiO_2 thermally grown on a silicon wafer; (a) Potential distribution with an SiO_2 wafer, and (b) Symmetric contact angle variation with an SiO_2 layer without potential distribution between the substrate and the auxiliary electrode.

The Si/SiO_2/Cytop substrate also provides reliable electrowetting. A challenge in EWOD is to achieve a reliable process. Reliable EWOD can be obtained in passivating systems by preventing electrochemical reactions [16-17]. However, in passivating systems, due to the diode-like behavior of alumina, reliable electrowetting holds only on anodic polarization of the wafer. This limits the EWOD applications, where both potential polarities of the wafer are desired. With

an SiO_2 layer, however, lifelong electrowetting can be achieved with both polarities of the wafer, with insignificant change in the initial and actuation angles. To demonstrate the reliability of the electrowetting systems with SiO_2, the reliability tests were performed for over 10,000 trials with 0.1 M citric acid and 0.1 M NaCl electrolyte solutions in air. In these tests, in each trial, the droplet voltage is switched between 0 V and 37 V (37 V was applied to achieve an initial contact angle near 75°) and is kept at each voltage for 50 ms, while the droplet images are taken in the middle of each voltage application. The results are shown in Figure 5-4. The reliability tests were performed on two substrates and two spots on each wafer over 10,000 trials. The curves show average contact angles of the four spots. The zero voltage curve shows the average of all measured contact angles.

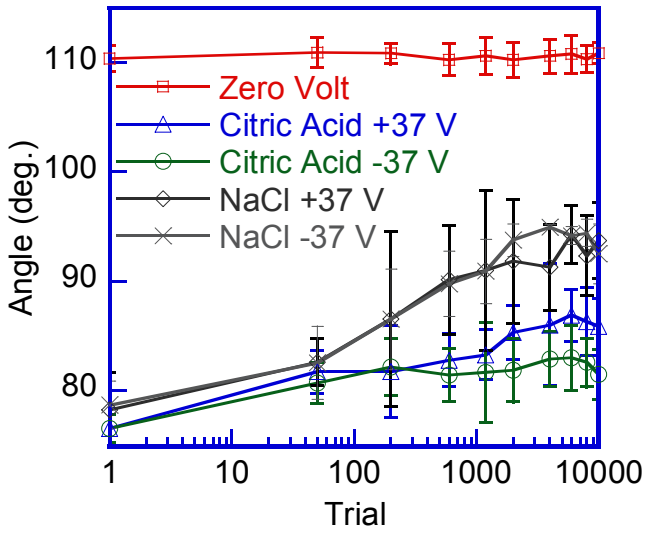

Figure 5-4. Demonstration of the electrowetting process. 37 V was applied to obtain a contact angle around 75°. The reliability tests were performed on two similar substrates (Si/SiO2 (500 nm)/Cytop (51±4 nm)) and two spots on each wafer over 10,000 trials. The curves show average contact angles from the four spots and the error bars show the standard deviation. The zero voltage curve shows the average of all measured contact angles (of all tests) and the error bars represent the corresponding standard deviation.

here, 51±4 nm Cytop layers were spin coated on two 500 nm SiO_2 wafers (SiO_2 layers were thermally grown on silicon wafers). Then the coated wafers were pre-baked at 100 °C for 90 seconds and post-baked at 200 °C for 1 h.

As shown in Figure 5-4, the droplet actuation does not fail, even though degradation in the contact angle modulation is obvious at all conditions. The contact angle degradation is the least with citric acid when +37 V is applied. The observed reliability is attributed to the high resistivity of the SiO_2 dielectric against electrolytes diffusion, which prevents electrochemical reactions.

5.4. Conclusions

In conclusion, symmetric electrowetting is observed with Si/SiO_2/Cytop substrates, which is attributed to the absence of electrochemical reactions in the auxiliary electrode. Additionally, reliable electrowetting is achieved with thermally grown SiO_2 layers. SiO_2 thermal growth and Cytop coating are the only fabrication steps, which are standard and cost-effective. Lab-on-a-chip devices would benefit from this stable electrowetting system.

In this study it was shown that a droplet with certain electrolytes can be actuated consistently on SiO_2 dielectric layer. In CEW devices, the dielectric layer is also SiO_2. Therefore, the results here indicate that it is possible to build reliable CEW devices with the aid of appropriate electrolyte solutions. This reliability is related to the dielectric component of the CEW devices. The results of these experiments indicate that, in CEW devices, electrolyte solutions with large anions (e.g. SO_4^{-2}) should be used. It is worth mentioning that the cations do not diffuse into the dielectric layer, so their size is not important. Cations diffuse into the dielectric layer if the substrate voltage becomes negative; however, in CEW, the substrate voltage increases (to positive values) at the leading edge of the droplet and remains at zero (or close to zero) at the trailing edge. This is why only anions can contribute in the degradation in the contact angle change via diffusion in the dielectric layer.

In chapter 6, reliable electrode/electrolyte combinations are also introduced, which are required to move a droplet sidewise for many times and with consistent force magnitude.

5.5. References

[1] T.B. Jones, J. Micromech. Microeng. 15 (2005) 1184.

[2] B.H.W. Hendriks, S. Kuiper, M.A.J. As, C.A. Renders, T.W. Tukker, Opt. Rev. 12 (2005) 255.

[3] B.J. Feenstra, R.A. Hayes, R.v. Dijk, R.G.H. Boom, M.M.H. Wagemans, I.G.J. Camps, A. Giraldo, B.v.d. Heijden, Electrowetting-Based Displays: Bringing Microfluidics Alive On-Screen, Micro Electro Mechanical Systems, 2006. MEMS 2006 Istanbul. 19th IEEE International Conference on (2006) 48.

[4] T. Krupenkin, J.A. Taylor, Nat. commun. 2 (2011) 448.

[5] W.C. Nelson, I. Peng, G.-A. Lee, J.A. Loo, R.L. Garrell, C.-J. "Cj" Kim, Anal. Chem. 82 (2010) 9932.

[6] J.L. Poulos, W.C. Nelson, T.-J. Jeon, C.-J.C.J. Kim, J.J. Schmidt, Appl. Phys. Lett. 95 (2009) 13706.

[7] M.L.H.S. W. Satoh, J. Appl. Phys. 96 (2004) 835.

[8] E.R.F. Welch, Y.-Y. Lin, A. Madison, R.B. Fair, Biotechnol. J. 6 (2011) 165.

[9] F. Mugele, J.-C. Baret, J. Phys.: Condens. Matter 17 (2005) R705.

[10] S. Chevalliot, S. Kuiper, J. Heikenfeld, J. Adhes. Sci. Technol. 26 (2012) 1909.

[11] E. Seyrat, R.A. Hayes, J. Appl. Phys. 90 (2001) 1383.

[12] M. Khodayari, B. Hahne, N.B. Crane, A.A. Volinsky, Floating Electrode Electrowetting on Hydrophobic Dielectric with an SiO2 Layer, Appl. Phys. Lett. revision submitted (2013).

[13] A. Schultz, S. Chevalliot, S. Kuiper, J. Heikenfeld, Detailed analysis of defect reduction in electrowetting dielectrics through a two-layer 'barrier' approach, Thin Solid Films, DOI: 10.1016/j.tsf.2013.03.008.

[14] B. Raj, M. Dhindsa, N.R. Smith, R. Laughlin, J. Heikenfeld, Langmuir 25 (2009) 12387.

[15] M. Khodayari, J. Carballo, N.B. Crane, Mater. Lett. 69 (2012) 96.

[16] C.W. Nelson, C.M. Lynch, N.B. Crane, Lab Chip 11 (2011) 2149.

[17] N.B. Crane, A.A. Volinsky, P. Mishra, A. Rajgadkar, M. Khodayari, Appl. Phys. Lett. 96 (2010) 104103.

CHAPTER 6: RELIABILITY IN CEW DEVICE

6.1. Objective

In CEW the electric potential difference of two metallic spots defines the droplet actuation force. Our goal is to obtain the highest droplet actuation force possible, which would help us improve droplet actuation. Therefore, the effects of influencing parameters are investigated to obtain a large potential difference between metallic spots with a long stable life. The investigated parameters consist of voltage ramp frequency, electrolyte solution, electrode pre-anodization, and electrode material.

In chapter 5, it was shown that reliable EWOD can be performed on SiO_2 dielectric with specific electrolyte solutions. This will help us fabricate reliable CEW devices. However, in addition to reliable dielectric/electrolyte combinations, we also require reliable electrode/electrolyte combinations (by electrode is meant metallic spot). In fact, in this chapter reliable electrode/electrolyte combinations are introduced. Finally, the electrolyte solution has to constitute both reliable dielectric/electrolyte and reliable electrode/electrolyte combinations to guarantee the stability of the CEW devices.

6.2. Electrowetting

Electrowetting on Dielectric (EWOD) is a process where a droplet/substrate contact angle can be modulated by applying an electric potential difference between the droplet and a substrate beneath the droplet as shown in Figure 6-1.

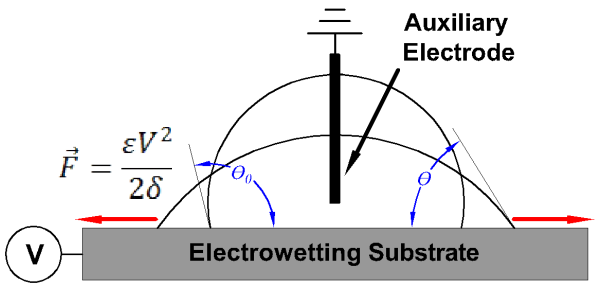

Figure 6-1. Schematic of contact angle variation in electrowetting process.

In EWOD, contact angle varies with voltage, following the Lippman equation [1]:

$$\cos\theta_1 = \cos\theta_0 + \varepsilon_0 \cdot \varepsilon_r \cdot V^2 / 2 \cdot \delta \cdot \gamma_{LO} \tag{6.1}$$

here, θ_0 and θ_1 are the initial and actuated contact angles, V is the power source voltage, γ_{LO} is the interfacial energy between the droplet and the second phase (here, air), δ and $\varepsilon_0\varepsilon_r$ are the dielectric thickness and permittivity, respectively. Droplet angle decreases with voltage up to a certain voltage, which is referred to as saturation voltage, and the corresponding angle is the saturation angle [1]. Saturation angle typically falls between 60° and 70° [2].

EWOD is an electromechanical process, in which an electrostatic force changes the droplet apparent contact angle [3]. The electrostatic force is perpendicular to the droplet surface and is only applied on the droplet surface [4-5]. The magnitude of the electrostatic force reaches a maximum close to Three Phase Contact Line (TCL), which is calculated as follows [6]:

$$\vec{F} = \varepsilon . \overrightarrow{V_r^2} / 2d \tag{6.2}$$

here, ε and d are respectively the dielectric permittivity and thickness. In equation 6.1, the dimension of the electrostatic force is N/m which defines the force applied per distance unit of the droplet perimeter. The electrostatic force magnitude decreases asymptotically by distance from the area in the vicinity of TCL. Hence, local contact angle remains constant at TCL while the apparent contact angle changes [7-8].

6.3. Continuous Electrowetting (CEW)

In the test setup shown in Figure 6-1, the electrostatic force is uniform over the droplet perimeter because of the voltage uniformity, which results in zero net electrostatic force. Hence, the droplet remains steady without any lateral movement [6]. However, if we apply a nonuniform voltage, the net force would be greater than zero, causing a planar movement of the droplet [9].

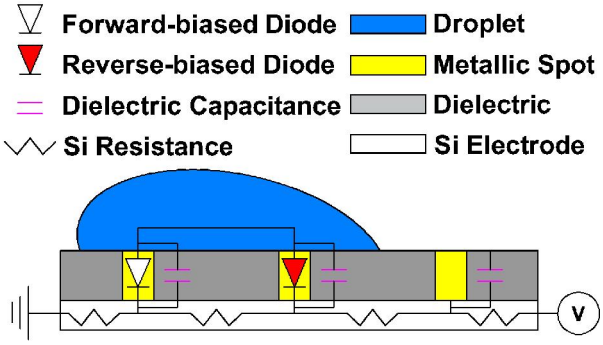

Figure 6-2. Schematic of Continuous Electrowetting on high resistivity silicon wafers.

Traditionally, this is accomplished using a series of different electrodes. Here we integrate metallic spots/electrolyte systems with diode-like properties [9] on high resistivity silicon wafers to create an electric potential difference [10] (Figure 6-2). With a sequence of metallic spots a droplet can be moved continuously on the substrate as shown schematically in Figure 6-2. This simplifies motion control by eliminating the need for numerous electrodes, which is particularly advantageous for 2D motion. This process is referred to as Continuous Electrowetting (CEW), inasmuch as the droplet moves continuously by applying a DC voltage.

In CEW, upon applying a voltage on the high resistivity silicon wafer, the metallic spots in contact with the droplet turn into electrochemical diodes causing a potential difference between the spots [9, 11]. The metallic spot with higher electrical potential becomes reverse biased because of its high resistance to charge transfer. The metallic spot diode on the grounded side gets forward biased, and hence the voltage change from electrode to droplet is insignificant. The potential difference between the metallic spots results in the droplet lateral movement towards the spot with higher potential. The voltage polarity of power source determines the direction of the droplet movement and the droplet always moves towards the side with higher voltage. This way we can change the direction of the droplet movement simply by changing the power source voltage polarity.

In essence, it is the lateral component of electrostatic force close to TCL that causes the droplet modulation. To find the net lateral force on the droplet, we integrate the lateral force on the perimeter of the droplet/substrate interface.

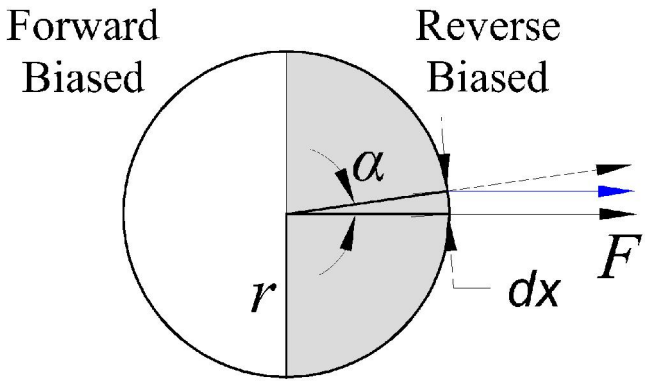

Figure 6-3. Concept of the estimation of net lateral force in CEW. In this figure, α is the angle between a force vector (perpendicular to the droplet perimeter) and its lateral component. r, dx, and F are respectively the droplet radius at TCL, the derivative of the TCL distance, and the electrostatic force that is obtained from equation 6.1.

Integrating over the perimeter of the droplet/substrate interface (Figure 6-3), the total lateral force can be obtained as follows:

$$\left.\begin{array}{l}\overrightarrow{dF_{t,\alpha}} = \overrightarrow{F_\alpha}\cos\alpha.dx \\ dx = rd\alpha\end{array}\right\} \Rightarrow \overrightarrow{dF_{t,\alpha}} = \overrightarrow{F_\alpha}\cos\alpha.r.d\alpha$$

$$\left.\begin{array}{l}\overrightarrow{dF_{t,\alpha}} = \overrightarrow{F_\alpha}\cos\alpha.r.d\alpha \\ \overrightarrow{F_\alpha} = \varepsilon.\left(V_\alpha - V_{drop}\right)^2 \Big/ 2d\end{array}\right\} \Rightarrow \overrightarrow{dF_{t,\alpha}} = \frac{\varepsilon.\left(V_\alpha - V_{drop}\right)^2}{2d}\cos\alpha.r.d\alpha \qquad (6.3)$$

The variables α, x, and r are respectively the angle between two force vectors, the force vector displacement on the droplet perimeter, and the droplet radius. The variable V_α is the substrate voltage on the perimeter of the droplet/substrate interface, which is a function of α. Here, $F_{t,\alpha}$ is the total lateral force on the droplet, which has the dimension of Newton. F_α is the specific lateral force on the droplet perimeter, which is a function of V_α.

To do integration, the relationship between the substrate voltage (V_α) and α on the perimeter of the droplet/substrate interface should be understood. To do so, we assume that the substrate voltage changes from zero (at the trailing edge of the droplet) to V_{max} (at the leading edge of the droplet) linearly by distance. Hence, V_α is related to α as follows:

$$V_\alpha = \left(\cos\alpha + 1\right).\left(\frac{V_{\max}}{2}\right) \qquad (6.4)$$

Combining equation 6.3 and 6.4, then:

$$\overrightarrow{dF_{t,\alpha}} = \frac{\varepsilon.r}{2d}\left[\left(\cos\alpha + 1\right).\left(\frac{V_{\max}}{2}\right) - V_{drop}\right]^2 \cos\alpha.d\alpha$$

$$\Rightarrow \vec{F}_{t,\alpha} = \int_0^{2\pi}\left(\frac{\varepsilon.r}{2d}\left[\left(\cos\alpha + 1\right).\left(\frac{V_{\max}}{2}\right) - V_{drop}\right]^2 \cos\alpha\right).d\alpha$$

$$\Rightarrow \vec{F}_{t,\alpha} = \frac{\varepsilon.\pi.r}{4d}.V_{\max}(V_{\max} - 2V_{drop}) \qquad (6.5)$$

Equation 6.5 shows how the total lateral force in CEW can be changed. The immediate conclusion from equation 6.5 is that $F_{t,\alpha}$ has a linear relationship with r (the droplet radius). In a previous work to perform CEW, we used droplets with different volumes and a droplet with 75 µl showed satisfactory results in terms of the droplet propensity to move sidewise. While this is also dependent on the spacing of the discrete diode spots, these effects are not considered in this model. Verifying the droplet volume/$F_{t,\alpha}$ relationship is the topic of future study.

Another conclusion from equation 6.5 is that to have higher $F_{t,\alpha}$, V_{max} has to be increased, or V_{drop} has to be decreased. This is possible in certain metal/electrolyte combinations and the objective of this study is to find the appropriate metal/electrolyte combinations. In fact, here, we are looking for electrolyte/metal systems where the metallic spots act like ideal theoretical diodes (V > 0 → R = infinity, V < 0→ R = 0). In such a case, V_{drop} would be close to zero when V_{max} is positive and V_{drop} would be close to V_{max} when V_{max} is negative, so:

$$\vec{F}_{t,\alpha} = \pm \frac{\varepsilon.\pi.r}{4d}.V_{\max}^2 \tag{6.6}$$

In equation 6.6, $F_{t,\alpha}$ is either positive or negative. $F_{t,\alpha}$ is positive when the droplet moves towards the right side (Figure 6-3) and vice versa. With a constant droplet/second phase surface tension, lateral electrostatic force reaches an upper bound on the maximum at saturation voltage, irrespective of d (the dielectric thickness) and ε (dielectric constant)—with the premise that saturation angle changes insignificantly with different dielectric materials and dielectric thicknesses [2]. The maximum lateral force can be improved by increasing the droplet/second phase surface tension using a specific second phase such as air. In our study, we use a SiO_2(500 nm)/Cytop (50 nm) dielectric stack with a saturation voltage of 40 V. In chapter four, it was shown that this dielectric layer is reliable where a citric acid droplet was manipulated for over 10000 cycles with acceptable consistency in the droplet modulation (over 10000 cycles, 19%

reduction in angle modulation has been observed), which is beneficial for making reliable CEW devices.

In this study, we are looking for electrode/electrolyte combinations that would improve the theoretical lateral force ($F_{t,a}$). Based on equation 6.5, when the right side of the droplet is reverse biased (as Figure 6-3), the maximum lateral force can be obtained by decreasing V_{drop} to zero volt. However, when the left side of the droplet is reverse biased, V_{drop} has to be increased up to V_{max} so as to obtain the highest lateral force. The parameter V_{drop} is also affected by the location of the droplet to the nearest diode and the spacing of the diodes. However, since this study focuses on electrochemical effects, the diodes are assumed to be ideally situated at the extreme leading and trailing edges of the droplet. A criteria that shows the actuation effectiveness of electrode/electrolyte combinations is obtained by dividing equation 6.5 by equation 6.6 as follows:

$$\eta_{actuation} = \left| \frac{\frac{\varepsilon.\pi.r}{4d}.V_{\max}(V_{\max} - 2V_{drop})}{\frac{\varepsilon.\pi.r}{4d}.V_{\max}^2} \right| = \left| 1 - 2\frac{V_{drop}}{V_{\max}} \right| \tag{6.7}$$

The $\eta_{actuation}$ is the coefficient of actuation, which varies between zero and one. To calculate $\eta_{actuation}$, the absolute value of the proportion is considered, so $\eta_{actuation}$ always varies between zero and one, irrespective of the movement direction of the droplet. When $\eta_{actuation}$ is one, the electrochemical diodes achieve the maximum possible actuation force. When it is zero, the voltage drop is the same on both sides of the droplet and there is no EW actuation. We investigate the diode behavior of the metallic spots in different electrode/electrolyte combinations and then calculate $\eta_{actuation}$ for each combination. The best electrode/electrolyte combinations are recommended for CEW devices.

6.4. Experimental Setup

As discussed earlier in chapter 3, the electric potential of the metallic spots, has to be measured directly without IR drop through high resistivity silicon substrates in CEW. To do so, pairs of metallic spots are evaluated using a test that simulates two consecutive metallic spots (diodes) in CEW. In this test, a conductive substrate (Si/SiO_2/Metallic Layer) is spin-coated with a 50 nm Cytop layer and then is divided into two pieces. Two tubes with a diameter of 4.5 mm are glued to the substrates and then electrolyte solution is poured into the tubes. The tubes are electrically connected via auxiliary electrodes. In this setup, the substrates resemble two consecutive metallic spots and the tubes with electrolyte solution and the connection resemble the droplet in CEW. The experimental setup is shown schematically in Figure 6-4.

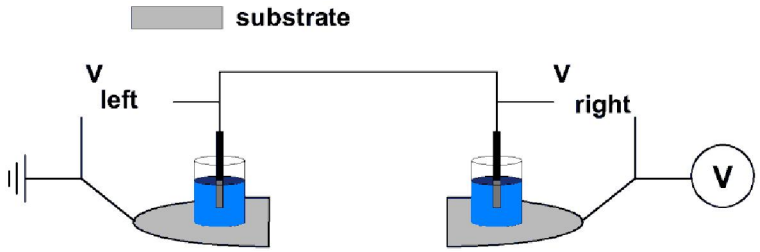

Figure 6-4. Schematic of experimental setup to measure the metallic spots potential difference in Continuous Electrowetting. In this test setup, the substrates resemble the metallic spots and the tubes with electrolyte solution connected via auxiliary electrode resemble a droplet which touches two consecutive metallic spots.

In essense, the used test setup is a combination of two diodes and two capacitors, which are connected in series and parallel as shown in Figure 6-5.

In the test setup circuit (Figure 6-5 (a)), the capacitors and diodes respectively indicate the capacitive behavior of Cytop and the diode-like behavior of conductive layer. Figure 6-5 (b) shows the circuit in CEW substrates, which is analogous with the test setup circuit. It is worth mentioning that in the CEW substrate the metallic spots are connected via the droplet from top and via the high resistivity silicon from bottom. Because the silicon resistance is much lower than the effective resistance of the droplet path through the diode pair, much more current passes

through the silicon than the droplet. Thus, the silicon substrate in CEW is replaced by fixed voltage difference between the two silicon pieces in the test arrangement. Therefore, in the test setup, the substrates are only connected through the electrolyte solution in the tubes. The measured quantity in this study is the applied voltage and the droplet voltage from which the voltage difference across each metal spot is calculated. In CEW, the dielectric layer over the other regions is expected to have much lower conductivity than the metal spots and have little impact on the electric potential of the substrates. Therefore, the experiment setup in this study represents two consecutive metallic spots in contact with droplet in CEW.

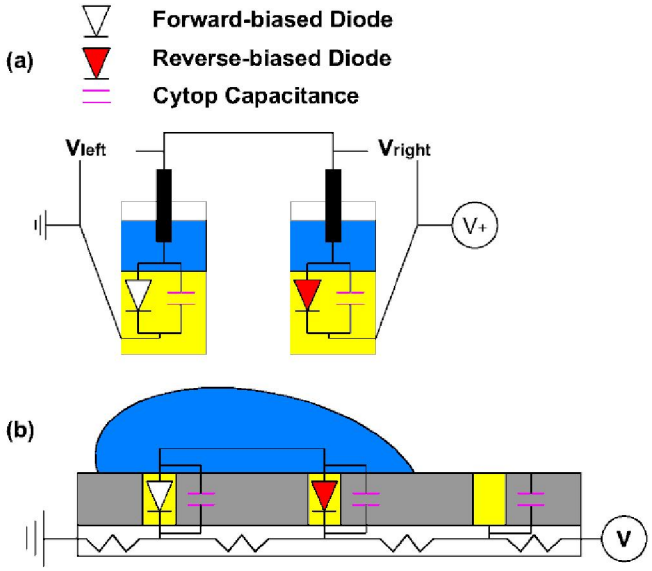

Figure 6-5. A comparison between the test setup circuit and Continuous Electrowetting circuit. (a)Schematic of the diodes and capacitors in the test setup constituting of the hypothetical circuit in CEW (the diodes and capacitors respectively indicate electrochemical diodes and Cytop), (b) schematic of Continuous Electrowetting with the underlying circuit.

To obtain the substrates potentials, a triangular voltage is applied as shown in Figure 6-9 and the droplet potential (V_{left}) is measured concurrently. The V_{right} is then calculated as follows:

$$V_{left} = V_{drop}$$
$$V_{right} = V_{applied} - V_{drop} \tag{6.8}$$

where V_{right}, $V_{applied}$, and V_{left} are respectively the calculated voltage (on the right hand of Figure 6-4), applied voltage, and measured voltage (on the left hand of Figure 6-4). In each test, this measurement is repeated for 500 trials and the average of 100, 101, and 102 trials are demonstrated. Between every two trials, the test is paused for seven seconds in order to allow any possible entraped charges to relax.

6.5. Results

In the following sections, the results of I-V tests on the single electrode tests and the results of the electrode pair measurements are shown. First, it is shown that, to obtain diode behavior, the electrodes have to be coated by a Cytop layer as thin as 50 nm. Second, the diode behavior of some single-electrode/electrolyte systems are shown. Finally, the results of the electrode pair measurements are demonstrated in the form of V-V plots as shown in Figure 6-10.

6.5.1. Single Electrode Measurements

6.5.1.1. Diode Behavior of Single Electrode with Thin Cytop

To observe effective diode behavior in the electrode, the electrolytes needs to be in contact with the electrode, which is feasible through pores in thin Cytop layers [12-13]. When a thin Cytop layer is used, the Cytop intrinsic pores provide channels for the electrolytes to reach the electrode, and hence diode behavior can be observed. To show how a thin Cytop pores contribute in the diode behavior, we have conducted I-V measurements on two $Si/SiO_2/Al/Cytop$ substrates with Cytop thickness of 50±4 nm (thin Cytop) and 240±7 nm (thick Cytop). In each test, a 16 µL droplet (0.1 M citric acid) is placed on the hydrophobobic substrate and then the substrate voltage (power source is connected to aluminum layer) is ramped to first +50 V and then to -50V with 1V/20 ms increments while the droplet is grounded. The results are shown in Figure 6-6.

With 50 nm Cytop, diode like behavior is obvious, which is attributed to the Cytop intrinsic pores. However, with 240 nm Cytop, aluminum substrate hardly shows diode-like behavior,

which is due to the resistance of Cytop against electrolytes diffusion. Therefore, in our tests, a Cytop layer of 50 nm is employed to permit the diode behavior of the electrodes.

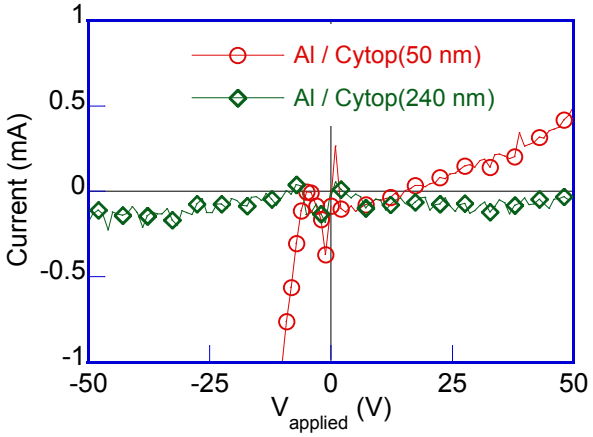

Figure 6-6. (a) I-V measurement on two Si/SiO_2/Al/Cytop substrates and (b) in a low Y axes scale. Power source is connected to the aluminum layer and the droplet is grounded. In each test, a 16 µL aqueous droplet (0.1 M citric acid) is placed on the substrate and the voltage is ramped to +50 V and then to -50 V with 1V/20ms increments and the current is measured concurrently.

6.5.1.2. Impact of Applied Voltage Frequency on Diode Behavior of Single Electrode

As explained before, CEW is based on diode behavior of electrodes. Here, the diode behavior of different electrode/electrolyte combinations are compared. In these tests, a 50 nm Cytop layer is spin coated on aluminum and titanium substrates. In each test, a 16 µl droplet is placed on the wafer and a triangular voltage is applied on the aluminum wafer while the droplet is grounded and the current is measured concurrently. Each test is repeated three times and the average of the measured currents is graphed (error bars in the graphs show the standard deviation of the measured currents). The applied voltage maximum and minimum are +50 V and -50 V, respectively. Each cycle consists of 400 points and the time between every two points is set based on the ramp frequency of the applied voltage. Two parameters are examined, first the ramp frequency of the applied voltage, and second the influence of electrode. Figure 6-7 shows the electrode diode behavior with three different ramp frequencies of 0.1 Hz, 1 Hz, and 10 Hz in aluminum/Na_2SO_4 combination. Generally, current is higher at 10 Hz, which is attributed to the

variation of the oxide layer (alumina) thickness by frequency. At high frequencies like 10 Hz, because of the time constraints for oxide layer thickening, electrochemical reactions would occur with relatively high speed due to the relatively low resistance of the oxide layer. With lower frequencies (1 and 0.1 Hz), the oxide layer thickness probably reaches a maximum and the resistance of the oxide layer against electrochemical reactions also reaches a maximum, which makes the current magnitudes less dependent on frequency—in Figure 6-7, the current magnitudes of I-V curves at 1 and 0.1 Hz are quite similar.

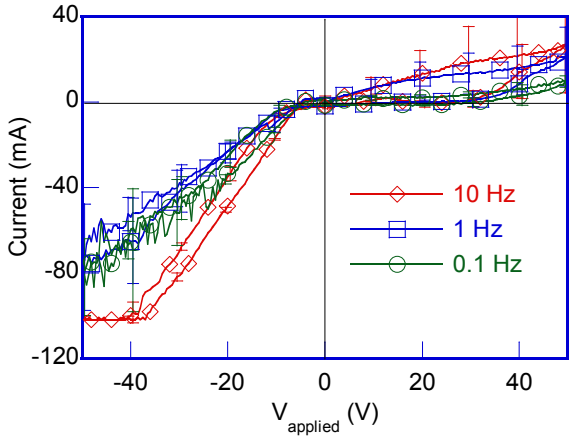

Figure 6-7. Diode behavior of aluminum electrode in contact with 0.1 Na_2SO_4 electrolyte solution. In this test, the aluminum substrate is coated by a 50 nm Cytop layer and then a 16 µl droplet is placed on the wafer. A triangular voltage is applied on the aluminum wafer while the droplet is grounded and the current is measured continuously.

6.5.1.3. Diode Behavior of Single Electrode in Different Electrode/Electrolyte Combinations

Typically, in the single electrode experimental setup, ramp frequency has insignificant impact on diode behavior of electrodes (as shown in Figure 6-7) below 1 Hz frequency.

However, variation of electrode/electrolyte combinations can cause noticeable change in electrodes diode behavior as shown in Figure 6-8.

Six different electrode/electrode combinations are used in this test, namely Al/Na_2SO_4, Al/citric acid, Al/NaOH, Ti/Na_2SO_4, Ti/citric acid, and Ti/NaOH. In each I-V measurement, a five µl droplet is placed on the corresponding electrode and then the droplet is grounded via a

platinum auxiliary electrode (with a 50 nm Cytop coating). A triangular voltage (0 to +50 to -50 to 0 V) is applied on the electrode with 0.5 V/250 ms increments and the current is measured concurrently.

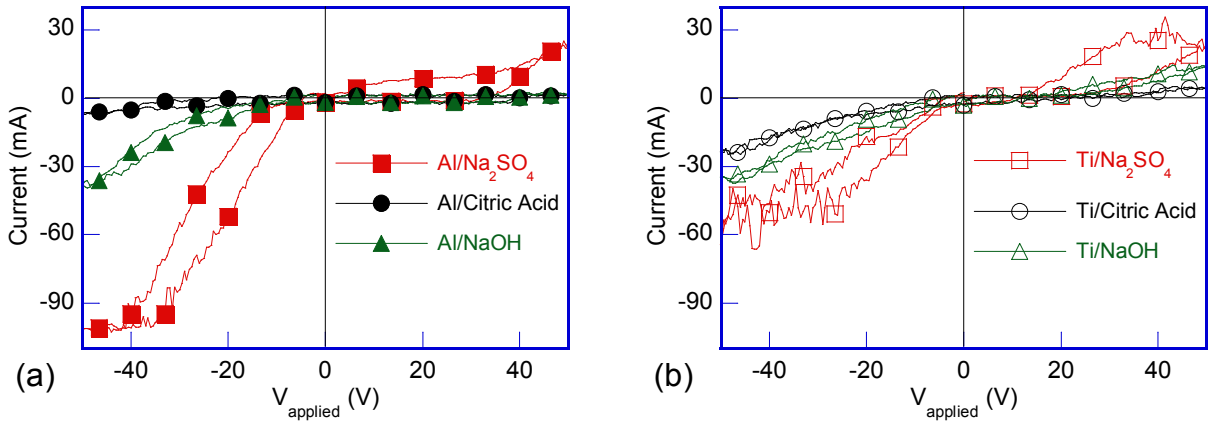

Figure 6-8. Diode behavior of eight different electrode/electrolyte combinations. In these test, the droplet is grounded via a platinum auxiliary electrode and the electrodes potential is first ramped up to +50 V and then to -50 V. A 5 µl droplet is used in each test. The frequency of the whole cycle is 1 Hz.

The results in Figure 6-8 show that, except aluminum/citric acid combination, almost all combinations behave as diodes to a greater or lesser extent. Comparing the I-V results with titanium and aluminum, titanium seems to have larger contrast in forward and reverse currents. At forward biased voltages, the tests with Na_2SO_4 in combination with both aluminum and titanium electrodes have the highest currents. This could be related to the high electrochemical charge transfer between Na^+ cations and electrodes at the alumina pores. With NaOH, the forward current is lower. Here, Na^+ cations are also the agents of cathodic charge transfer, but their concentration is half of that with Na_2SO_4, which can be the reason of lower forward current. At reverse biased voltages, the tests with Na_2SO_4 have the highest currents with both aluminum and titanium electrodes, yet their corresponding I-V curves indicate diode characteristics. One possible reason for the high magnitude of currents with Na_2SO_4 can be the porous structure of

aluminum oxide and titanium oxide, which paves the way for anions to reach the electrodes surface with subsequent electrochemical reactions.

As will be shown in the next sections, all of the electrode/electrolyte combinations with diode behavior can cause a difference in V_{left} and V_{right} behaviors in the electrode pair measurements. However, the absolute current measurements in single diode circuits are not always good indicators of the electrowetting actuation potential of an electrolyte/electrode pair. The parmeters V_{left} and V_{right} have to be directly measured in the electrode pair measurements and have to be related to the diode behavior characteristics in the single electrode tests with caution.

Overall, to evaluate the effectiveness of the electrochemical diodes in CEW devices, the direct measurement of V_{left} in the electrode pair measurements is recommended. In the next sections, the results of the electrode pair measurements with simulation and in different electrode/electrolyte combinations are shown.

6.5.2. Electrode Pair Measurements

As discussed in the experimental setup section, an electrode pair setup is used to evaluate CEW performance in different electrode/electrolyte combinations. CEW performance is related to V_{drop} ($V_{left}= V_{drop}$) via $\eta_{actuation}$ (actuation coefficient). The goal of the next sections is to present $\eta_{actuation}$ behavior in different electrode/electrolyte combinations.

Before presenting the actual experimental results, here we show how V_{right} and V_{left} vary in the electrode pair measurements with some simulation results (performed with Simulink in Matlab) as shown in Figure 6-9. Two simulations were performed with two different diodes and V_{left} and V_{right} are shown respectively in Figure 6-9a and b. First, a linear diode is employed (assuming ideal diodes) with V_{TurnON} = 0, zero forward-biased resistance, and infintie reverse-biased resistance. In the second simulation, an exponential diode is used, which behaves closer to the diodes in CEW.

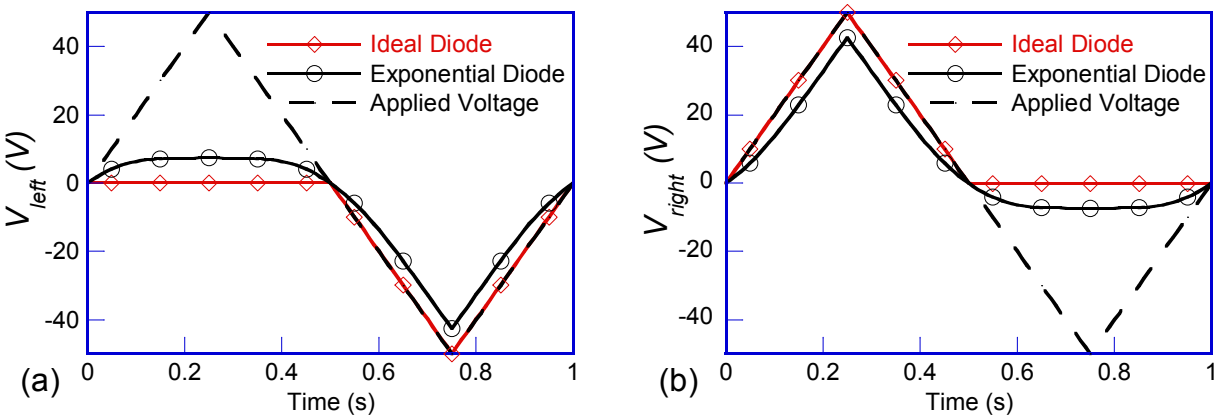

Figure 6-9. Triangular voltage in the test setup shown in Figure 6-4. In this figure, it is also shown how the substrates would behave in the case they are acting as (a) ideal diodes and (b) exponential diode. To obtain exponential diode behavior, saturation current is 0.00685 A, ideality voltage (V_{to}) is 6 V, and the resistance of the forward biased diode is 468 Ω, which are obtained by fitting equation 6.9 on an I-V curve obtained from an aluminum/Na_2SO_4 combination.

The exponential diode current is related to voltage as follows:

$$I = -I_s.(e^{-\frac{V}{V_{to}}} - 1) \tag{6.9}$$

here, V is the applied voltage and V_{to} is the diode turn on voltage at forward biased voltages. I_s (scale current) is the current when the diode voltage is close to the negative of the lowest V_{to} (26 mv). Additionally, in this model, when the diode is forward biased, a resistor (R_s) is considered in series with the diode. The R_s value accounts for the electrical resistance through a forward biased diode. In the electrodes used here, cations diffusion through Cytop pores and/or oxide pores can possibly cause such resistance.

In the simulation, I_s, V_{to}, and R_s are respectively considered 6.9 mA, 6 V, and 468 Ω, which are obtained by fitting equation 6.9 on an I-V curve obtained from an aluminum/Na_2SO_4 combination. After simulation, for better clarity, V_{left} and V_{right} are plotted against the applied voltage (V_{app}) as shown in Figure 6-10.

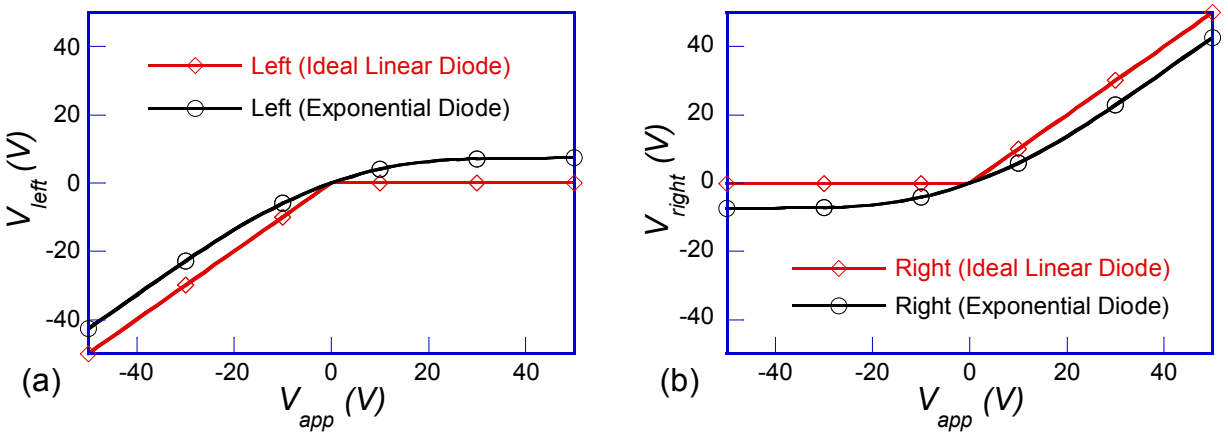

Figure 6-10. Demonstration of (a) Vleft and (b) Vright variation versus applied voltage in the electrode pair setup for ideal and exponential diodes. The ideal diode resistance when reverse biased and forward biased is respectively zero and infinity (V > 0 → R = infinity, V < 0 → R = 0).

The applied voltage varies as shown in Figure 6-9. In the first half cycle of the applied voltage, the electrode on the right side of Figure 6-4 becomes reverse biased and the other electrode becomes forward biased. In the second half cycle of the applied voltage, the voltage polarities of the electrodes are switched. When an ideal diode is used (Figure 6-10a and b), the voltage of one side increases and is equal with the applied voltage, while the voltage of the other side stays at zero—in this case, $\eta_{actuation}$ is one. However, with exponential diode, both of V_{left} and V_{right} change, which results in a reduction in $\eta_{actuation}$. The exponential behavior of the metallic diodes in CEW can be considered as the general reason for $\eta_{actuation}$ reduction.

The diodes effectiveness in CEW can be sought in $\eta_{actuation}$ which can be simply calculated via equation 6.5 using V_{left} (V_{drop} =V_{left}) values from the electrode pair measurements. In the next sections, the experimental $\eta_{actuation}$ values are shown. The impact of four experimental parameters on $\eta_{actuation}$ are investigated, which are V_{app} ramp frequency, electrolytes, substrate preanodization, and electrode material. To do so, $\eta_{actuation}$ values are plotted versus V_{app} as shown in Figure 6-11 (in this figure, to calculate $\eta_{actuation}$, V_{left} is extracted from the curves in Figure

6-10a). By repeating the electrode pair experiments, we also investigate the consistency of $\eta_{actuation}$ in different electrode/electrolyte combinations.

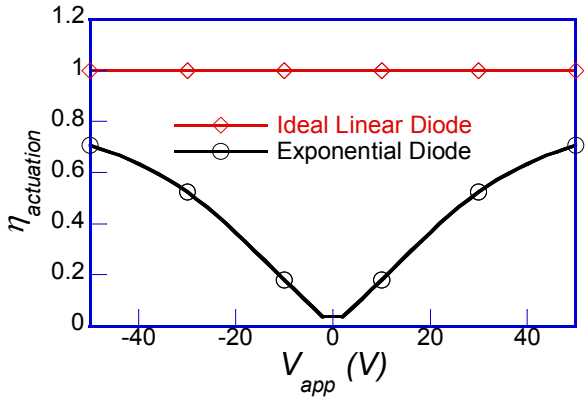

Figure 6-11. Actuation coefficient versus voltage plot. In this figure, to obtain actuation coefficient values, the data in Figure 6-10a are used as V_{left} or V_{drop}.

To show the experimental results, the average of 100, 101, and 102 trials are plotted. It should be mentioned that the curves of 100, 101, and 102 trials are identical to their average, which shows the stability of the system under study. Figure 6-12 shows the consistency of V_{left} (black curve) and V_{right} (red curve) of 100, 101, and 102 trials of titanium/Na_2SO_4 combination.

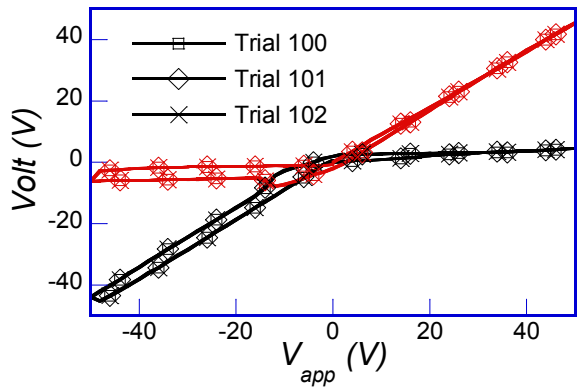

Figure 6-12. V_{left} (black curve) and V_{right} (red curve) of 100, 101, and 102 trials of titanium/Na_2SO_4 combination.

6.5.2.1. Impact of Frequency

The triangular V_{app} as shown in Figure 6-9 is applied at three frequencies of 100 Hz, 1 Hz, and 0.025 Hz. V_{left} and V_{right} and their corresponding ideal case (dashed line) respectively are shown in Figure 6-13 a and b.

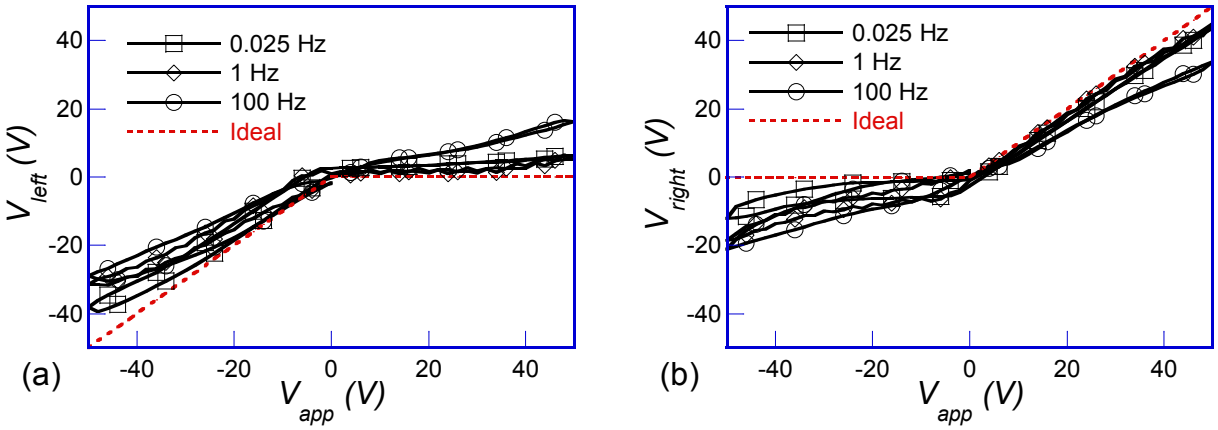

Figure 6-13. Impact of ramp frequency on (a) V_{left} and (b) V_{right} in the electrode pair test setup. In these tests, two Al/Cytop (50 nm) electrodes are used. The theoretical ideal V_{left} and V_{right} are also shown as a reference (red dashed lines).

The shown V_{left} and V_{right} curves are the average of V_{left} and V_{right} curves of 100, 101, and 102 trials. In this test, a combination of 0.1 M Na_2SO_4 as the electrolyte solution and a Si/SiO_2/Al(300 nm)/Cytop(50 nm) as the substrate is used and V_{app} is applied on Al layer. The auxiliary electrodes are activated titanium.

Figure 6-13 a and b show slight differences between V_{left} and V_{right} at the three frequencies. To better visualize the impact of frequency, the $\eta_{actuation}$ values are plotted versus V_{app} as shown in Figure 6-14. To calculate $\eta_{actuation}$ values, V_{left} curves of Figure 6-13 a (the average of 100, 101, and 102 trials) are used.

Figure 6-14 shows that, when V_{app} is positive, $\eta_{actuation}$ has the highest values at 1 Hz and the lowest values at 100 Hz. When V_{app} is negative, $\eta_{actuation}$ has the lowest values at 100 Hz and the highest values at 0.025 Hz. The low values of $\eta_{actuation}$ at 100 Hz is attributed to the poor diode behavior of aluminum due to the continuation of oxide layer formation when the electrode is reverse biased. In other words, the formation of aluminum oxide takes time to reach a maximum thickness (when the oxide resistance against electrochemical reaction reaches a maximum) and at high frequencies it cannot reach the maximum thickness, which decreases the aluminum

resistance when reverse biased, so $\eta_{actuation}$ decreases. In general, the electrodes diode behavior is a lot better at 1 Hz and slower than 100 Hz. Limiting frequencies are likely to be different for different electrode/electrolyte combinations and this is likely impacted even by the concentration of the electrolytes. The subsequent results were measured using 1Hz input frequency—in practice, a low response time of the CEW devices is desired, so we tend to evaluate $\eta_{actuation}$ with a relatively high input frequency (e.g. 1 Hz).

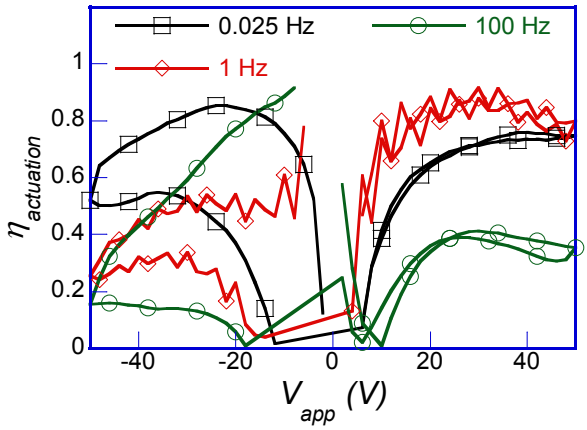

Figure 6-14. Actuation coefficient versus voltage plot in the electrode pair experiments (with aluminum/Na_2SO_4 combination at three frequencies of 0.025, 1, and 100 Hz). In this figure, to obtain actuation coefficient values, the data in Figure 6-13a are used as V_{left} (V_{drop}).

6.5.2.2. Impact of Electrolyte

Electrolytes strongly affect the formation of passivation layers during oxidation. Hence, they change diode behavior of electrodes in our tests. To investigate the impact of electrolytes on $\eta_{actuation}$ with aluminum electrode, three electrolyte solutions, namely 0.1 M citric acid, 0.1 M Na_2SO_4, and 0.1 M NaOH are tested. These tests are performed at 1 Hz and substrates are Si/SiO_2/Al(300 nm)/Cytop(50 nm). The results are shown in Figure 6-15. The shown V_{left} and V_{right} curves are the average of V_{left} and V_{right} curves of 100, 101, and 102 trials.

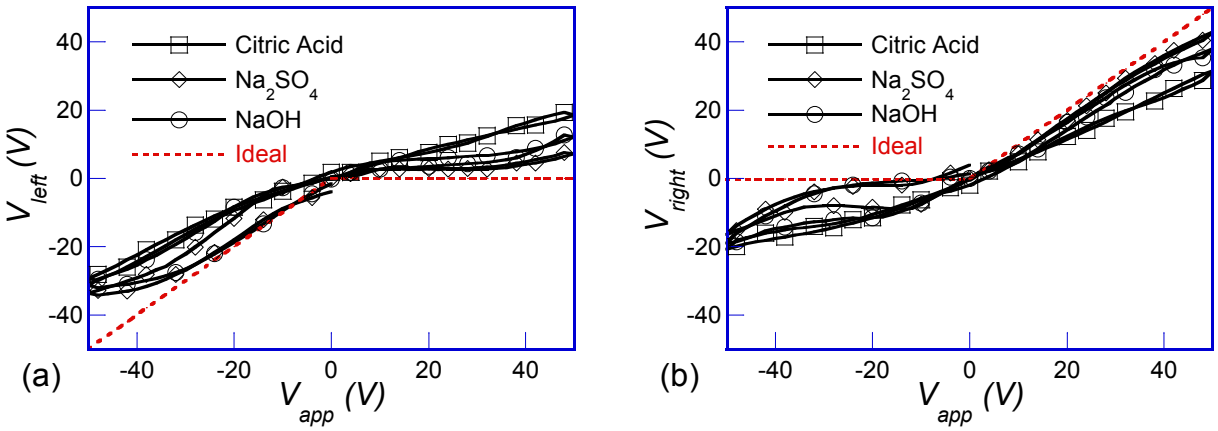

Figure 6-15. Impact of electrolytes on the (a) Vleft and (b) Vright behavior (in the electrode pair tests). The Vleft and Vright are plotted versus the applied voltage. The dashed red lines show the simulated Vleft and Vright behavior with the linear ideal diodes (as seen in Figure 6-10). 0.1 M citric acid, 0.1 M Na2SO4, 0.1 M NaOH are used as electrolyte solutions.

Figure 6-15 a and b show V_{left} and V_{right} of aluminum electrodes with three different electrolyte solutions, namely 0.1 M citric acid, 0.1 M N_2SO_4, 0.1 M NaOH. The V_{left} and V_{right} curves show some differences. For better comparison among the test results in the electrode pair measurements with aluminum electrode, the $\eta_{actuation}$ values are plotted versus V_{app} as shown in Figure 6-16. To calculate $\eta_{actuation}$, V_{left} is obtained from the data in Figure 6-15a. To calculate $\eta_{actuation}$ values, V_{left} curves of Figure 6-15 a (the average of 100, 101, and 102 trials) are used.

The results with citric acid show significant deviation from the ideal case, which is attributed to the passive alumina formation on aluminum. In fact, with aluminum/citric acid combination, aluminum oxidation results in a non-porous alumina formation. The resulting alumina layer impedes electrolyte diffusion at both cathodic and anodic potential polarities of the electrode, which results in the poor behavior observed in electrode pair experiments. Hence, the substrates hardly behave as ideal diodes.

With Na_2SO_4 and NaOH, $\eta_{actuation}$ improves, yet it is not ideal and also some asymmetric behavior in $\eta_{actuation}$ with the applied potential polarity (Figure 6-16) is obvious. Additionally, the

electrode pair tests with aluminum/Na_2SO_4 and aluminum/NaOH combinations cause some damages to the aluminum substrates (aluminum etching is obvious after the tests). In CEW, this could quickly damage the thin aluminum spots and eliminate the diode behavior. Therefore, aluminum/electrolyte combinations used in this study are inappropriate for making a reliable CEW device. To minimize the aluminum etching, we pre-anodized the aluminum electrode and performed the electrode pair tests. The results are shown in the next section.

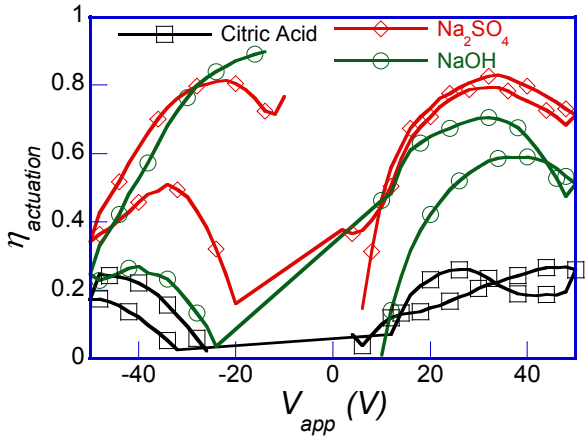

Figure 6-16. Actuation coefficient versus voltage plot. In this figure, to obtain actuation coefficient values, the data in Figure 6-15a are used as Vleft or Vdrop.

6.5.2.3. Impact of Pre-anodization

As stated in the previous section, the conductive layer oxidation affects electrodes diode behavior. In this section, it is shown how alumina layer can affect the test results. To do so, an aluminum substrate is first anodized at +50 V in 0.1 M citric acid bath, which creates a 70 nm alumina layer [14], and then a 50 nm Cytop is spin coated. Then, the electrode pair tests are performed at 1 Hz with three electrolyte solutions, consisting of 0.1 M citric acid, 0.1 M Na_2SO_4, and 0.1 M NaOH. Results are shown in Figure 6-17.

Pre-anodized electrodes show poor CEW actuation behavior with nearly linear voltage response. There are two main issues with the pre-anodized electrodes in terms of diode behavior. First, alumina layer increases the resistance of the forward biased substrates at cathodic

potentials, so V_{left} behavior deviates from ideal case as shown in Figure 6-17a. Second, Al_2O_3/Cytop dielectric stack possesses a high time constant, which could be due to the entrapment of the diffused electrolytes in the dielectric (alumina) pores. The entrapped electrolytes, in fact, require more time and voltage to be removed. This is why, in between around +20 V and -20 V, V_{left} is lower than the ideal diode voltage (Figure 6-17a) and V_{right} is higher than the ideal diode voltage (Figure 6-17b). This shows that $V_{right} + V_{left}$ is higher than V_{app} between +20 V and -20 V, which is an indication of electrolytes entrapment in the Al_2O_3/Cytop dielectric stack. Practically, this means CEW devices with pre-anodized aluminum spots would have poor response time. Therefore, metallic spots pre-anodization is not appropriate for CEW.

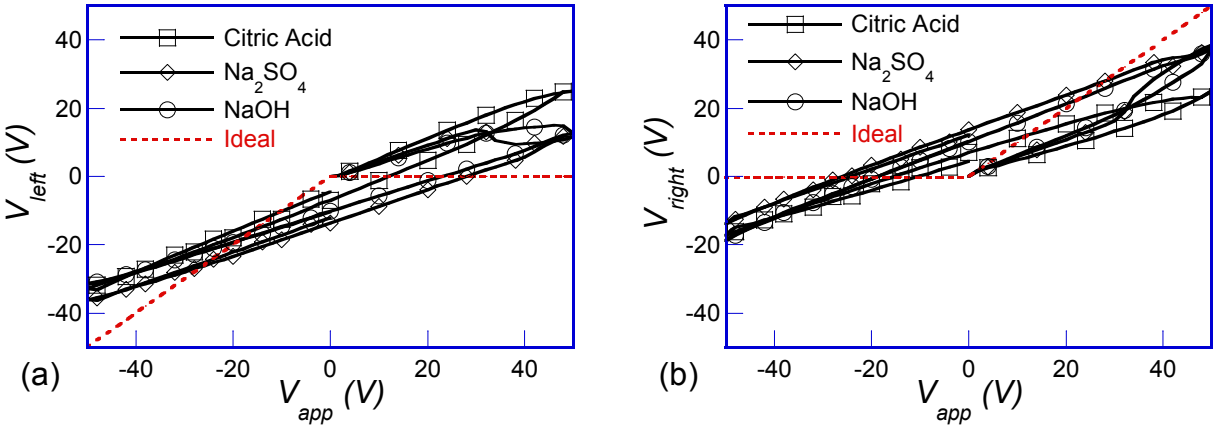

Figure 6-17. Impact of electrodes pre-anodization on the (a) V_{left} and (b) V_{right} behavior. The V_{left} and V_{right} are plotted versus the applied voltage. The dashed red lines show the simulated V_{left} and V_{right} behavior when the diodes are ideal (as seen in Figure 6-10). 0.1 M citric acid, 0.1 M Na_2SO_4, 0.1 M NaOH are used as electrolyte solutions.

So far, it was shown that, with non-preanodized aluminum electrodes, the use of Na_2SO_4 results in the highest $\eta_{actuation}$ values where its magnitude varies with voltage (Figure 6-16). The use of only specific electrolytes limits the application of CEW devices to those electrolytes, which has to be addressed. In the next section, it is shown how high values of $\eta_{actuation}$ can be obtained in different titanium/electrolyte combinations.

6.5.2.4. Impact of Electrode Material

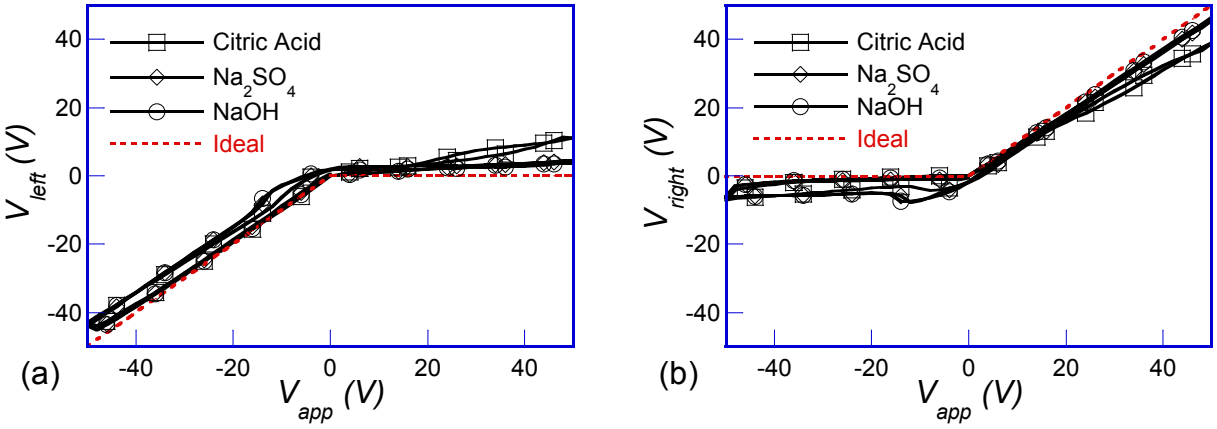

Figure 6-18. Impact of electrodes material on (a) V_{left} and (b) V_{right} in the electrode pair tests. The V_{left} and V_{right} are plotted versus the applied voltage. The dashed red lines show the simulated V_{left} and V_{right} behavior when the diodes are ideal (as seen in Figure 6-10). 0.1 M citric acid, 0.1 M Na_2SO_4, 0.1 M NaOH are used as electrolyte solutions.

The electrode material also influences $\eta_{actuation}$ (actuation coefficient). To investigate the effect of the conductive layer material, we used titanium instead of aluminum as the electrode and performed the electrode pair tests at 1 Hz with 0.1 M citric acid, 0.1 M Na_2SO_4, and 0.1 M NaOH. The results are shown in Figure 6-18a and b. The shown V_{left} and V_{right} curves are the average of V_{left} and V_{right} curves of 100, 101, and 102 trials.

As shown in Figure 6-16, with aluminum the use of only Na_2SO_4 and NaOH as electrolyte can result in relatively high $\eta_{actuation}$ values. However, titanium shows quasi-ideal diode behavior with almost all electrolyte solutions as shown in Figure 6-18, which can be attributed to the titanium oxide nature.

Like previous sections, the $\eta_{actuation}$ is plotted versus V_{app} for better clarity as shown in Figure 6-19. To calculate $\eta_{actuation}$ values, V_{left} curves of Figure 6-16a (the average of 100, 101, and 102 trials) are used.

As shown in Figure 6-19, the $\eta_{actuation}$ values of titanium/Na_2SO_4 and titanium/NaOH combinations are higher than of titanium/citric acid combination. Comparing Figure 6-19 and

Figure 6-16, the $\eta_{actuation}$ values with titanium are greater than the $\eta_{actuation}$ values with aluminum. We attribute the high $\eta_{actuation}$ values with titanium to the thermodynamical stability of titanium oxide films [15-16] and also insignificant tendency of titanium to produce titanium ions at anodic polarities [17] during the electrode pair measurement.

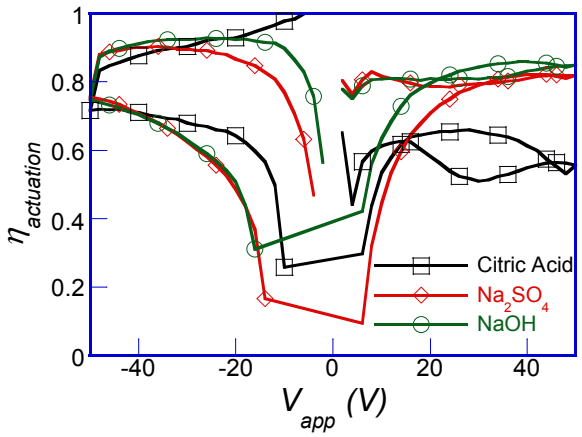

Figure 6-19. Actuation coefficient versus voltage plot of titanium electrode. In this figure, to obtain actuation coefficient values, the data in Figure 6-18a are used as V_{left} or V_{drop}.

Oxides of metals such as aluminum, tantalum, and titanium are amorphous at low voltages and, depending on the electrode/electrolyte combination used, at a certain voltage the oxides become crystalline. The oxides crystallization has been attributed to local heating and internal compressive stresses in the amorphous oxide layers [18-20]. Titanium oxide at low voltages below around 6 V is amorphous and at higher voltages becomes crystalline [18], and then the growth of the crystalline titanium oxide continues at higher voltages [21]. However, during aluminum anodization, alumina crystallization occurs at much higher voltages than 6 V, which is associated with the alumina breakdown [21]. In fact, the oxides crystallization is accompanied by a volume shrink of the oxide layer, which imposes significant stress at the oxide/metal interface [22]. At higher voltages this stress would be more significant and cause mechanical breakdown of the oxide. That may be why in the electrode pair measurements with aluminum, the electrodes

etch away (due to the alumina breakdown at high voltages), while with titanium, the electrodes remains stable.

In fact, in the very first trial of the electrode pair experiments, electrode/electrolyte combinations with both aluminum and titanium result in high values of $\eta_{actuation}$ (except with aluminum/citric acid). However, after the first trial, $\eta_{actuation}$ values with aluminum decrease, while those with titanium remain high, which is attributed to the consistency in titanium oxide films during the electrode pair measurements. In the next section, to show the variation in $\eta_{actuation}$ values in different combinations, the $\eta_{actuation}$ are plotted versus trial number for repeated trials.

6.5.2.5. Actuation Coefficient Variation over Repeated Trials

To evaluate the consistency of the $\eta_{actuation}$ values over repeated trials, we performed the electrode pair measurements for 500 and 2000 trials respectively with aluminum and titanium electrodes (with the three electrolyte solutions of 0.1 M citric acid, 0.1 M N_2SO_4, 0.1 M NaOH). Figure 6-20 a and b show the values of $\eta_{actuation}$ at the extremes of applied voltage (+50 V and -50 V).

In the first trials of the electrode pair measurements with aluminum/Na_2SO_4 and aluminum/NaOH combinations, the $\eta_{actuation}$ values are above 0.6 except for Al/Na_2SO_4 at -50 V (Figure 6-20 a) and they significantly decrease after repeated trials (Figure 6-20 b). In these measurements, the reduction of the $\eta_{actuation}$ values is attributed to the instability and etching of aluminum oxide during the electrode pair measurements, which decreases the aluminum electrodes resistance when they are reverse biased. The aluminum/citric acid combination is an exception because the $\eta_{actuation}$ values are significantly low from the very first trials (Figure 6-20 a) and stay low all over the test (Figure 6-20 b), which is attributed to the immediate aluminum passivation. Generally, with aluminum electrode, the $\eta_{actuation}$ behavior over repeated trials show

that the CEW devices with aluminum spots would perform appropriately in the beginning, but their performance degrades after repeated use.

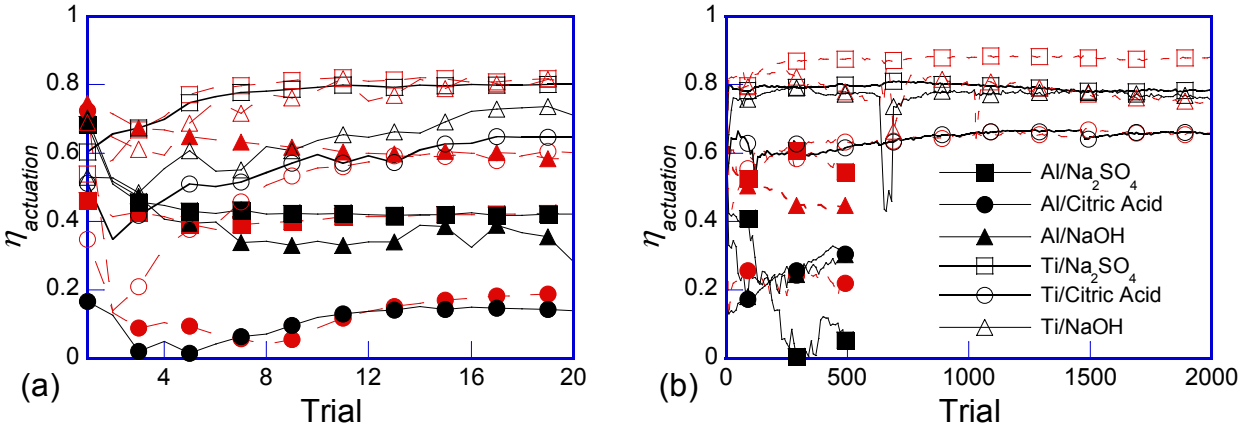

Figure 6-20. Evaluation of actuation coefficient ($\eta_{actuation}$) reliability. Six electrode/electrolyte combinations, namely Al/Na_2SO_4, Al/Citric Acid, Al/NaOH, Ti/Na_2SO_4, Ti/Citric Acid, and Ti/NaOH are used. Equation 6.7 is used to calculate $\eta_{actuation}$ where $V_{drop}=V_{left}$. The solid black and dashed red lines show the $\eta_{actuation}$ values at the extremes of applied voltage of +50 V and -50V, respectively. Figure 6-11 (a) and (b) respectively show the $\eta_{actuation}$ values over the first 20 trials and 2000 trials.

However, the reliability of the CEW devices can be improved by the use of titanium spots. As shown in (Figure 6-20 a), with titanium the $\eta_{actuation}$ values start from around 0.5 and even increase after repeated trials (Figure 6-20 b). This behavior of $\eta_{actuation}$ indicates that CEW devices made with titanium spots can perform appropriately from the first use and its performance even improves after repeated trials—the improvement of the $\eta_{actuation}$ values is attributed to a gradual formation of titanium oxide. Additionally, after the $\eta_{actuation}$ values reach a plateau (Figure 6-20 b), their consistency can be related to titanium oxide stability over repeated trials. In conclusion, in the beginning, the CEW devices made with aluminum spots might perform as well as those made with titanium spots; however, after repeated use, it is expected that aluminum spots performance would degrade, while titanium spots would keep actuating droplets consistently.

6.6. Conclusion

In this chapter, we showed how metallic spots voltages in CEW are theoretically related to the electrostatic force moving the droplets sidewise. An equation was developed (equation 6.5) that relates the total electrostatic force to the droplet radius, applied voltage, and droplet voltage (which is measured experimentally). To evaluate the performance of different electrode/electrolyte combinations, an electrode pair experiment is designed, and then the experimental results are related to the metallic spots performance in real CEW devices via a coefficient which here is referred to as actuation coefficient ($\eta_{actuation}$).

6.6.1. CEW in Different Electrode/Electrolyte Combinations

The $\eta_{actuation}$ values in six electrode/electrolyte combinations, namely Al/Na_2SO_4, Al/citric acid, Al/NaOH, Ti/Na_2SO_4, Ti/citric acid, and Ti/NaOH are evaluated. We performed the electrode pair measurements over repeated trials (500 trials with aluminum electrode and 2000 trials with titanium electrode). Altogether, two kinds of graphs are obtained from the electrode pair measurements. First, the $\eta_{actuation}$ values are plotted versus V_{app}, which shows how $\eta_{actuation}$ varies with voltage. Second, the $\eta_{actuation}$ values of the trials at the applied voltage extremes (±50 V) are plotted versus the trial number, which show the reliability of the $\eta_{actuation}$ values over repeated trials.

6.6.1.1. CEW with Aluminum Electrode

With aluminum, the use of citric acid caused a significant reduction of $\eta_{actuation}$, which is due to the passivation of aluminum electrode—once passivating, the electrodes impede the ions diffusion at both anodic and cathodic polarities of the electrode, which is the reason of low values of $\eta_{actuation}$ in Al/citric acid combinations. The $\eta_{actuation}$ magnitudes in Al/NaOH and Al/Na_2SO_4 combinations are higher than those in Al/citric acid, but they vary with voltage. With Al/NaOH and Al/Na_2SO_4 combinations, the $\eta_{actuation}$ values reach a maximum of around 0.7 at

middle voltages (around ±30 V) and decrease down to 0.4 at ±50 V. This raises the question as to whether it is possible to fabricate CEW devices with higher $\eta_{actuation}$ values by reducing the dielectric thickness (which reduces the droplet actuation voltage). To answer this question, as a future plan, we are performing the electrode pair measurements up to ±30 V with aluminum electrodes to see how the results would differ from the current ones. In the repeated electrode pair measurements with aluminum, in the first trials, the $\eta_{actuation}$ values are high for all but the Al/citric acid combination—in this combination, the $\eta_{actuation}$ values are low from the very first trial, which is attributed to the immediate passivation of aluminum. Aluminum electrode performance declined significantly with repeated cycling—the reduction in $\eta_{actuation}$ values is possibly due to the alumina etching. In general, the results of the electrode pair measurements with aluminum shows that CEW devices with aluminum spots might perform well in the first trials, but a significant degradation in their performance is expected.

6.6.1.2. CEW with Titanium Electrode

With titanium electrode, all of the $\eta_{actuation}$ values (around 0.8) were higher than those obtained with the aluminum electrode. However, with citric acid the $\eta_{actuation}$ values were slightly lower than others at positive applied voltages, which can be attributed to a high resistance of the titanium oxide (formed with citric acid) against electrolytes diffusion. With the titanium electrode, another aspect of the $\eta_{actuation}$ curves is that they do not decrease around the extreme voltages (unlike the $\eta_{actuation}$ curves with the aluminum electrodes). The consistency of the $\eta_{actuation}$ curves can be related to the stability of titanium oxide over the electrode pair measurements. In the repeated electrode pair measurements, titanium electrodes showed consistent performance over 2000 cycles. Here, the consistency of the $\eta_{actuation}$ values is also attributed to the titanium oxide stability. Practically, with the use of titanium spots, we can

fabricate CEW devices which are expectedly reliable for repeated use. In the future, some CEW devices will be fabricated with both aluminum and titanium spots and the droplet actuation performance will be compared on both devices in terms of the droplet lateral force and the device reliability. The droplet lateral force would be measured by a tool designed and fabricated in our lab [23]. Moreover, we will perform the electrode pair measurements with more valve metals such as tantalum and zirconium with some other electrolyte solutions such as $Ca(OH)_2$ and tartaric acid.

6.7. References

[1] F. Mugele, J.-C. Baret, Electrowetting: from basics to applications, Journal of Physics: Condensed Matter, 17 (2005) R705-R774.

[2] S. Chevalliot, S. Kuiper, J. Heikenfeld, Experimental Validation of the Invariance of Electrowetting Contact Angle Saturation, Journal of Adhesion Science and Technology, 26 (2012) 1909-1930.

[3] T.B. Jones, An electromechanical interpretation of electrowetting, Journal of Micromechanics and Microengineering, (2005).

[4] C.E. Rosenkilde, A Dielectric Fluid Drop an Electric Field, Proceedings of the Royal Society of London. A. Mathematical and Physical Sciences, 312 (1969) 473-494.

[5] T.B. Jones, J.D. Fowler, Y.S. Chang, C.-J. Kim, Frequency-Based Relationship of Electrowetting and Dielectrophoretic Liquid Microactuation, Langmuir, 19 (2003) 7646-7651.

[6] K.H. Kang, How electrostatic fields change contact angle in electrowetting, Langmuir, 18 (2002) 10318-10318.

[7] J. Buehrle, S. Herminghaus, F. Mugele, Interface profiles near three-phase contact lines in electric fields, Phys. Rev. Lett., 91 (2003) 86101-86101.

[8] F. Mugele, J. Buehrle, Equilibrium drop surface profiles in electric fields, Journal of Physics: Condensed Matter, 19 (2007) 375112-375112.

[9] N.B. Crane, A.a. Volinsky, P. Mishra, A. Rajgadkar, M. Khodayari, Bidirectional electrowetting actuation with voltage polarity dependence, Applied Physics Letters, 96 (2010) 104103-104103.

[10] C.W. Nelson, C.M. Lynch, N.B. Crane, Continuous electrowetting via electrochemical diodes, Lab on a chip, 11 (2011) 2149-2152.

[11] C.W. Nelson, C.M. Lynch, N.B. Crane, Continuous electrowetting via electrochemical diodes, Lab on a chip, 11 (2011) 2149-2152.

[12] M. Khodayari, J. Carballo, N.B. Crane, A material system for reliable low voltage anodic electrowetting, Materials Letters, 69 (2012) 96-99.

[13] A. Schultz, S. Chevalliot, S. Kuiper, J. Heikenfeld, Detailed analysis of defect reduction in electrowetting dielectrics through a two-layer 'barrier' approach, Thin Solid Films.

[14] S. Wernick, R. Pinner, P.G. Sheasby, The surface treatment and finishing of aluminum and its alloys, in, ASM International, Finishing Publication Ltd., 1987.

[15] R.J. Solar, S.R. Pollack, E. Korostoff, In vitro corrosion testing of titanium surgical implant alloys: An approach to understanding titanium release from implants, Journal of Biomedical Materials Research, 13 (1979) 217-250.

[16] D.F. Williams, Corrosion of Implant Materials, Annual Review of Materials Science, 6 (1976) 237-266.

[17] P. Tengvall, I. Lundström, Physico-chemical considerations of titanium as a biomaterial, Clinical Materials, 9 (1992) 115-134.

[18] J. Yahalom, J. Zahavi, Electrolytic breakdown crystallization of anodic oxide films on A1, Ta and Ti, Electrochimica Acta, 15 (1970) 1429-1435.

[19] J. Yahalom, J. Zahavi, Experimental evaluation of some electrolytic breakdown hypotheses, Electrochimica Acta, 16 (1971) 603-607.

[20] J.S.L. Leach, B.R. Pearson, Crystallization in anodic oxide films, Corrosion Science, 28 (1988) 43-56.

[21] C.K. Dyer, J.S.L. Leach, Breakdown and Efficiency of Anodic Oxide Growth on Titanium, Journal of The Electrochemical Society, 125 (1978) 1032-1038.

[22] J.-H. Xing, Z.-B. Xia, J.-F. Hu, Y.-H. Zhang, L. Zhong, Growth and Crystallization of Titanium Oxide Films at Different Anodization Modes, Journal of The Electrochemical Society, 160 (2013) C239-C246.

[23] N.B. Crane, Q. Ni, T. Marschke, S. Steele, S. Najafi, Contact Angle Friction and Contact Angle Hysteresis (CAH) through Force Measurements, in: IMECE, 2012, pp. 1-3.

CHAPTER 7: CONCLUSION

The goal of this study was to select reliable material combinations for Continuous Electrowetting (CEW) devices. In this context, the devices reliability is associated with two parts of the CEW devices. First part is the dielectric substrate, as the droplet actuation on the dielectric substrate has to be consistent over many cycles. The second part is the metallic spots, in that the droplet actuation force has to be persistent over many tests cycles, which is provided by the metallic spots reliability. To test the dielectric capabilities, a droplet was placed on a hydrophobic substrate and then a potential difference is applied between the droplet (via an auxiliary electrode placed in the droplet) and the substrate. In the electrode pair measurements, two separate identical electrodes are connected in a way that they resemble two consecutive metallic spots in the CEW devices.

7.1. Key Conclusions

7.1.1. EWOD Reliability in Passivating Systems

To evaluate the substrate's reliability, a pulse voltage (for many cycles) is applied in the conventional test setup and then the variation in the contact angle modulation is evaluated over cycles (a combination of one zero voltage and one applied pulse voltage is considered one cycle). In the reliable systems, the degradation of the angle modulation over cycles is negligible.

In this study, the early reliability measurements were performed on aluminum substrates of Si/SiO_2(500 nm)/Al(300 nm)/Cytop (various thicknesses). In these tests, the power source is connected to the droplet via an auxiliary electrode and the aluminum layer. We used three different electrolyte solutions, consisting of 0.1 M NaCl, 0.1 M Na_2SO_4, and 0.1 M citric acid. It

was found that with citric acid the droplet modulation continues consistently with negligible variation in the contact angle change. However, with NaCl and Na_2SO_4, the droplet modulation fails after a couple of test cycles. The EWOD failure is attributed to the aluminum layer etching which is inhibited with citric acid due to the passive nature of the aluminum/citric acid combination.

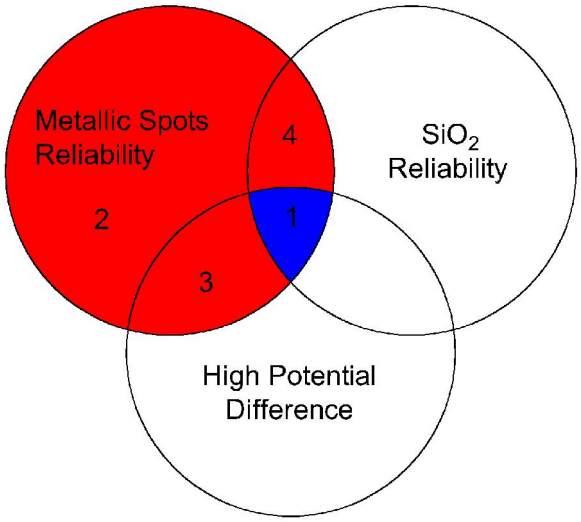

Figure 7-1. The contribution of the metallic spots reliability in the CEW devices reliability.

The results of this study help us better understand the failure mechanisms in CEW devices. First, the inhibition of electrochemical reactions would result in a consistent EWOD for many cycles as occurs in the aluminum/citric acid passivating combination. Second, in CEW devices when positive voltages are applied on the substrate, electrochemical reactions can lead to the etching of metallic spots as occurs in aluminum/NaCl and aluminum/Na_2SO_4 combinations (when negative voltages are applied on the substrate, cathodic reactions occur); therefore, the electrode/electrolyte combinations selected for CEW devices have to resist etching. Our tests results in electrode pair measurements show that titanium should be used as the metallic spots in CEW devices to fabricate reliable devices. Titanium resists electrochemical etching, which

results in a persistent droplet actuation in CEW for over 2000 trials. The contribution of the metallic spots reliability in the reliability of CEW devices is shown in Figure 7-1.

In this diagram, the reliability of metallic spots can be met in four regions. Region 1 corresponds to the metallic spots reliability when titanium is used with citric acid electrolytes and region 3 when titanium is used with sodium sulfate electrolytes. Region 2 and 4 are related to metallic spots reliability when a passivating system is used. Among all the regions, only region 1 has to be considered for the fabrication of reliable CEW devices because region 1 is the overlap among the three circles. In the next sections it is explained how the other circles are divided into regions.

7.1.2. EWOD Reliability with SiO_2 Dielectrics

As stated in the previous section, the electrochemical reactions can cause the EWOD failure due to the electrode etching and the damages they cause to the dielectric layer. In CEW devices, the dielectric layer underneath the droplet is a SiO_2(500 nm)/Cytop(50 nm) stack. Hence, in this study, the dielectric stack reliability is evaluated.

Our second reliability measurements are performed on SiO_2(500 nm)/Cytop(50 nm) stack dielectric layer with 0.1 M NaCl and 0.1 M citric acid electrolyte solutions. The results show that, over 10,000 cycles, the contact angle change can degrade with NaCl and citric acid respectively up to 47% and 19%. With both electrolyte solutions, the SiO_2 layer resists the electrolytes solutions, and hence electrochemical reactions are prevented. The better consistency in the contact angle change with citric acid is attributed to the large size of the anions which limits the anions diffusion into the SiO_2 layer. However, with NaCl, chloride anions can possibly diffuse to the SiO_2 layer, which degrades the contact angle modulation up to 47% due to charge entrapment. The contribution of the metallic spots reliability in the reliability of CEW devices is shown in Figure 7-2.

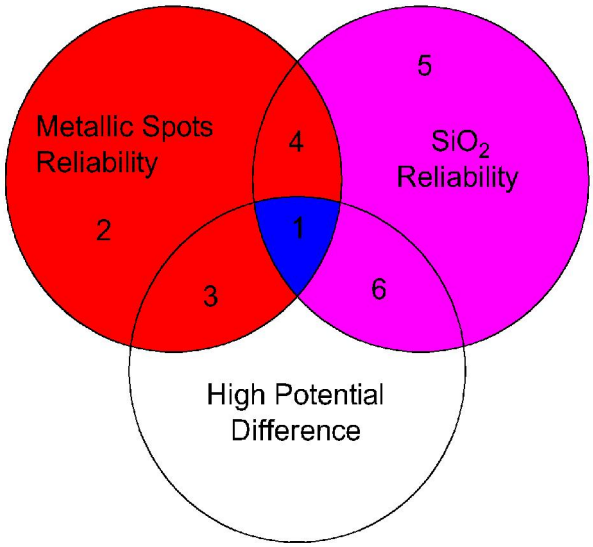

Figure 7-2. The contribution of SiO_2 reliability in the reliability of CEW devices.

The all four regions in the SiO_2 reliability circle correspond to the SiO_2 dielectric in contact with large electrolytes. However, here, the SiO_2 reliability circle is divided into four regions and each region is related to the use of a specific metallic spot, so that the overlap among the circles can be demonstrated. Region 1 and 4 are related to the reliability of the SiO_2 dielectric when titanium and aluminum is used respectively. Region 5 and 6 are related to any other metals that are not fit in the metallic spots reliability circle.

Based on the results of these experiments, it can be expected that, in CEW devices, electrolyte solutions with Na_2SO_4 should be used to guarantee the reliability of the SiO_2 dielectric. This could be related to the larger size of the SO_4^{-2} ions relative to Cl^{-1}, but additional testing is necessary to draw clear conclusions and identify other high performance materials. It is worth mentioning that the cations should not diffuse into the dielectric layer, so their properties may not be important. Cations diffuse into the dielectric layer if the substrate voltage becomes negative; however, in CEW, the substrate voltage increases (to positive values) at the leading edge of the droplet and remains at zero (or close to zero) at the trailing edge. This is why only anions can contribute in the degradation in the contact angle change via diffusion in the dielectric

layer. With the use of only Cytop instead of the SiO_2/Cytop stack, it was shown how the small size of the cations lead to the significant cathodic reaction on the electrode, which degrades the contact angle change. Here, the use of SiO_2 prevents cathodic reactions.

7.1.3. Reliability in CEW Devices

At the end, it is important to evaluate the metallic spots behavior in CEW in terms of their effectiveness to actuate droplets and also their reliability. To have an estimate of the metallic spots effectiveness in CEW, the metallic spot voltages are theoretically related to the electrostatic force on the droplet via an equation. Then, a criteria is extracted from the relationships between the metallic spots voltage and the electrostatic force, which is referred to as actuation coefficient ($\eta_{actuation}$). The $\eta_{actuation}$ values of six electrode/electrolyte combinations, (namely Al/Na_2SO_4, Al/citric acid, Al/NaOH, Ti/Na_2SO_4, Ti/citric acid, and Ti/NaOH) are evaluated. It is observed that, over tests trials, the $\eta_{actuation}$ values with aluminum decrease from around 0.7 to around 0.3, while those with titanium remains at around 0.8. The consistency of the $\eta_{actuation}$ values with titanium is attributed to the titanium oxide stability. The conclusion of these experiments is that, to fabricate reliable CEW devices, the metallic spots should be titanium. The contribution of the consistency of the potential difference of metallic spots in the reliability of CEW devices is shown in Figure 7-3.

In the circle related to high potential difference, region 3 is related to the initial high potential difference in passivating systems, region 6 is related to the initial high potential difference in non-passivating systems with large electrolytes, region 7 is related to the initial high potential difference in non-passivating systems with small electrolytes, and region 1 corresponds to the persistent high potential difference when titanium and large electrolytes are used. In fact, to fabricate reliable CEW devices, all the conditions of region 1 have to met.

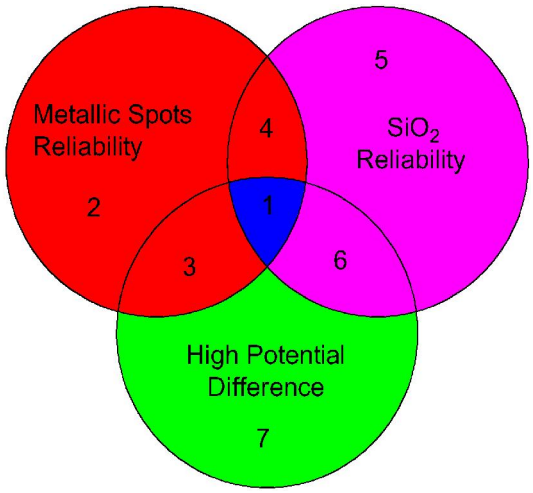

Figure 7-3. The contribution of the consistency of the potential difference of metallic spots in the reliability of CEW devices.

7.2. Future Plan

The results of this study have provided us with the bases for the future studies to improve the CEW devices. That electrode/electrolyte materials influenced the $\eta_{actuation}$ values has encouraged us to conduct other material related tests as future studies, which are as follows:

1- Test Titanium in single polarity testing

2- Evaluate other valve metals (e.g. tantalum and zirconium)

3- Test impact of electrolyte concentration on performance

4- Compare different electrolytes—in this study we have used three different electrolyte solutions which were acidic, neutral, and alkaline. In the next experiments other electrolyte solutions such as tartaric acid (acidic), sulfuric acid (acidic), NaCl (neutral), CaOH (alkaline), and etc. can be used.

5- Test whether silicon will work by itself:

1- Electrochemical diodes. Silicon in contact with electrolytes behaves as diode too, which is similar to electrochemical diode behavior of the metallic spots. If silicon can be used (without metallic spots) the CEW device fabrication would be easier and more cost effective.

2- Schottky diodes using a liquid metal droplet. The CEW device of this study works based on electrochemical diodes, which can fail due to intense electrochemical reaction and the subsequent electrode etching. If Schottky diodes can be used, the electrochemical reactions would be eliminated, which is expected to improve the devices lifetime.

Testing materials parameters listed above, we expect to find materials that bear higher (close to one) $\eta_{actuation}$ values. Then the appropriate material systems are to be used to fabricate reliable, efficient CEW devices. To obtain better CEW performance, some other factors are also tested, which are:

1- Test the limits of frequency to assess the impact of higher frequencies

2- Consider the case of three diodes connected since droplets often have three connections at a time

In the past, we have demonstrated CEW with aluminum spots. In future, two more CEW devices will be fabricated, consisting of:

3- New CEW devices with Titanium

4- Create 2D CEW

APPENDICES

Appendix A: Permission for Use of Figure 1-3.

RSC | Advancing the Chemical Sciences

Terms & Conditions

This web site and any RSC information accessed from this site are protected by copyright.

The RSC maintains this site for your information, education, communication, and personal entertainment. You may browse, download or print out one copy of the material displayed on the site for your personal, non-commercial, non-public use, but you must retain all copyright and other proprietary notices contained on the materials. You may not further copy, distribute or otherwise use any of the materials from this site without the advance, written consent of RSC.

RSC shall use its best endeavours to ensure that the information contained on this site is accurate and up-to-date, but RSC accepts no liability for omissions or errors therein or their consequences. RSC shall not be liable for any consequential direct or indirect loss or damage of any nature whatsoever alleged to be caused by errors or omissions in the information contained on this site.

RSC makes no representations whatsoever about the suitability of the information contained in the documents and related graphics published on this site for any purpose. All such documents and related graphics are provided "as is" without warranty of any kind, express or implied, without limitations, warranties of title or implied warranties of merchantability or fitness for a particular purpose.

In no event shall RSC be liable for any general, special, direct, indirect, consequential or incidental damages, or any damages whatsoever, resulting from loss of use, data or profits, whether in an action of contract, negligence or other tortious action, arising out of or in connection with the use of information available from this site.

In no event shall RSC be liable for any damage to your computer equipment or software which may occur on account of your access to or use of the site, or your downloading of materials, data, text, or images from the site, whether caused by a virus, bug or otherwise.

The information published on this site could include technical inaccuracies or typographical errors. RSC may make improvements and/or changes to the information published on this site at any time.

This site is linked to third party sites. The linked sites are outside the control of RSC and RSC is not responsible for the contents of any linked site or any link contained in a linked site. RSC provides these links only as a convenience, and the inclusion of any link does not imply endorsement or approval by RSC of the site. RSC is not responsible for the contents of any site linking to this site.

Certain areas of this web site can only be accessed on a subscription or pay-per-view basis. In this case more specific Terms and Conditions apply, in addition to the general web site Terms and Conditions above.

Amazon Associates Programme

The Royal Society of Chemistry is a participant in the Amazon Europe S.à r.l. Associates Programme, an affiliate advertising programme designed to provide a means for sites to earn advertising fees by advertising and linking to Amazon.co.uk.

Open Access image

The Open Access image used on this website can be downloaded from: **www.openaccessweek.org/page/downloads-2** and is distributed under a **Creative Commons Attribution License**.

Copyright & Permissions
What you need to know about copyright and requests for permission to use RSC or third party material.

Appendix B: Permission for Use of Chapter 4.

Rights & responsibilities

At Elsevier, we request transfers of copyright, or in some cases exclusive rights, from our journal authors in order to ensure that we have the rights necessary for the proper administration of electronic rights and online dissemination of journal articles. Authors and their employers retain (or are granted/transferred back) significant scholarly rights in their work. We take seriously our responsibility as the steward of the online record to ensure the integrity of scholarly works and the sustainability of journal business models, and we actively monitor and pursue unauthorized and unsubscribed uses and re-distribution (for subscription models).

In addition to authors' scholarly rights, authors have certain responsibilities for their work, particularly in connection with publishing ethics issues. View our webinar on Ethics for Authors for a useful resource of information.

Rights	FAQ	Responsibilities	Permissions

As a journal author, you have rights for a large range of uses of your article, including use by your employing institute or company. These rights can be exercised without the need to obtain specific permission.

How authors can use their own journal articles

Authors publishing in Elsevier journals have wide rights to use their works for teaching and scholarly purposes without needing to seek permission.

Table of Authors' Rights

	Preprint version (with a few exceptions- see below *)	Accepted Author Manuscript	Published Journal Articles
Use for classroom teaching by author or author's institution and presentation at a meeting or conference and distributing copies to attendees	Yes	Yes with full acknowledgement of final article	Yes with full acknowledgement of final article
Use for internal training by author's company	Yes	Yes with full acknowledgement of final article	Yes with full acknowledgement of final article
Distribution to colleagues for their research use	Yes	Yes	Yes
Use in a subsequent compilation of the author's works	Yes	Yes with full acknowledgement of final article	Yes with full acknowledgement of final article
Inclusion in a thesis or dissertation	Yes	Yes with full acknowledgement of final article	Yes with full acknowledgement of final article
Reuse of portions or extracts from the article in other works	Yes	Yes with full acknowledgement of final article	Yes with full acknowledgement of final article
Preparation of derivative works (other than for commercial purposes)	Yes	Yes with full acknowledgement of final article	Yes with full acknowledgement of final article
Preprint servers	Yes	Yes with the specific written permission of Elsevier	No